

**ANALYSIS OF FACTORS AFFECTING PERFORMANCE OF A LOW-
TEMPERATURE ORGANIC RANKINE CYCLE HEAT ENGINE**

By

TISAYE BERTRAM KALUA

Student number: 215118707

Submitted in fulfilment of the requirements for the degree of

MAGISTER TECHNOLOGIAE: MECHANICAL ENGINEERING

In the

FACULTY OF ENGINEERING, THE BUILT ENVIRONMENT AND IT

at the

NELSON MANDELA METROPOLITAN UNIVERSITY

Supervisor: Prof Russell Phillips

Co-supervisors: Mr Gys Kleyn and Mr Karl du Preez

2017

DECLARATION

I, Tisaye Bertram Kalua, Student Number 215118707, hereby declare that the dissertation for a Masters in Mechanical Engineering is my own work and that it has not previously been submitted for assessment to another University or for another qualification.

Tisaye Bertram Kalua

DATE:

DEDICATION

Dedicated to my wife, Helen, and children Tapiwa, Yewo, Uwemi and Makhumbo....
not used to living as apart as for this cause! Namusobani mwabanthu!

I love you!

ACKNOWLEDGEMENTS

I would like to thank the following people who made my dream come true.

Professor Russell Phillips. You rekindled my dream and made it a possibility with all the support and daring... stopping at nothing. Your encouragement and zeal resulted in this work we can point at today.

Co-supervisors, Mr Gysbert Kleyn and Mr Karl du Preez, for all the necessary criticisms, contributions and financial support, all so dear to this work.

Louwrens Hercules Kok. Every research project seemed to be in your hands. What an organizer, what a dedicated person you are.

Colleagues Greystone and Saulos for the untiring support in coming up with this document.

Technology Innovation Agency (TIA) for sufficient financial support.

ABSTRACT

Organic Rankine Cycle (ORC) heat engines convert low-grade heat to other forms of energy such as electrical and mechanical energy. They achieve this by vaporizing and expanding the organic fluid at high pressure, turning the turbine which can be employed to run an alternator or any other mechanism as desired. Conventional Rankine Cycles operate with steam at temperatures above 400 °C

The broad aspect of the research focussed on the generation of electricity to cater for household needs. Solar energy would be used to heat air which would in turn heat rocks in an insulated vessel. This would act as an energy storage in form of heat from which a heat transfer fluid would collect heat to supply the ORC heat engine for the generation of electricity.

The objective of the research was to optimize power output of the ORC heat engine operating at temperatures between 25°C at the condenser and 90 to 150°C at the heat source. This was achieved by analysis of thermal energy, mechanical power, electrical power and physical parameters in connection with flow rate of working fluid and heat transfer fluids.

KEYWORDS

Organic Rankine Cycle heat engine, "ORC", electricity, low grade heat, pressure differential, temperature, cycle, optimisation.

TABLE OF CONTENTS

	Page
DECLARATION.....	i
DEDICATION.....	ii
ACKNOWLEDGEMENTS	iii
ABSTRACT.....	iv
KEYWORDS.....	iv
TABLE OF CONTENTS	v
LIST OF FIGURES.....	x
LIST OF TABLES.....	xii
LIST OF APPENDICES.....	xiii
ABBREVIATIONS	xiv
GREEK SYMBOLS	xv

CHAPTER 1

RESEARCH PROJECT PROPOSAL AND OVERVIEW

1.1	INTRODUCTION	1
1.2	ORGANIC RANKINE CYCLE HEAT ENGINES.....	1
1.3	PROBLEM STATEMENT.....	3
1.4	SUB PROBLEMS	3
	1.4.1. Sub-problem 1 (Operating Pressures and Temperatures).....	3
	1.4.2 Sub-problem 2 (Unit Physical Structure).....	3
	1.4.3 Sub-problem 3 (Cavitation).....	3
	1.4.4 Sub-problem 4 (Start-up).....	4
1.5	HYPOTHESIS.....	4
1.6	DELIMITATIONS	4

1.7	SIGNIFICANCE AND FEASIBILITY OF RESEARCH.....	5
1.8.	RESEARCH METHODOLOGY.....	5
1.8.1	Preliminary work	5
1.8.1.1	Literature survey	5
1.8.1.2	Prototype construction	6
1.8.1.3	Analysis of results	6
1.8.1.4	Construction of final prototype	6
1.9	COST ESTIMATE.....	8
1.10	RESEARCH PROJECT PLAN.....	9

CHAPTER 2

LITERATURE REVIEW

2.1	INTRODUCTION	10
2.2	OPTIMISATION.....	10
2.2.1	Fluid selection criteria.....	11
2.2.2	Blends and Pure Substances	12
2.2.3	Scroll expanders.....	12
2.2.4	Condensers	13
2.2.5	Recirculators.....	14
2.2.6	Evaporators	15
2.2.7	Regenerators.....	16

CHAPTER 3

TEST SET-UP

3.1.	INTRODUCTION	17
3.2.	THE ORGANIC RANKINE CYCLE HEAT ENGINE.....	17
3.3.	MODELLING AND REBUILDING THE PROTOTYPE	18

3.3.1	Heat exchangers	19
3.3.3	Evaporator	22
3.3.4	Condenser	25
3.4.	PIPES	25
3.4.1	Pipe types.....	25
3.4.2	Pipe dimensioning	26
3.5.	CAVITATION	27
3.6.	WORKING FLUID.....	31
3.7.	RECIRCULATION PUMP	31
3.8.	CHARGING THE SYSTEM.....	32
3.9.	PARAMETERS FOR CONSIDERATION.....	33
3.8.1	Pressure	33
3.8.2	Temperature	35
3.8.3	Working fluid flow rate	35
3.8.4.	Shaft power	36
3.9.	SUMMARY	38

CHAPTER 4

RESULTS AND DISCUSSIONS

4.1	INTRODUCTION	39
4.2	COMPARISON OF HEAT SOURCE AND EXPANDER INLET PRESSURE	39
4.3	COMPARISON OF PUMP AND SCROLL SPEEDS.....	40
4.4	FEED PUMP BEHAVIOUR.....	41
4.5	THERMODYNAMIC PERFORMANCE OF PROTOTYPE 1 AND 2	43
4.6	SUMMARY OF PROTOTYPE 1 AND 2.....	45
4.7	FINAL PROTOTYPE	45

4.7.1	Tests with R-134a.....	47
4.7.1.1	Thermal Efficiency.....	47
4.7.1.2	Mechanical, thermodynamic and electrical power.....	51
4.7.1.3	Turbine speed.....	53
4.7.1.4	Relationship of pumping speed with scroll rotational speed.....	54
4.7.1.5	Effect of pressure differential.....	55
4.7.2	Tests with R-245fa.....	56
4.7.2.1	Pressure differential (R-245fa).....	56
4.7.2.2	Effect of temperature on scroll rotational speed.....	58
4.7.2.3	Effect of temperature difference on power output.....	58
4.7.2.4	Shaft power.....	61
4.7.2.5	Thermal efficiency.....	62
4.8	START UP.....	66
4.9	OVERALL EFFICIENCY.....	68
4.10	SUMMARY OF RESULTS.....	69

CHAPTER 5

OBSERVATIONS

5.1	INTRODUCTION.....	70
5.2	FLOW RATE.....	70
5.3	PRESSURE RISE.....	70
5.4	SUCTION VOLUME.....	70
5.5	HEAT SOURCE.....	71
5.6	TYPE OF WORKING FLUID.....	71
5.7	CAVITATION.....	71
5.8	SELF-STARTING.....	72

CHAPTER 6

CONCLUSIONS AND SUMMARY

6.1	THE PROBLEM.....	73
6.2	ISSUES RESOLVED.....	74
6.3	FUTURE WORK.....	74
	REFERENCES.....	76

LIST OF FIGURES

Figure 1.1	ORC main components and the T-s diagram.....	2
Figure 1.2	ORC flow chart.....	7
Figure 2.1	GWP of common working fluids for ORCs	11
Figure 2.2	ORC cycle with regenerator	16
Figure 3.2	ORC schematic and T-s diagram for the unit	20
Figure 3.3	Coil evaporators, A- single coil, B- multiple coil	22
Figure 3.4	Cooling water flow meter.....	28
Figure 3.5	Effect of cooling water on condenser temperature	29
Figure 3.6	P-h Chart as simulated by Genetron ORC Simulator	30
Figure 3.7	Prototypes used to investigate NPHS regarding cavitation	30
Figure 3.8	Wika pressure gauges (max 15 bar)	33
Figure 3.9	Bourdon pressure gauges.....	34
Figure 3.10	TEMPpoint temperature module with K-type thermocouples	35
Figure 3.11	Picture of a flow meter for working fluid	36
Figure 3.12	Shaft power for prototype 2.....	37
Figure 4.1	Pressure temperature relationship for prototype 2	40
Figure 4.2	Comparison of pump and scroll speeds of prototype 2	41
Figure 4.3	Feed pump power with and without load.....	42
Figure 4.5	The final prototype	46
Figure 4.6	Thermodynamic performance of 3 prototypes tested with R-134a....	48

Figure 4.7	Temperature conditions at different positions in the cycle.....	49
Figure 4.8	Apparatus for measuring shaft power	51
Figure 4.9	Comparison of shaft power - prototype 2 and 3 (R-134a)	52
Figure 4.10	Electrical power input and output (R-134a).....	52
Figure 4.11	Power output and generator rotational speed (R-134a)	54
Figure 4.12	A comparison of pump and expander speeds (R-134a).....	55
Figure 4.13	Effect of fluid feed on pressure differential (R-134a).....	56
Figure 4.14	Pressure differential pattern with varying temperatures (R-245fa)	57
Figure 4.15	Variation in speed patterns with temperature (R-245fa).....	58
Figure 4.16	Power output curves at different temperatures. (R-245fa)	59
Figure 4.17	A comparison of power outputs (R-245fa).....	60
Figure 4.18	Effect of flow rate on pressure differential. (R-245fa).....	61
Figure 4.19	Shaft power output at different weights and flowrates (R-245fa).....	62
Figure 4.20	P-h diagram for R 245fa	63
Figure 4.21	TEMPpoint display for R 245fa at high temperature	65
Figure 4.22	Power output and expander speeds for R-245fa.....	66
Figure 4.23	Manual start self-sustenance unit with power measuring devices.....	67
Figure 4.24	Results from a self-sustaining system.....	68

LIST OF TABLES

Table 1.1	Estimated budget for the research project.....	8
Table 1.2	Research project plan.....	9
Table 3.1	Fluid heat transfer coefficients in heat exchangers.....	24
Table 3.2	Comparison of copper and stainless steel.....	25
Table 3.3	Properties of R-134a and R-245fa as ORC working fluids.....	31
Table 3.4	Charging working fluid with R-134a.....	32
Table 4.1	Genetron Simulation results.....	43
Table 4.2	Specifications of main components.....	47
Table 4.3	Thermodynamic performance data for prototype 1,2 and3 (R-134a)....	50
Table 4.4	Expander power outputs and pump power inputs (R-134a).....	53
Table 4.5	Thermal performance of low and high temperature cycles on R-245fa	64

LIST OF APPENDICES

Appendix 1	Properties of saturated refrigerant R-134a.....	84
Appendix 2	Properties of superheated refrigerant R134a	85
Appendix 2	Properties of superheated refrigerant R134a (cont.	86
Appendix 3	Mourrier (P-h) chart for R-134a.....	87
Appendix 4	Properties of saturated refrigerant R-245fa.....	88
Appendix 5	Mourrier (P-h) chart for R-245fa.....	89
Appendix 6a	Simulation of thermal performance of R-245fa at low temperature	90
Appendix 6b	Simulation of thermal performance of R-245fa at high temperature.....	91
Appendix 6c	Simulation of thermal performance of R-134a.....	92
Appendix 7	Pressure conversion tables.....	93
Appendix 8	Properties of ORC heat engine working fluids	94

ABBREVIATIONS

\dot{Q}_{in}	heat absorbed by working fluid
\dot{Q}_{out}	heat rejected by working fluid
\dot{m}	mass flow rate
h_1	enthalpy, condenser exit and entry to pump [kJ/kg]
h_2	enthalpy at exit from pump and entry to evaporator [kJ/kg]
h_3	enthalpy, evaporator exit and expander entry [kJ/kg]
h_4	enthalpy, scroll expander exit and pump entry [kJ/kg]
kW	Power, kilowatt
LMTD	Logarithmic Mean Temperature Difference
mm	millimetre
MW	Power, Megawatt
ORC	Organic Rankine Cycle
P_1	pressure, low side [bar]
P_2	pressure, high side [bar]
P-h Diagram	Pressure / enthalpy diagram
P-h	pressure /enthalpy (chart)
PWR	power [W]
r	radius [mm]
R-134a	refrigerant, 1,1,1,2-tetrafluoroethane
R-245fa	refrigerant, 1,1,1,3,3-pentafluoropropane
Revs/min	rotational speed in revolutions per minute
T	temperature[°C]
TIA	Technology Innovation Agency

T-s diagram	Temperature / entropy diagram
U	heat transfer coefficient [W/m ² K]
v _f	specific volume [m ³ /kg]
W/ m ²	Watt per square metre
W _{net}	difference between turbine work and pump work [kJ/kg]
W _{out. turb}	turbine work output [kJ/kg]
W _{pump in}	work done to fluid across pump [kJ/kg]

GREEK SYMBOLS

ΔP	pressure differential, (P ₂ - P ₁)
Δh_{3-4}	enthalpy across the scroll expander
η_{Carnot}	Carnot efficiency (the maximum possible for a cycle)
η_{ise}	isentropic efficiency
η_{thermal}	thermal efficiency
ω	angular velocity [radians/second]

CHAPTER 1

RESEARCH PROJECT PROPOSAL AND OVERVIEW

1.1 INTRODUCTION

The importance of researching energy sources cannot be overemphasised with the current escalated energy demand. Increased industrialisation and global population increases the demand for more energy for increased comfort and productivity. This is causing a depletion of non-renewable energy sources such as petroleum, coal and wood. The environment is threatened by use of the conventional energy sources. Deforestation, for example, has resulted in silting - which has made hydroelectric power unreliable. Petroleum and coal are increasing carbon pollution, resulting in global warming, which also alters climatic seasons - putting man on the verge of survival crisis. Energy cost has escalated, leading to high cost of living ⁽¹⁾. Is there a way of containing the situation? This question can be answered by use of renewable energy that is abundant. The research is one of the answers to that question.

1.2 ORGANIC RANKINE CYCLE HEAT ENGINES

Organic Rankine Cycle (ORC) heat engines are a variation of Rankine Cycle heat engines that employ organic fluids as the working substance. Rankine Cycle heat engines were conceptualised by a Scottish Polymath and Glasgow University Professor, William J.M. Rankine.

Figure 1.1 shows the thermodynamic cycle of the ORC heat engines with a closed circuit ⁽²⁾. The fluid in liquid state, is pumped to the evaporator where it is vaporised and superheated after which the dry vapour is expanded in the turbine, doing the desired work. It proceeds to the condenser where it is liquefied to be recycled. The conventional cycles work with high-temperature steam in ranges above 300°C ⁽³⁾, used to turn turbines at high pressures while generating various magnitudes of electric power. Most such plants are made for commercial purposes producing in the range of tens of kilowatts to hundreds of

megawatts of power. In most cases, the steam is rejected to the atmosphere upon usage (open systems). They are economically too large to suit household applications.

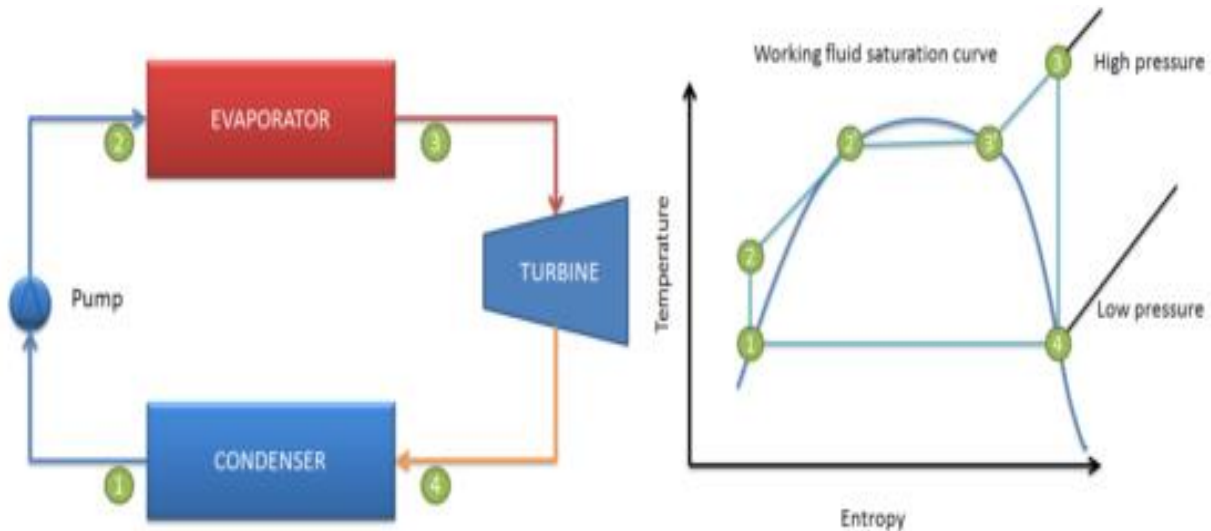


Figure 1.1 ORC main components and the T-s diagram

ORC heat engines of the same magnitudes have been successfully made since their introduction in 1961. Currently, many engineers are making strides in the experimentation of small household units such as the one-kilowatt range of products. Another challenge that has been taken on board is the lowering of operating temperatures of the units. Most Rankine cycle units operate at temperature ranges above 300°C as already stated. Working in such high temperatures requires availability of steam and other high-temperature sources which can readily be found in industry setup rather than households.

This is the reason exploration of low-temperature units is important. It is easier and affordable to achieve temperatures below 100 °C at household levels using simple technologies such as solar heat harnessing. The ORC can be suited to such environments since the working fluid boils at much lower temperatures and can change between phases under easier to achieve conditions.

1.3 PROBLEM STATEMENT

The research will focus on improving the performance of a 1kW Organic Rankine Cycle heat engine studied by a previous scholar, Jason Humm ⁽⁴⁾ to enable it to work with lower temperatures in the range of 85 -140°C, while producing at least 80% of the rated power. Low-temperature ORCs have been successfully developed elsewhere using refrigerants such as R-134a ⁽⁵⁾.

1.4 SUB PROBLEMS

Various sub-problems will be considered in order to successfully accomplish the intended purpose and objective of this research project. These will include the following:

1.4.1. Sub-problem 1 (Operating Pressures and Temperatures)

Conditions that influence the optimum performance of the Organic Rankine Cycle heat engines such as pressure differential and temperature ranges and differential will be investigated.

1.4.2 Sub-problem 2 (Unit Physical Structure)

The optimum volume and weight of the Organic Rankine Cycle heat engine will be investigated.

Whilst working on the performance of the machine, work will also be done to investigate the possible size reduction of the initial unit to reduce on material consumption and space occupation while increasing performance. A compact unit will be considered without compromising performance output.

1.4.3 Sub-problem 3 (Cavitation)

There is need to eliminate all possibilities for pump cavitation (a condition when the liquid pump fails to pump liquid due to presence of bubbles).

Condenser capabilities will be tested against the dryness factors of working fluid to achieve a cooling level where cavitation may not occur. Also, it will be tested if construction conditions such as Net Positive Suction Head (NPSH) and pipe diameters can contribute to cavitation.

1.4.4 Sub-problem 4 (Start-up)

A possibility for the unit to start without using the motor will be investigated by identifying the operational control characteristics such as the use of electromagnetic valves and pressure storage devices. A sprocket /chain arrangement will be tested with the two linking the pump and the scroll expander.

1.5 HYPOTHESIS

The low-temperature Organic Rankine Cycle heat engines can work efficiently with correct conditions of volume ratio and pressure ratio.

1.6 DELIMITATIONS

Since an initial prototype was developed which will have to be optimised ⁽⁴⁾, and bearing in mind the fact the cost of the components is high, the research will be constrained by the following:

- The study will only be done on refrigerant R-134a; whose initial investigations show that it can provide the anticipated results besides being cheaper. This will change depending on the results.
- The 1kW scroll expander will be used with a plunger pump of 138 bar maximum pressure capabilities as it is already available.
- Copper pipes are preferred owing to their low cost and ease of workability whilst achieving the operating parameters. Copper pipes are generally compatible with R-134a and R-245fa ⁽⁶⁾.
- The refrigerant will be recovered ⁽⁷⁾ for re-use ⁽⁸⁾ each time there is a need to change on piping circuitry.

1.7 SIGNIFICANCE AND FEASIBILITY OF RESEARCH

This research will contribute towards the following:

- The research will lead to the provision of portable sources of electricity which are reliable and cost effective since most of the running cost is credited to nature and industrial waste. This somehow takes care of the low efficiencies as the input energy is abundantly available so long it can be harnessed. In this particular research, the source of energy will be heat stored in rocks.
- The research will enable provision of electricity to the remotest of areas where the national grid may not reach. This can encourage people to move to remote places like farm lands and rural villages with a readily available source of electricity.
- This research will encourage the use of green energy which may be abundant and free to use - consequently reducing the overall depletion and degradation of nature. Most of such energy is clean as it does not pollute the environment.
- This research will encourage savings on energy usage by increasing the reuse of waste heat energy in industries. Most energy usage audits show inefficiencies in excess of 50% ⁽⁹⁾

1.8. RESEARCH METHODOLOGY

1.8.1 Preliminary work

The research steps to carry out the study are discussed below:

1.8.1.1 Literature survey

Literature regarding the existing Organic Rankine Cycle heat engines will be reviewed extensively and continuously with the view to fully understand the functionalities, existing challenges and the solutions available.

1.8.1.2 Prototype construction

The initial ORC unit will be reconstructed more than once while establishing power output, flow rates, fluid temperature differences, fluid pressure differentials and thermodynamic efficiencies.

1.8.1.3 Analysis of results

The results will be analysed and interpreted by use of numerical computation analysis using computer programs such as Excel and Genetron simulation.

1.8.1.4 Construction of final prototype

Based on analysis of results, adjustments and improvements will be carried out on the unit to curb the challenges identified and further tests carried out to establish the required procedures and framework for achieving optimum performance of low-temperature ORCs. This procedure has been chosen for the following reasons:

- The experiment is a continuing process where improvements will be made on existing research done by the previous scholar, Jason Humm.
- The unit's components are expensive such that no control prototypes will be built.

The summarized research methodology is illustrated in Figure 1.2 as a flow chart showing the critical steps that will be followed during the study.

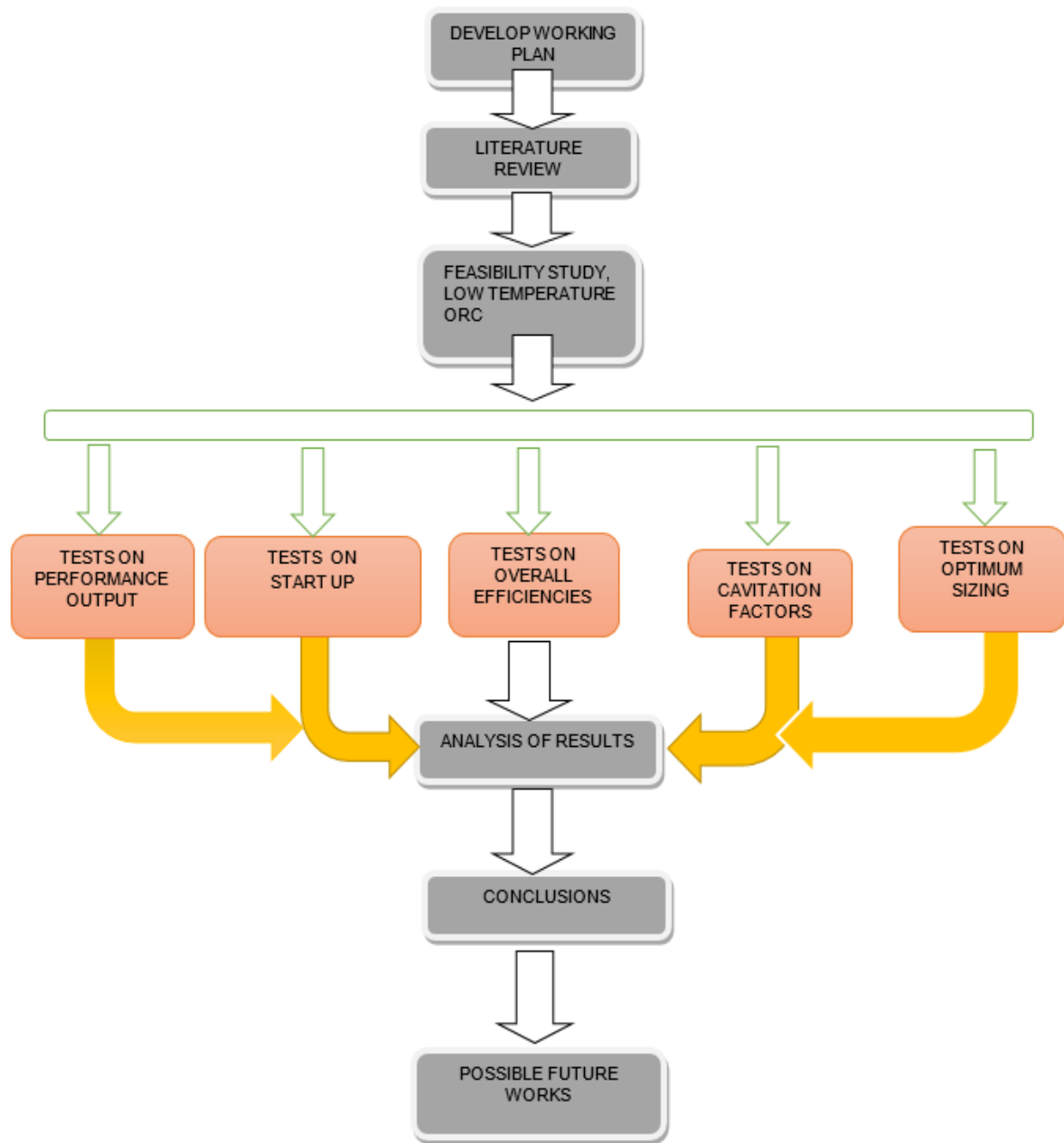


Figure 1.2 ORC flow chart

1.9 COST ESTIMATE

Table 1.1 shows the estimated cost of prototype and dissertation.

Table 1.1 Estimated budget for the research project

PROJECTED COST (RANDS)	
Prototype	
Copper tubing	1,900.00
Installation materials and fittings	6,000.00
R-410a refrigerant	1,500.00
R-245fa	21,000.00
R-134a	3,000.00
Plate heat exchangers	20,000.00
Sub-total	53,400.00
Dissertation	
Transport	2,000.00
Editing	6,000.00
Printing and binding	5,000.00
Sub-total	13,000.00
Total	66,400.00

1.10 RESEARCH PROJECT PLAN

The research project activities and schedules are listed in Table 1.2.

Table 1.2 Research project plan

Description	Start Date	End Date
Literature review	February 2015	November 2015
Research proposal	March 2015	January 2016
Identification of design parameters	October 2015	February 2016
Experimental set-up at NMMU- Renewable Energy	October 2015	June 2016
Data drafting for thesis	June 2016	August 2016
Thesis write-up	August 2016	November 2016
Paper Writing for Journal	May 2016	November 2016

CHAPTER 2

LITERATURE REVIEW

Information regarding the research was gathered by use of journals, text books and suppliers' manuals. Information from internet was also considered. The findings are presented below.

2.1 INTRODUCTION

Supplying electricity to populations away from an urban setup is a challenge to many organisations and governments around the world. Many challenges include transportation cost and economic viability, especially if the location is very remote and does not have an economic activity to offset the cost of supply ⁽¹⁰⁾. Other sources of electricity that would suit such setups include small scale remote generation such as nuclear energy generation, fossil fuel generation, solar power ⁽¹¹⁾, wind, biomass, biogas, ⁽¹²⁾ geothermal as well as industrial waste heat. ⁽¹³⁾.

Some energy sources, though viable, have their disadvantages including pollution, technical challenges in maintenance and source of energy to achieve generation. This is where an Organic Rankine Cycle heat engine ⁽¹⁴⁾ fits better.

ORC heat engines make use of fluids that require less heat energy to translate to power output, and ably fit remote generation with less cost on inception and during operation. They stand to be a solution to power supply for isolated populations. One case of success was the implementation of such a project at a clinic in Lesotho ⁽¹⁵⁾, with the result that cost of supply of electricity was reduced considerably.

2.2 OPTIMISATION

Generally, ORC heat engines have low efficiencies ranging within 10% of the energy input ⁽¹⁶⁾. This is the reason optimisation becomes important to get the most possible power output. Studies are being conducted in component performance improvement ⁽¹⁷⁾ as well as working fluid ⁽¹⁸⁾ and operating temperatures ⁽¹⁹⁾. ORC units almost always are closed circuit

engines such that pressure differentials are an important factor unlike open systems whose low pressure side is atmospheric.

2.2.1 Fluid selection criteria

There is need to select the best combination of the heat source and working fluids as the results of installing the unit range from energy efficiencies ⁽²⁰⁾ to environmental issues ⁽¹²⁾. Many researchers have evaluated performances of different working fluids in different conditions while being guided by performance efficiencies, safety, and international protocols. Some suggestions indicate that fluids which can be used in ORC engines must be of the following characteristics ⁽²¹⁾: low specific volume, high efficiency, moderate pressure in heat exchangers, low cost, low toxicity, low Ozone Depletion Potential (ODP) and low Global Warming Potential (GWP) ⁽²²⁾.

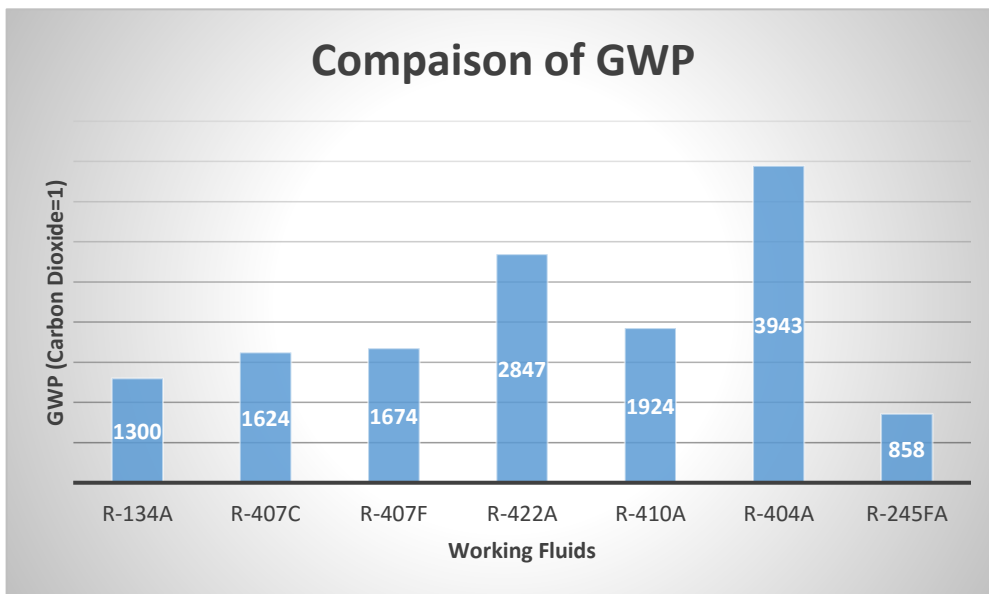


Figure 2.1 GWP of common working fluids for ORCs

From January 2015 the European Union fluorine gas regulation prohibits the production of new equipment that uses fluids with GWP greater than 2500 (comparing with Carbon Dioxide whose index is 1), and restricts services of such equipment to 2020 ⁽²³⁾. Figure 2.1 shows GWP of some substances ⁽²⁴⁾ including R-134a (source Danfoss).

2.2.2 Blends and Pure Substances

The most active refrigerants used in ORC heat engines are R-134a ⁽²⁵⁾, and R-245fa ⁽²⁶⁾. Others include the flammable hydrocarbons like Isobutane, Isopentane ⁽²⁷⁾. Most of these refrigerants operate at typical temperatures of 100-350°C at evaporator outlet conditions and a typical 20-40 °C at the condenser. *Refer to Appendix 8* ⁽²⁸⁾ The higher efficiencies come in with a higher temperature difference between the evaporator and the condenser conditions ⁽²⁹⁾.

The working fluids are classified as either wet, isentropic or dry ⁽³⁰⁾. Wet fluids are those that are saturated such that when the vapour reaches the expander some droplets will have formed already. Isentropic fluids have a balance of energy such that it is assumed they do not collect or lose heat during expansion in the expander. Most such processes are ideal. Dry fluids are regarded highly superheated such that they do not form liquid droplets while in the expander; owing to high enthalpy held by such fluids. ⁽²⁸⁾ Operating the unit at supercritical conditions increases the power output, hence those fluids that are able to achieve this are preferred.

It is claimed that use of zeotropic mixtures ⁽³¹⁾ (mixtures of different fluids which have different phase change temperatures at a given pressure) can considerably increase the efficiency of the cycle ⁽³²⁾. They take advantage of a variation in boiling and condensing temperatures, known as a temperature glide ⁽³³⁾ at evaporator and condenser respectively. Also, Whang and Zhao ⁽²⁷⁾ observed that use of mixtures led to reduced required flow rates and expansion ratios, resulting in reduced turbine dimensions and cost.

2.2.3 Scroll expanders

There are several types of turbines that have been developed for the operation of electricity generators ⁽³⁴⁾. It is, therefore, necessary to select suitable turbines for the desired output based on operating conditions. Most Organic Rankine Cycle heat engines operate at low temperatures, hence necessary to determine which turbines can give the best power output.

Axial turbines and radial turbines, also known as turbo expanders or centrifugal turbines, are some of those employed in generating shaft power from fluids ⁽³⁵⁾. Axial turbines are used with higher temperature heat sources ⁽³⁶⁾ and are more applicable in high energy output applications, while radial turbines are feasible in low energy output applications. The latter is smaller in physical dimensions, yet with higher efficiencies ⁽³⁷⁾. On the other hand, scroll, screw and piston expanders are widely used in smaller ORC engines ⁽³⁶⁾ due to their high efficiencies, simplicity, compactness, among other reasons ⁽³⁸⁾. The performance of expanders depends on flow characteristics. Scroll expanders are an even better choice on smaller generators as they are more reliable with minimal moving parts and constant flow. They are classified as oil lubricated or dry, (not requiring oil lubrication) ⁽³⁹⁾.

2.2.4 Condensers

A condenser is a part of the cycle where the organic fluid vapour is allowed to cool off, getting rid of the heat and being brought to the condensed (liquid) state ⁽⁴⁰⁾. It is an important part of the cycle as it prepares the fluid for recirculation since the recirculator is a liquid pump ⁽⁴¹⁾. There are many designs of condensers defined by the following:

- The cooling medium

Condensers can be classified as either air cooled, water cooled or evaporative. Water cooled condensers work more effectively than air cooled condensers owing to the ability of water to collect more heat ⁽⁴²⁾. Smaller load air cooled condensers depend on natural convection while those that extract more heat load use fans, a method known as forced convection. Water cooled condensers may be of any of the following designs, shell and tube, shell and coil, annulus or submersible ⁽⁴³⁾. Evaporative condensers use both water and air.

- Physical construction

This class ranges from bare tube to microchannel condensers. In general, microchannel condensers are the most effective. ⁽⁴⁴⁾ The brazed plate type, such as car air conditioning condensers, are an example of micro-channel condensers ⁽⁴⁵⁾.

Water cooled condensers with micro-channels, such as the brazed plate heat exchangers, bring into play a strong combination of wide surface area and effective heat transfer between fluids ⁽⁴⁶⁾.

2.2.5 Recirculators

Fluid recirculators for Organic Rankine Cycle heat engines are normally liquid pumps ⁽⁴⁷⁾. These can be in the form of piston pumps, diaphragm pumps, centrifugal as well as plunger pumps, just to mention a few. Different application limits of pressure, temperature, suction head and flow rate determine the type of pump that suits the most.

In ORCs, the energy generated must operate the unit and a substantial percentage remain for consumption by the intended users ⁽⁴⁸⁾. This remainder is the net energy (the whole purpose of investing in the plant). More energy spent by the plant itself reduces the performance and efficiency of the unit. It is for this reason that issues to do with challenges of discharge and suction head management be carefully analysed before a pump can be selected. Another aspect is cavitation, ⁽⁴⁹⁾ which is a phenomenon that occurs as a result of the following:

- Insufficient fluid charge resulting from undercharging or loss of charge due to leakages leaves the fluid mostly in vapour state due to reduced pressure. This can be avoided by making sure the system is void of leakages by thoroughly checking for leaks and determining the required charge through system performance. Electronic leak detectors may be required for such a task.
- Air being trapped in the system, in which case the air forms bubbles that prevent smooth flow and in doing so increase the compressibility of the fluid. A way of separating the air

from the fluid must be found to solve such a problem, such as inserting purge valves at highest point of fluid path.

- When the vapour is condensed and left at saturation temperatures, a slight decrease in pressure causes “boiling” which forms bubbles. Such phenomenon is common at pump entry where pressures tend to reduce with suction and can be solved by sub cooling.
- At constant pressures, a saturated liquid boils off with a slight increase in temperature by the addition of heat from the surroundings, or by virtue of friction caused by flow. A sub cooling of at least 5°C solves such a problem.

All the situations above result in cavitation, which is damaging to the pump life as referred to in the textbook “Cavitation and Bubbles Dynamics” by Brennen, page 27 ⁽⁴⁹⁾. An improved condenser capacity must be able to sub-cool the fluid sufficiently ⁽⁵⁰⁾, reducing chances of boiling off. However, some literature suggest increased Net Positive Suction Head (NPSH) as a solution ⁽⁵¹⁾.

2.2.6 Evaporators

Evaporators, just like condensers, are heat exchangers. The difference lies in the direction of heat flow. With evaporators, heat moves from the surrounding to the working fluid, causing it to evaporate. Studies on evaporator performance show that the type of evaporator can have significant effects on performance. Yuh-Ren Lee(et-al) ⁽⁵²⁾ reported in their study on the effects of types of evaporators on ORC heat engines. They used R-245fa as a working fluid and noted that with plate evaporators they hardly reached 10°C superheat while with a shell and tube evaporator they were able to superheat to 17 °C. The significance of such a superheat was the ability to completely phase out of the saturation zone, which resulted in the expander running smoothly and more efficiently. This means a higher superheat temperature is a goal to achieve with evaporators. The design pressures must also be taken into consideration when selecting the evaporator ⁽⁴⁸⁾. The evaporator is the highest pressure region of the system and unrealistically high pressures may rupture it. The manufacturers of the brazed plate heat exchangers ⁽⁵³⁾, Danfoss, limit the working pressures to 30 bar.

Tailu Li, et al ⁽⁵⁴⁾ studied on evaporator options where evaporators were placed in parallel and efficiencies were improved. This could basically have an increase in heat transfer surface area and a decrease in frictional resistances to flow, with minimal pressure losses.

2.2.7 Regenerators

A fluid leaving the expander has substantial heat which must be extracted in the condenser. This heat can be used to preheat the fluid from the pump entering the evaporator (refer to Figure 2.2⁽⁵⁵⁾) thereby reducing the evaporator duty ⁽⁵⁶⁾. This reduces the condenser duty⁽⁵⁷⁾ on the fluid from the expander as some heat is already given up to the fluid from the pump thereby reducing the required condenser size and saving on cost. Consequently, the size of the evaporator and energy required to evaporate the fluid is reduced. Regenerators help in the reuse of heat energy and reduction of required evaporator and condenser capacity while increasing system efficiency and performance ⁽⁵⁸⁾.

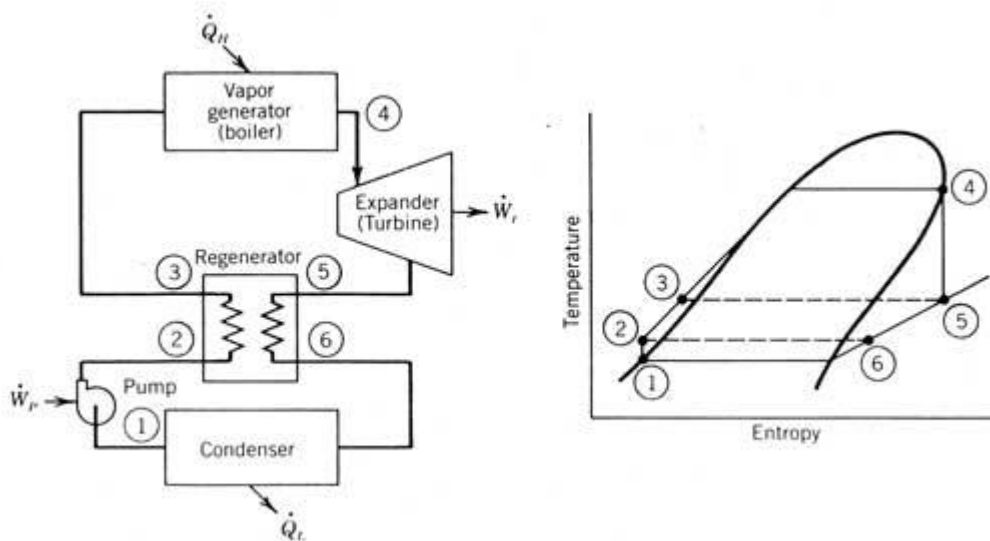


Figure 2.2 ORC cycle with regenerator

CHAPTER 3

TEST SET-UP

3.1. INTRODUCTION

This chapter provides details of the approach towards achieving optimisation of the Organic Rankine Cycle heat engine. This is based on extensive literature reviews and initial experiments on the unit which involved construction of two prototypes, refer to Figure 3.7, the findings of which led to construction of the current prototype as shown in Figure 4.5. In summary, the chapter will look into optimisation in areas that will lead to increasing power output.

3.2. THE ORGANIC RANKINE CYCLE HEAT ENGINE

The heat engine to be optimised was built by the previous scholar, Jason Humm,⁽⁴⁾ as seen in Figure 3.1. It comprised the following main components; the plunger pump, an evaporator, a scroll expander, a condenser and a booster pump. The unit utilised R-245fa as a working fluid. Literature review and test results led to an optimised design.

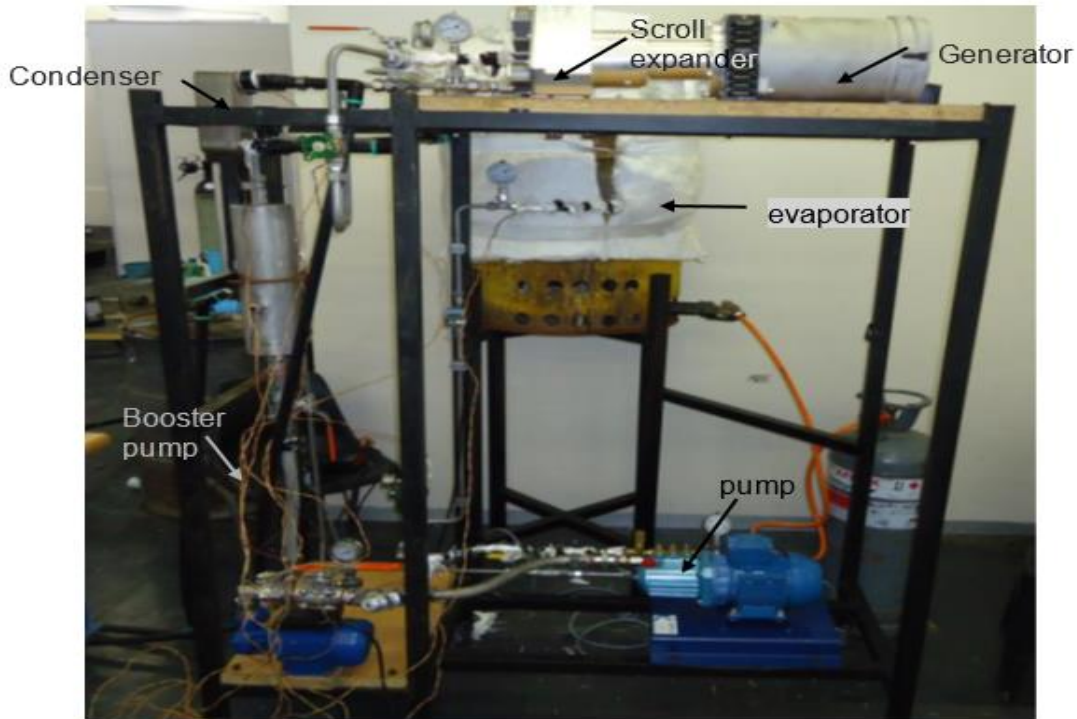


Figure 3.1 Initial set up of the Organic Rankine Cycle heat engine

3.3. MODELLING AND REBUILDING THE PROTOTYPE

There was need to understand the working principle of the cycle, especially the performance characteristics. The first replica was constructed and tested to understand the following issues:

- Cavitation
- Pressure differentials
- Power output

During the rebuild, some main components such as the scroll expander and the plunger pump remained unchanged components around which system optimisation could be explored. Some components got eliminated, simplifying the unit. Pipes were changed from stainless steel to refrigeration grade copper pipes. This simplified the workability as brazing

became the most relevant joining method, cutting the cost on fittings and resulting in reduced occurrence of leakages.

3.3.1 Heat exchangers

The capacity of the unit at different stages was determined with regards to energy balances. A mass flow rate was determined using the volume flow rate as deduced from the energy balance equations from equation 3.1 to 3.6 below with the targeted power output of 1 kW from the scroll expander. Pressure and temperature boundaries were set by the ambient conditions, critical fluid temperatures' and manufacturers specifications which together with results from previous experiments enabled determining enthalpies from NIST Tables of fluid properties. Refer to *Appendices 1 to 5*. Also use of Genetron Properties (a Honeywell refrigeration properties program) helped predict and confirm expected results as given in *Appendices 6a, b and c*. The analysis of the process started with pump working on incompressible liquid. From the properties chart, specific volume, v_f , and enthalpy, h_f across the pump positions 1-2 in Figure 3.2⁽⁵⁹⁾ were read at given pressure and temperature. Since the fluid was assumed incompressible, v_f remained the same and work was determined by the difference in a change of pressure as follows:⁽⁵⁹⁾

$$W_{pump\ in} = v_f (P_2 - P_1) / \eta_{ise} \quad (3.1)$$

The boundary temperature and pressure of the unit were used to read the enthalpies across the evaporator (boiler) from the NIST property charts and heat energy gained in the evaporator was determined by the formula:

$$\dot{Q}_{in\ evap} = \dot{m}(h_3 - h_2) \quad (3.2)$$

The mass flow rate was derived from the volume flow rate read from the flow meter.

As the fluid caused the turbine to spin, a drop in pressure and temperature was evident. If the turbine were absolutely efficient, all the drop would translate into work done by turbine.

Considering mechanical and thermodynamic inefficiencies, the isentropic efficiency, η , of the turbine was taken into consideration.

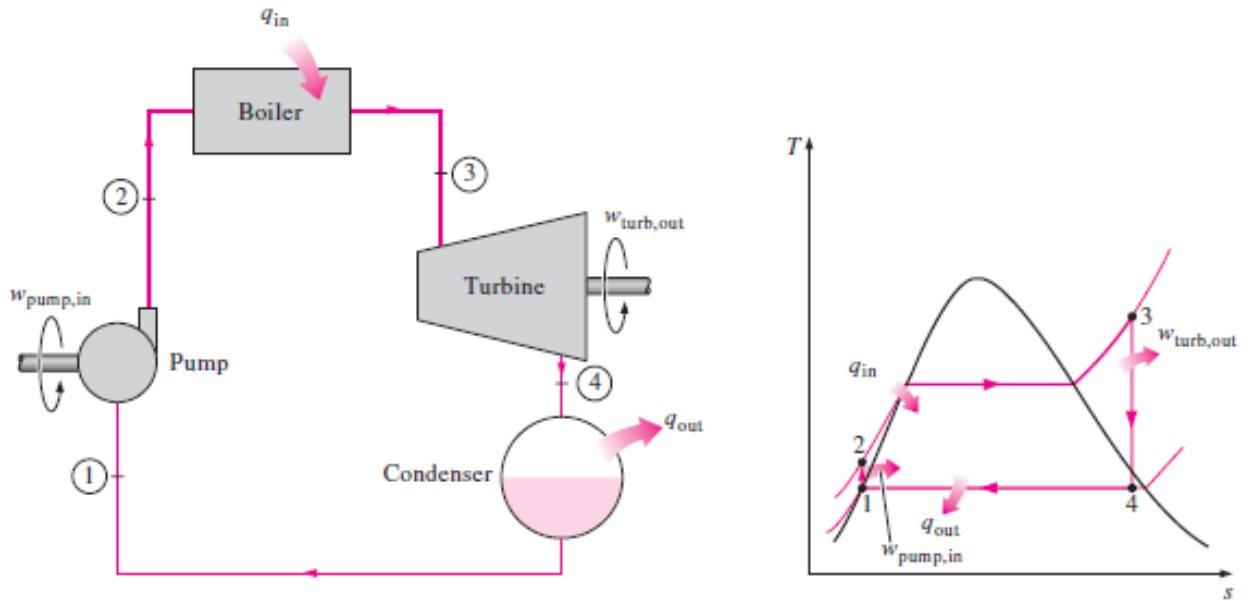


Figure 3.2 ORC schematic and T-s diagram for the unit

Work by turbine was given as:

$$W_{out\ turb} = \eta_{ise} \dot{m}(h_3 - h_4) \quad (3.3)$$

The fluid got to the condenser at low pressure but at almost exit temperature from turbine. A regenerator was not considered in the analysis, and reading the conditions of pressure and temperature from the charts determined the enthalpies as well as dryness factor of the fluid. The heat extracted from the condenser before the fluid started another cycle was given by:

$$\dot{Q}_{out\ cond} = \dot{m}(h_4 - h_1) \quad (3.4)$$

Thermal efficiency of the unit was given by

$$\eta_{thermal} = 1 - (\dot{Q}_{out} / \dot{Q}_{in}) \quad (3.5)$$

$$\text{Or } \eta_{thermal} = W_{net} / \dot{Q}_{in} \quad (3.6)$$

Where

\dot{Q}_{in} was heat absorbed by working fluid

\dot{Q}_{out} was heat rejected by working fluid [W]

\dot{m} was mass flow rate [kg/s]

h_2 was enthalpy at exit from pump and entry to evaporator [kJ/kg]

h_3 was enthalpy, evaporator exit and expander entry [kJ/kg]

h_4 was enthalpy, scroll expander exit and pump entry [kJ/kg]

h_1 was enthalpy, condenser exit and entry to pump [kJ/kg]

η_{ise} was isentropic efficiency of turbine

$W_{out. turb}$ was work done by the turbine [W]

W_{net} was difference between turbine work and pump work. [W]

The pump does little (negligible) work on the fluid. Refer to Table 4.1. However, the energy required by the pump and motor was observed to be 3.5 times more than that used by fluid. Pump and turbine isentropic efficiency is normally given by the supplier as such there was no need to calculate it.

Carnot efficiency, which is the highest ideal efficiency the cycle can achieve was given by

$$\eta_{Thermal,Carnot} = 1 - (T_{low} / T_{high}) \quad (3.7)$$

The Carnot efficiency is a comparison of cycle thermal performance against highest possible performance.

3.3.2 Evaporator

The evaporator was made of a single coil 12.5 mm diameter and 10 m long copper tubing, refer to Figure 3.3A. This had a surface area of 3.95 m² which could have been sufficient at high operating temperatures as was the case with a gas burner as a source of heat. However, the evaporator did not give the desired outcome hence another one was worked out and can be seen in Figure 3.3B.

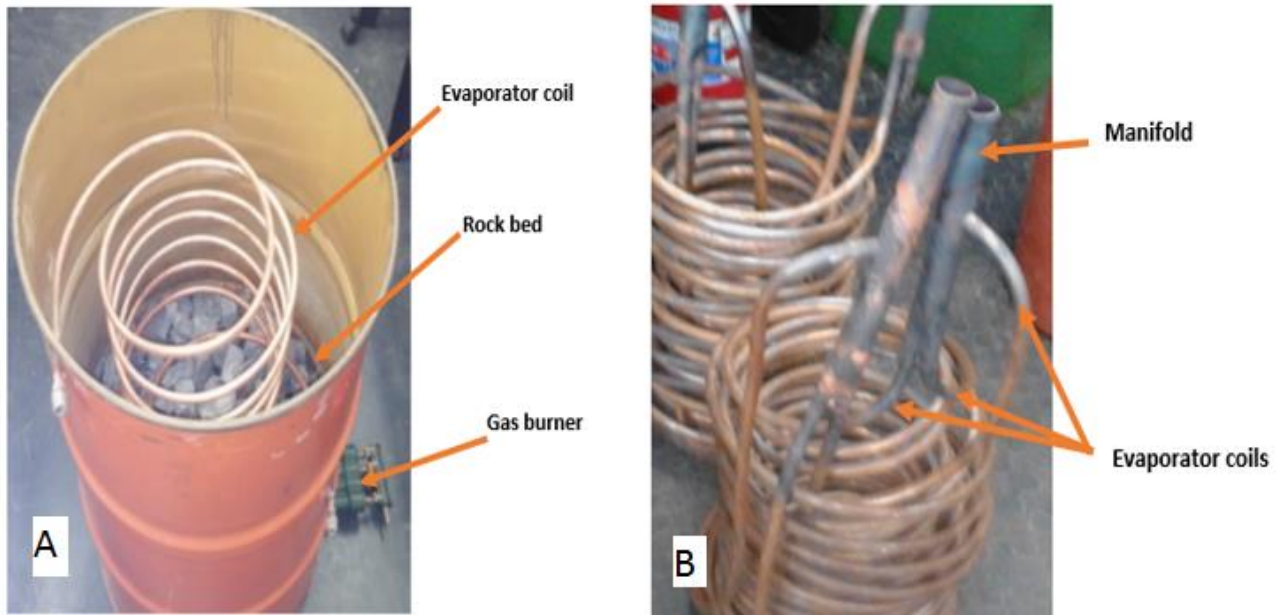


Figure 3.3 Coil evaporators, A- single coil, B- multiple coil

Apart from low efficiency, friction losses were also experienced, which led to adjustment from a single coil to 3 coils in parallel, as in Figure 3.3B., thus increasing heat exchange surface area and achieving more heat transfer. LMTD method was used to establish required surface area. This was achieved using the following relationships:

$$\dot{Q} = UAs\Delta T_{lmtd} \text{ (kW)} \quad (3.8)$$

Temperature difference between the incoming hot fluid and the outgoing cold fluid:

$$\Delta T_1 = T_{H \text{ in}} - T_{C \text{ out}} \text{ (}^\circ\text{C)} \quad (3.9)$$

Temperature difference between the outgoing hot fluid and the incoming cold fluid:

$$\Delta T_2 = T_{H\ out} - T_{C\ in} \text{ (}^\circ\text{C)} \quad (3.10)$$

A logarithmic mean temperature difference is determined as follows:

$$\Delta T_{lmt d} = \frac{\Delta T_1 - \Delta T_2}{\ln\left(\frac{\Delta T_1}{\Delta T_2}\right)} \text{ (}^\circ\text{C)} \quad (3.11)$$

Where

\dot{Q} was the rate of heat transfer [W]

LMTD was Logarithmic Mean Temperature Difference[$^\circ\text{C}$]

U was heat transfer coefficient [W/m²K]

$T_{H\ in}$ was entry temperature of hot fluid to heat exchanger [$^\circ\text{C}$]

$T_{H\ out}$ was exit temperature of hot fluid from heat exchanger [$^\circ\text{C}$]

$T_{C\ in}$ was entry temperature of cold fluid to heat exchanger [$^\circ\text{C}$]

$T_{C\ out}$ was exit temperature of cold fluid from heat exchanger [$^\circ\text{C}$]

A thermal balance was determined with the knowledge of mass flow rate and coefficient of heat transfer as below:

$$\dot{Q} = \dot{m}C_p (T_2 - T_1) \text{ (kW)} \quad (3.12)$$

$$\text{Thus: } \dot{m}C_p (T_2 - T_1) = UA_S \Delta T_{lmt d} \quad (3.13)$$

This heat equated to the LMTD equation gave the required surface area of the heat exchanger. Values of U were found from the tables as a range ⁽²⁾, refer to Table 3.1. The minimum as well as the maximum were calculated giving a range of heat exchanger surface area. For optimum benefit, the larger area was used for the design of the heat exchangers.⁽⁶⁰⁾

The coil was immersed in a small drum provided with electric heaters that simulated the stored thermal energy. Improved heat transfer ensured that the scroll received sufficient superheat ⁽⁶¹⁾ so that the exit vapour remained with a little superheat to prevent condensation within the scroll expander. The condenser had to sub-cool the fluid at least 5°C ⁽⁶²⁾ because such conditions would improve the performance of the recirculation pump. This would ensure that almost incompressible fluid was pumped by the plunger, resulting in increased pumping efficiencies, and would result in the elimination of cavitation; as will be discussed in the preceding sections.

The modified type of heat exchanger was utilised both as evaporator and condenser.

Table 3.1 Fluid heat transfer coefficients in heat exchangers

Type of heat exchanger	U , W/m ² · °C
Water-to-water	850–1700
Water-to-oil	100–350
Water-to-gasoline or kerosene	300–1000
Feedwater heaters	1000–8500
Steam-to-light fuel oil	200–400
Steam-to-heavy fuel oil	50–200
Steam condenser	1000–6000
Freon condenser (water cooled)	300–1000
Ammonia condenser (water cooled)	800–1400
Alcohol condensers (water cooled)	250–700
Gas-to-gas	10–40
Water-to-air in finned tubes (water in tubes)	30–60
	400–850
Steam-to-air in finned tubes (steam in tubes)	30–300
	400–4000

3.3.3 Condenser

The condenser initially utilised a plate type heat exchanger which was later used as a recuperator. One of the coils was immersed in 220l drum supplied with tap water, thus being utilised as a condenser (Figure 3.7 under cavitation).

The parallel coil setup resulted in improved heat transfer as expected. Pressure changes were also observed (only across the pump and the scroll expander) suggesting a reduced impact of friction.

3.4. PIPES

3.4.1 Pipe types

Steel pipes had 10 times more frictional factors compared to copper pipes which contributed to energy demands required to transport the fluid. For optimisation in energy efficiency, comparisons of stainless steel and copper give copper a better advantage over steel in this application, refer to Table 3.2.

Table 3.2 Comparison of copper and stainless steel

PARAMETERS	COPPER	STAINLESS STEEL
Absolute roughness ϵ ⁽⁶⁰⁾	0.0015mm	0.015mm
Cost of 25mm diameter /m	R92	R504
Rigidity	Low	High
Method of joining	Mostly soldering	Unions and fittings
Leakages Possibility	Low	High
Thermal conductivity k ⁽⁶⁰⁾	401 W/m.K	14.2 -15.1 W/m.K

3.4.2 Pipe dimensioning

Pipe diameters and lengths had a direct effect on pressure differentials (Pressure differential is the difference between the turbine entry pressure and exit pressure at any instance), and analysis of friction factors and pumping energy requirements was done based on pipe dimensions. Changing the setup to shorter pipe runs reduced pressure drop across piping, the same result was observed in the heat exchanger piping in parallel. The following was the method of calculation:

A volume flow rate, Q , was determined from the flow meter readings in litres per minute.

$$Q = \frac{\pi d^4}{128 \mu l} (\text{Poiseuille's equation}) \quad (\text{m}^3/\text{s}) \quad (3.14)$$

The limiting lengths given particular diameter were determined, and examined at different diameters. The coefficient of dynamic viscosity, μ remained the same for a range of conditions of a fluid. Or alternatively:

$$Q = \left(\frac{\pi D^2}{4}\right) \tilde{u} \quad (\text{m}^3/\text{s}) \quad (3.15)$$

The average velocity of a fluid in motion is denoted \tilde{u} , which is the maximum velocity divided by 2 as the minimum velocity on the walls is close to zero (0).

The expected pressure drop due to flow and pipe characteristics was given as follows:

$$\Delta P = f \frac{l v^2}{2d} \rho \quad (\text{kPa}) \quad (3.16)$$

Reynold's number was used to determine flow characteristics of the fluid, whether laminar or turbulent, with the relationship below.

$$\text{Re} = \frac{\rho u d}{\mu} \quad (3.17)$$

The frictional factor f was read from the Moody's chart, having determined the relative roughness, $\frac{\varepsilon}{d}$ where ε was the absolute roughness and d the diameter of pipes for a particular Reynold's number.

In the above equations:

ΔP was the pressure differential registered across pipe sections, (kPa)

\tilde{u} was the average velocity of a fluid in a pipe (m/s)

l was the length of a pipe under examination (m),

f was the frictional factor (dimensionless)

d was the bore diameter of a pipe. (m)

ρ was the density of the fluid in question (kg/m³)

v was the velocity (m/s)

3.5. CAVITATION

Another factor to be investigated was cavitation. Tests by the previous scholar registered this as a major challenge to be investigated further. It was noted that the liquid pump would run without registering a flow rate. This was due to vapour occupying the pump region, resulting in no significant suction. An investigation to verify whether this phenomenon was to do with suction head or dryness factor of working fluid was launched by the construction of a tall unit, about 3.5 m high (Figure 3.7) to increase the Net Positive Suction Head (NPSH), and installing a flow meter (Figure 3.4) along the tap water supply line to monitor the volume flow rates. Sight glasses were installed in different areas of interest to observe the condition of working fluid at different condenser flow rates. At increased condenser cooling fluid flow rates, it was expected that the sight glass would be full indicating all liquid and no vapour. A reduced condensation would show bubbles at the sight glass indicating a

mixture of vapour and liquid. The dryness factor regions as evident from sight glasses can be seen on the Genetron Simulation chart in Figure 3.6



Figure 3.4 Cooling water flow meter

The results were compared at different flow rates of the cooling water. It was observed that at lower flow rates, there would be no pumping and bubbles would be seen through a sight glass fitted at the exit of the condenser. Optimum flow rates were established, as seen in Figure 3.5, beyond which cavitation was eliminated and the sight glass was clear. It was further noted that more cooling in the condenser resulted in better pump performance as there was more liquid in the pump intake region.

Plotting the refrigerant conditions on the P-h chart indicated that it was still in the saturation zone as a mixture, suggesting that sub cooling conditions had not been reached.

The flow rate results and condenser performance results were recorded and presented in the graph in Figure 3.5

The system was left to run with about 200 litres of water and in about 30 minutes' performance had significantly dropped and the water temperature was about 40°C. This resulted in reduced condensation causing cavitation of system pump. Water was supplied in intervals of volume flow rates while observing the steady state conditions of temperature. An optimum range was reached where temperature of the water dropped no more and the unit performance improved.

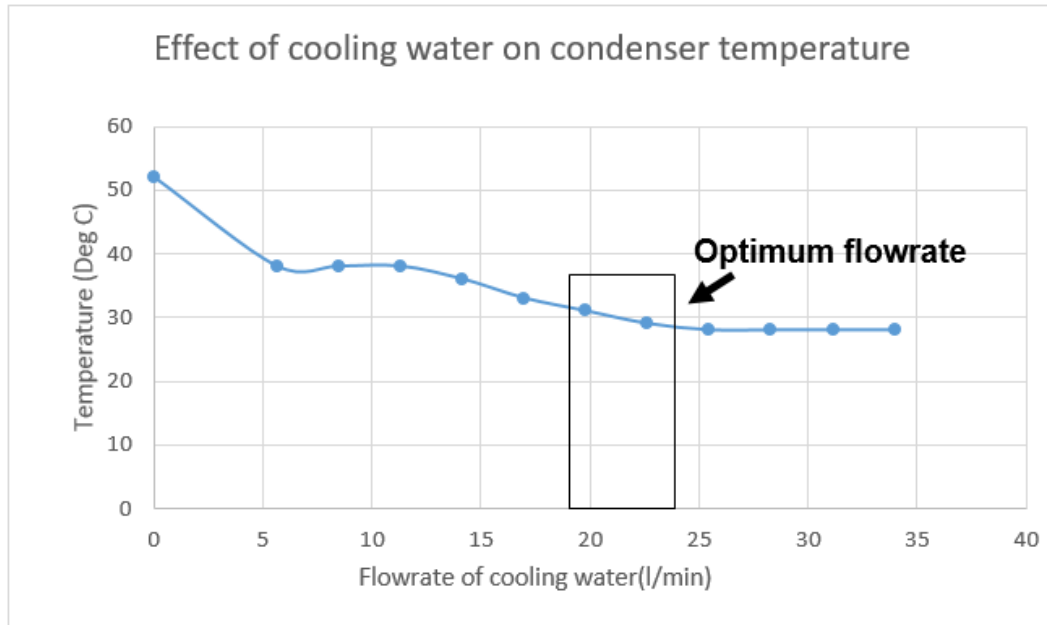


Figure 3.5 Effect of cooling water on condenser temperature

The same was the case with the shorter unit (Figure 3.7), resulting in the conclusion that cavitation was dependent on the dryness factor of working fluid. Hence, height being eliminated as a constraint.

The P-h chart in Figure 3.6 shows fluid conditions at different processes in the system. The liquid saturation region of zero dryness fraction is the desired condition at the pump while the superheat region beyond 100% dryness fraction is desired at the outlet of the expander. The transition region which is the mixture phase occurs in the evaporator and condenser, the direction of which is dependent on direction of heat flow.

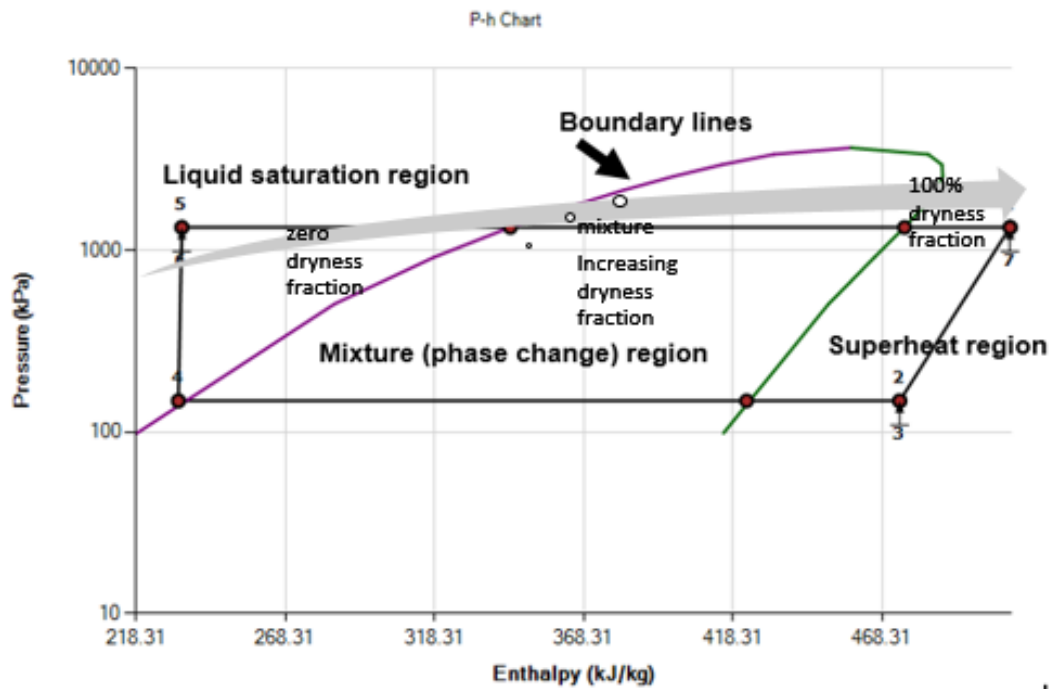


Figure 3.6 P-h Chart as simulated by Genetron ORC Simulator

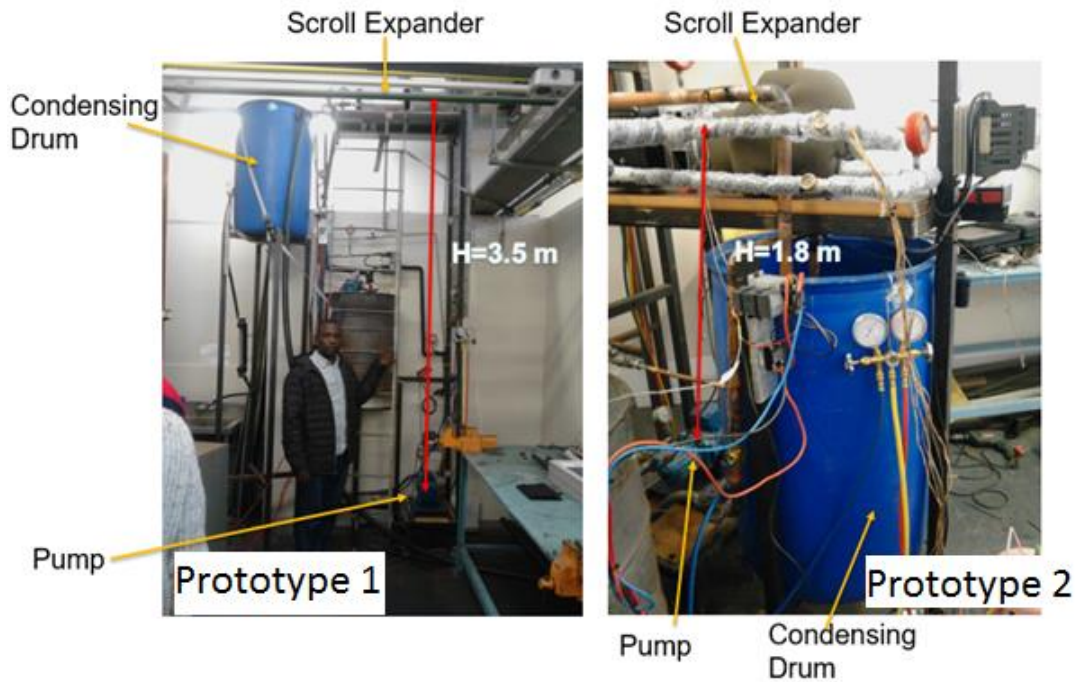


Figure 3.7 Prototypes used to investigate NPHS regarding cavitation

3.6. WORKING FLUID

R-134a was used for development due to its lower cost, availability and low critical temperatures which are below 100°C. The refrigerant used water as a heat transfer fluid as it required a temperature just about the boiling point of water. Using the Genetron Simulation program, it was noted that R-245fa would produce 30% more power output compared with R-134a. Refer to *Appendices 6a, b and c*. However, R-245fa requires about 130°C temperature heat source to operate efficiently. Meanwhile, heat transfer oil was used to give energy to R-245 fa as it requires temperatures higher than water can reach at atmospheric pressure. Some characteristics of the two fluids are shown in Table 3.3 below.

Table 3.3 Properties of R-134a and R-245fa as ORC working fluids

Fluid	Relative Density	Boiling Point (atmospheric)	Critical temperature	Latent heat of vaporisation	GWP	State at Pump	Cost
	Pure water=1	°C	°C	(kJ/kg)	CO ₂ = 1		R/ kg
R-134a	1.168	-26	101	245	1410	liquid	92
R-245fa	1.32	15.1	154	197.5	1030	liquid	2200

3.7. RECIRCULATION PUMP

A recirculation plunger pump by CAT Pumps (model 2SF 30) was used which could achieve a flow rate up to 12 l /minute. However, driving the pump and motor required more power than driving the working fluid. If a pump achieving high pressures above 20 bar could be employed at lower energy consumption, it would be a saving to the heat engine energy demands. The behaviour of the feed pump can be seen in section 4.3 and Figure 4.3 where it was discussed further ⁽⁶³⁾. Another selection in the supplier's catalogue was a CAT pumps 2SF 10 plunger pump with a maximum flow rate of just about 4l/minute. Unfortunately, the pump required to run at much higher speeds compared with the former, to achieve a

particular flow rate, compromising on power input. It also required that it run longer than the bigger pump considered above for it to achieve adequate flow.

3.8. CHARGING THE SYSTEM

The unit was pressurised to check for leaks using an electronic leak detector and soap bubbles. Once convinced that there were no leakages, the unit was evacuated from atmospheric pressure, 760,000 microns to about 500 microns using a vacuum pump. (See *Appendix 7*, pressure conversion table by H. Tring and T. Stec). A heat source was prepared to the expected operating temperatures. Working fluid was added at intervals with increments as shown in Table 3.4 using a weighing scale and charging gauges.

Table 3.4 Charging working fluid with R-134a

MASS (kg)	EFFECT ON EXPANDER	REVS/ MIN (NO LOAD)
1	No response	0
2	Runs for 8 seconds	90
3	Runs for 23 seconds	200
4	Runs for 2 minutes	500
5	Runs continuously	1200
6	Runs continuously	4000

A 10% mass refrigerant was added to ensure sufficient charge at all times. Once the required mass was established, it could be used as a guide for future charging. This method was preferred because different working fluids would be required in different quantities for the same unit.

A refrigerant cylinder was connected to the access port with a valve via manifold gauges and hoses. A vacuum was pulled, cylinder opened and placed on a weighing scale such that liquid refrigerant was supplied. Manifold gauges were opened and closed at mass intervals as tabulated above. A point was reached when the cylinder pressure was equal to system pressure and no further transfer would occur. The cylinder was warmed with warm water to allow flow. This process raised the cylinder vapour pressure. CARE MUST BE TAKEN NOT TO EXCEED 48°C AS EXCESS VAPOUR FORMATION MAY EXPLODE THE CYLINDER.⁽⁶⁴⁾

Refrigerant recovery was done by pulling vacuum on empty cylinders and connecting them to the unit for drainage while placed in ice. This method was capable of recovering up to 80% of R-134a and almost 100% for R-245fa.

3.9. PARAMETERS FOR CONSIDERATION

Some of the parameters that were monitored included temperature and pressure at different points in the system as it was being operated.

3.8.1 Pressure

Initial pressure reading gauges were limited to 15 bar as shown in Figure 3.8 and could not be used on R-134a whose operating pressures were above 20 bar in the first 2 prototypes



Figure 3.8 Wika pressure gauges (max 15 bar)

thus were replaced by the high pressure refrigeration bourdon gauges limited to 80 bar as in Figure 3.9. The gauges were set to read the inlet and outlet of the scroll expander as well as the inlet and outlet of the working fluid circulation pump.

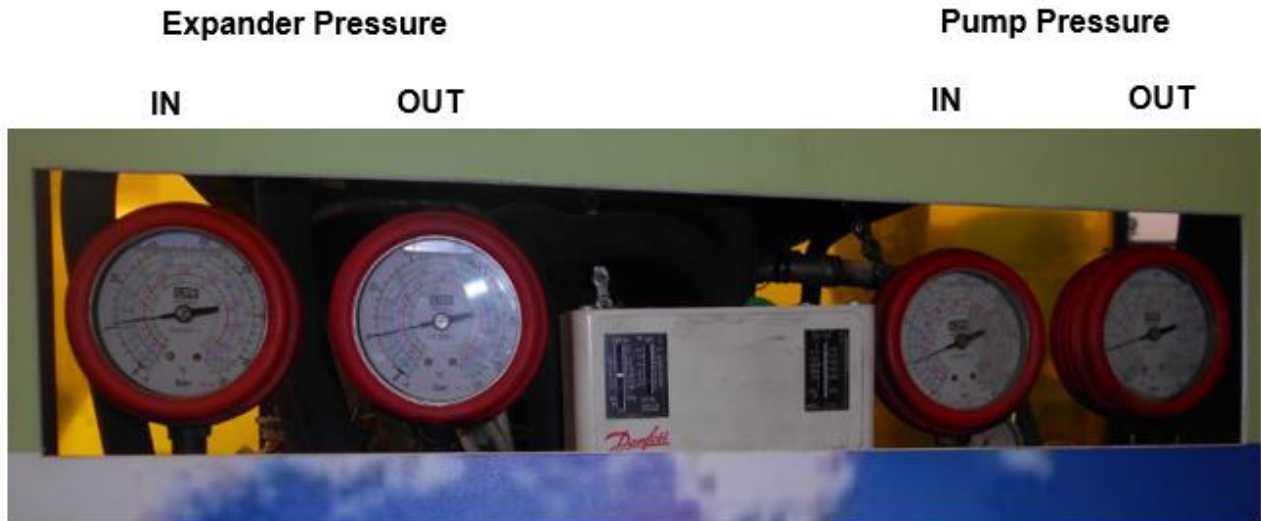


Figure 3.9 Bourdon pressure gauges

An electronic pressure transducer was placed in comparison with the bourdon gauges.

The areas to be monitored were at the entry and exit of the scroll expander, and entry and exit of the liquid circulating pump. (Figure 3.9)

In the first prototype setup, the unit showed significant pressure drop between expander outlet and pump inlet as much as 3 bar, as well as between pump outlet and expander inlet in the region of 5 bar. This suggested a high friction loss as a result of the length of piping. Moreover, most parts of the unit had steel pipes, which had higher friction factors in comparison with copper pipes.

Pipe dimensioning confirmed that bigger pipes reduced friction and pumping power, as expected. Also, bigger heat exchangers were more effective in heat transfer processes in spite of their cost. Despite the recommended pressure ratio across the expander being 3.5 to 1, the two set-ups had pressure ratios around 2 to 1.

3.8.2 Temperature

Temperature was monitored using K-type thermocouples whose one end was bonded to the pipes, and the other plugged to a TEMPpoint module as shown in Figure 3.10. Computer software Measurement Instruments Calibration Utility was used to calibrate the thermocouples with the help of a K-type thermometer, and Measurement Applications software read the temperatures at different positions.



Figure 3.10 TEMPpoint temperature module with K-type thermocouples

Pressure and temperature relations were used to plot the process on the P-h or T-s chart from which enthalpies could be read or calculated respectively. These values were interpreted as work input and output as well as the heat that was transferred to and from the fluid. Thermodynamic efficiencies were also analysed.

3.8.3 Working fluid flow rate

A flow meter was included in the circuit to read the volume flow rate which was translated to a mass flow rate with the knowledge of specific fluid conditions of temperature and pressure to determine density. The flow meter in Figure 3.11 shows a liquid flow rate of 2.44 litres per minute. It was noted that beyond certain limits of flow, pressure and scroll rotational speeds could not be increased with increasing flow rates. This established the optimum flow rate of the ORC unit to be 3.2 l/min for prototype 1 and 2.



Figure 3.11 Picture of a flow meter for working fluid

3.8.4. Shaft power

Two methods were used to measure shaft power. The first one employed an electric generator with the speed of 3600 revs/min. The second one used a dynamometer that measured mechanical shaft power.

Whilst using an electricity generator, a minimum speed of 1500 revs/min was required for it to switch to current supply. The highest scroll speed of 2200 revs/min was reached with prototype 2, an increase from the previous 1650 from the first prototype. Multimeters were used to measure current and voltage which was translated to power using the following equation:

$$\text{PWR} = V \times I \text{ [W]} \quad (3.18)$$

Where V is voltage and I is current.

Maximum voltage recorded from the high setup was 78 Volts, translating to 180 W power. The preceding setup produced a maximum of 142 Volts with an average of 120V. This translated to 320 W of power.

A dynamometer was set up and the results were calculated as shaft power using the following relationships:⁽⁶⁵⁾

$$PWR = T \omega \text{ [W]} \tag{3.19}$$

$$T = F \times r \text{ [Nm]} \tag{3.20}$$

$$\text{And } \omega = 2\pi \frac{\text{revs/min}}{60} \text{ radians.} \tag{3.21}$$

Where T was torque which was a product of force and pulley radius
 ω was the angular velocity in radians

Force was determined by use of a spring balance and brake rope, with a dead weight on the other side. The difference between spring balance reading and dead weight gave the applied force on the shaft. while reducing the speed of the expander. The effect was interpreted to shaft power output using the above formulation. Refer to Figure 3.12 for the plot of the power output. Whilst maintaining the feed pump flow rate, the expander was allowed to accelerate to a maximum rotational speed and a gradual increase in dead weight increased braking force.

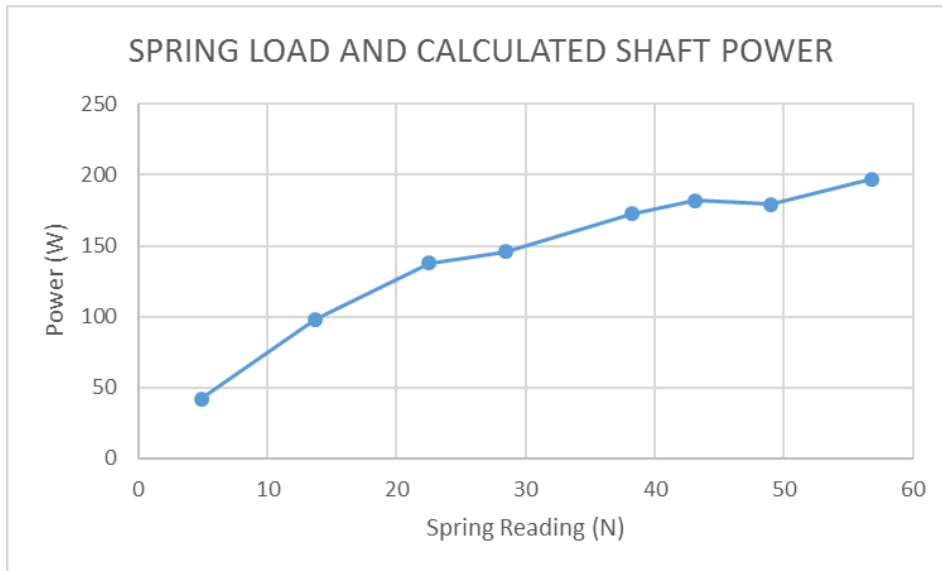


Figure 3.12 Shaft power for prototype 2

3.9. SUMMARY

In summary, the heat source power requirements were established to be 16 kW for the unit to produce 1 kW. The capacity of heat exchangers was found to be in the range of 15 kW.

Flow rates of cooling water and working fluid were established as well. the unit required not more than 4l/ min of working fluid while the condenser optimum coolant flow rate was about 23l/ min of tap water.

Power output for the first and second prototype was determined to be lower than the pump power intake.

CHAPTER 4

RESULTS AND DISCUSSIONS

4.1 INTRODUCTION

This chapter summarises the results obtained from the experiments and their impact on the remodelling of the new unit. The model was studied in two stages to compare the performances at different heights. A three-metre-high and a one-and-a-half-meter unit were tested and a comparison of results was made. Refer to Figure 3.7. Test areas included pressure differential, cooling water volumes, fluid circulation pump behaviour, evaporator and condenser temperatures, power input, and power output of the unit. Thermal efficiencies were also analysed and used for the design of the current prototype.

4.2 COMPARISON OF HEAT SOURCE AND EXPANDER INLET PRESSURE

Evaporator temperatures were varied at the source and the unit operated. It followed that the expander inlet pressure indicated higher limits with increased temperature, as well as lower with low evaporator temperatures. Boiler temperature was observed to have a direct impact on the achievable speed of the expander. It was observed that at low temperature the sight glass to and from the scroll expander revealed presence of liquid in the working fluid. This suggested that the fluid could well be below saturation conditions. This resulted in reduced power output and vulnerability of the scroll expander to damage. significantly. It was noted that the temperature of the working fluid was in many cases 15°C less than the heat source temperature referred to in the graph. The left hand part of the graph in Figure 4.1 shows saturated liquid whose pressure did not significantly change with a change in temperature. The right hand part illustrates a highly superheated vapour, whose increase in temperature did not change the pressure

These results suggested that the fluid was not superheated as required to a point around 18 bar on the graph indicating a temperature of 80°C. Increasing beyond 80°C, no evidence of liquid was detected in sight glasses, indicating that the fluid was superheated. It is desired of the expander that the exiting vapour should be slightly superheated to eliminate chances

of droplets forming in the expander. It was noted from the results that, at some higher temperature range, the pressure did not have a significant change. This compared with the fluid properties, *Appendices 1 to 5*, in regions of high superheat such that the properties did not change significantly with increasing temperatures. Operating the ORC unit with R-134a at heat source temperatures beyond 100°C did not contribute substantially to power output or pressure differential. Better unit performance occurred at temperatures within 80 and 100°C.

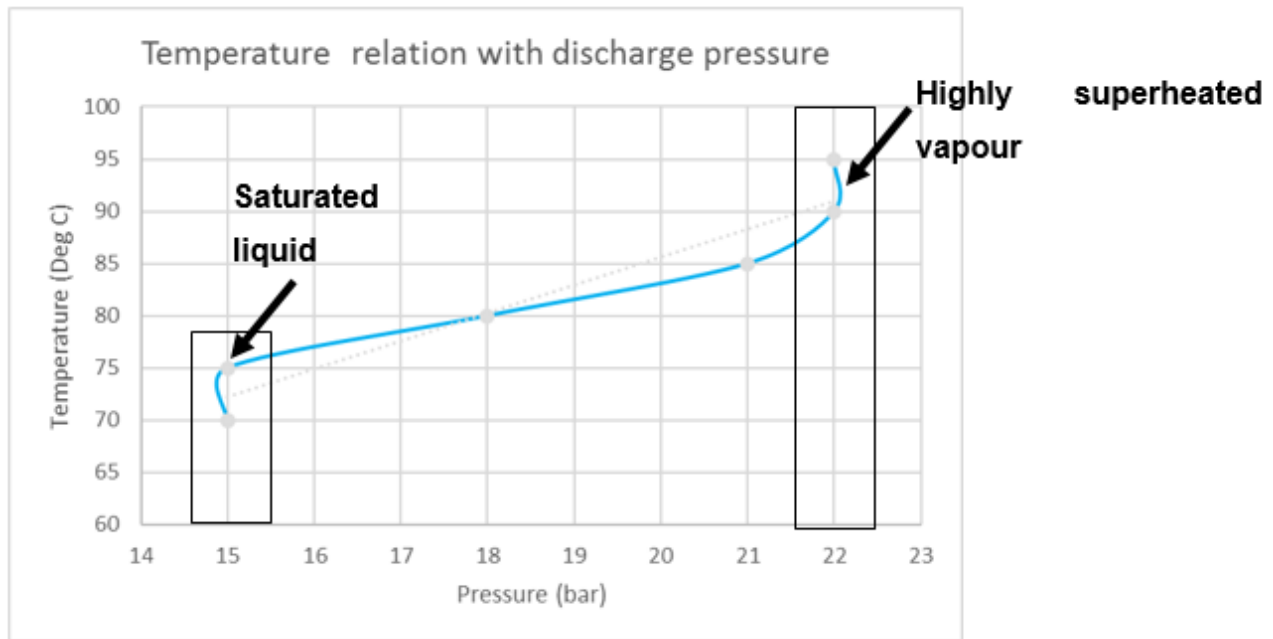


Figure 4.1 Pressure temperature relationship for prototype 2

4.3 COMPARISON OF PUMP AND SCROLL SPEEDS

Increased pump speed automatically increased the flow rate of the working fluid. An optimum flow rate was reached at about 3.5 litres per minute, at which the scroll expander reached the highest speed of 2200 revs/min. Figure 4.2 illustrates the comparison between pump and scroll speed. As was observed, the scroll speed was dependent on pump speed, which related to fluid flow. However, the expander speed reduced at flow rates beyond 3.5l/min.

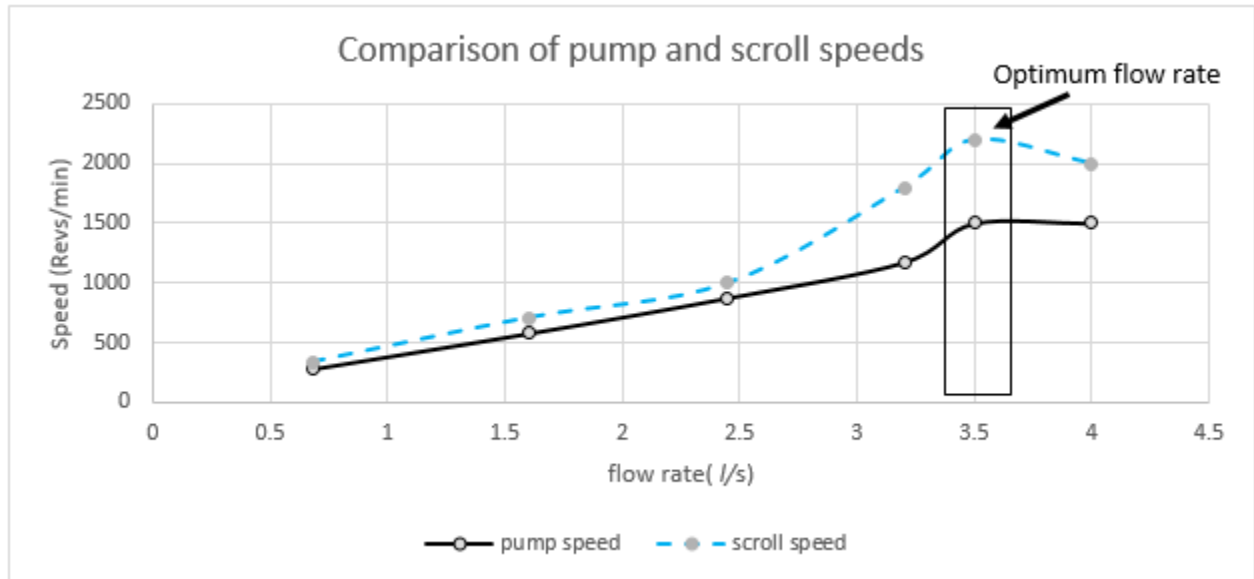


Figure 4.2 Comparison of pump and scroll speeds of prototype 2

Optimum flow rate was determined and used as a basis for fluid pump design as indicated in Figure 4.2. At 4 litres per minute, the fluid arriving at the scroll was very wet, suggesting that it did not collect much heat from the evaporator. This was a possible reason for decline in performance as this trend kept repeating in subsequent tests. This might also be the reason any increase in pump speed did not increase the efficiency of the unit.

From the above observations, improved results were expected with slightly bigger heat exchangers and 15 kW heat exchangers were proposed. It was found that the nearest on the range were 20 kW heat exchangers.

4.4 FEED PUMP BEHAVIOUR

It was noted that pump work was significant in the cycle such that the power output was in some cases less than the input. Simulations showed insignificant energy demand by the fluid across the pump. A study was done on pump behaviour with a full charge of working fluid and without working fluid.

Results indicated that the difference of power consumption between the two was consistently small through a set of speeds. Refer to Figure 4.3.

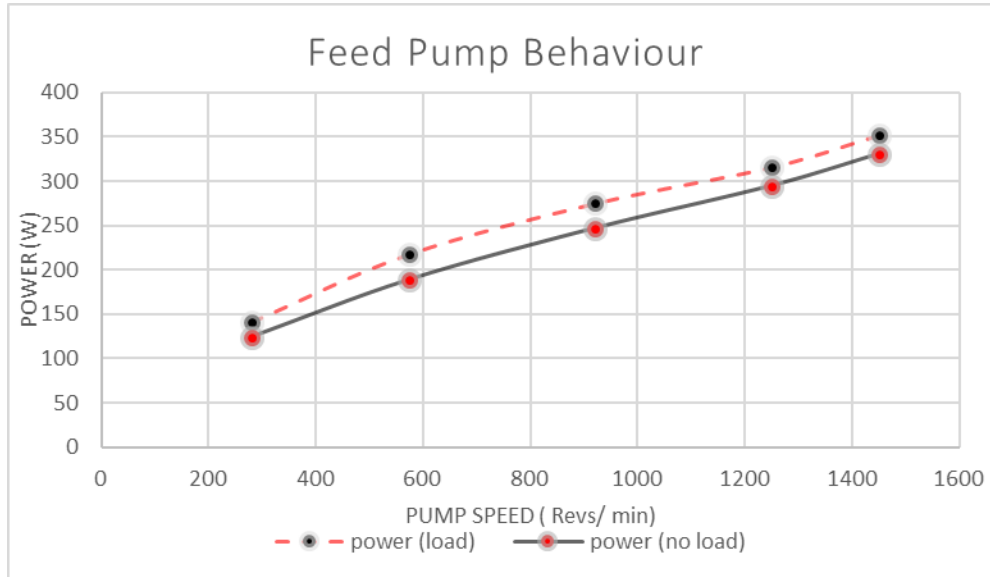


Figure 4.3 Feed pump power with and without load


This agreed with Genetron simulation results that did not take into account power demands of the motor or the pump, but of the fluid alone as observed in Table 4.1. The results are also consistent with the thermodynamic property results plotted on NIST charts in this report.

Again it was observed that a constant power demand by the working fluid was maintained across a set of pump speeds. This raised the question if flow rates did not have significant effect on the power consumption of the fluid in a given setup of the unit. It also suggested that the pump performance curves be understood before deciding on the pump to employ, as most of the input energy was spent on driving pump rather than working fluid.

Table 4.1 Genetron Simulation results

Performance Parameters					
Refrigerant	R134A		Thermal Eff.	-	0.0598
GWP	1300		Turb. Exit Quality	-	1
Mass Flow	kg/s	0.06763	Turb. Exit Superheat	°C	52.73
Boiler Heat Input	W	16500	Boiler Temp.	°C	50.49
Turbine Output	W	990.11	Condensation Temp.	°C	25
Heat Rejection Cond.	kW	15.56	Pump Power	kW	0.05

Typical fluid power demand for a 1kW unit



4.5 THERMODYNAMIC PERFORMANCE OF PROTOTYPE 1 AND 2

Two cycles, one over 3 metres high and the other about half the height, were examined. The pressure patterns on the continuous cycle points 2 - 3 and 4 -1, in Figure 4.4, showed a reduction across pipes, indicative of frictional factors. The shorter construction with dotted lines in the same Figure 4.4 had comparisons B to C and D to A, which did not show a pressure differential at a precision of 0.1bar on the gauges. The shorter unit had more restrictions removed by setting the evaporator and condenser tubing in 3 parallel passes. Shorter routes were achieved which reduced the friction losses. Pipe diameters remained the same.

Despite operating at lower pressure of 16 bar, the second unit had an increased power output of 320 W compared with 180 W for the first and achieved a higher scroll speed.

Both units had an unexpected behaviour of gradually increasing the suction as well as discharge pressure when running, as opposed to the expected decrease of suction and increase of discharge pressures. This phenomenon was not readily understood.

It must be mentioned that the second unit was built primarily to find out if cavitation would be a setback in the final design, and if the pipe characteristics could affect pressure loss. Hence it was built with mostly recycled material from parent prototype for the purpose of cost reduction.

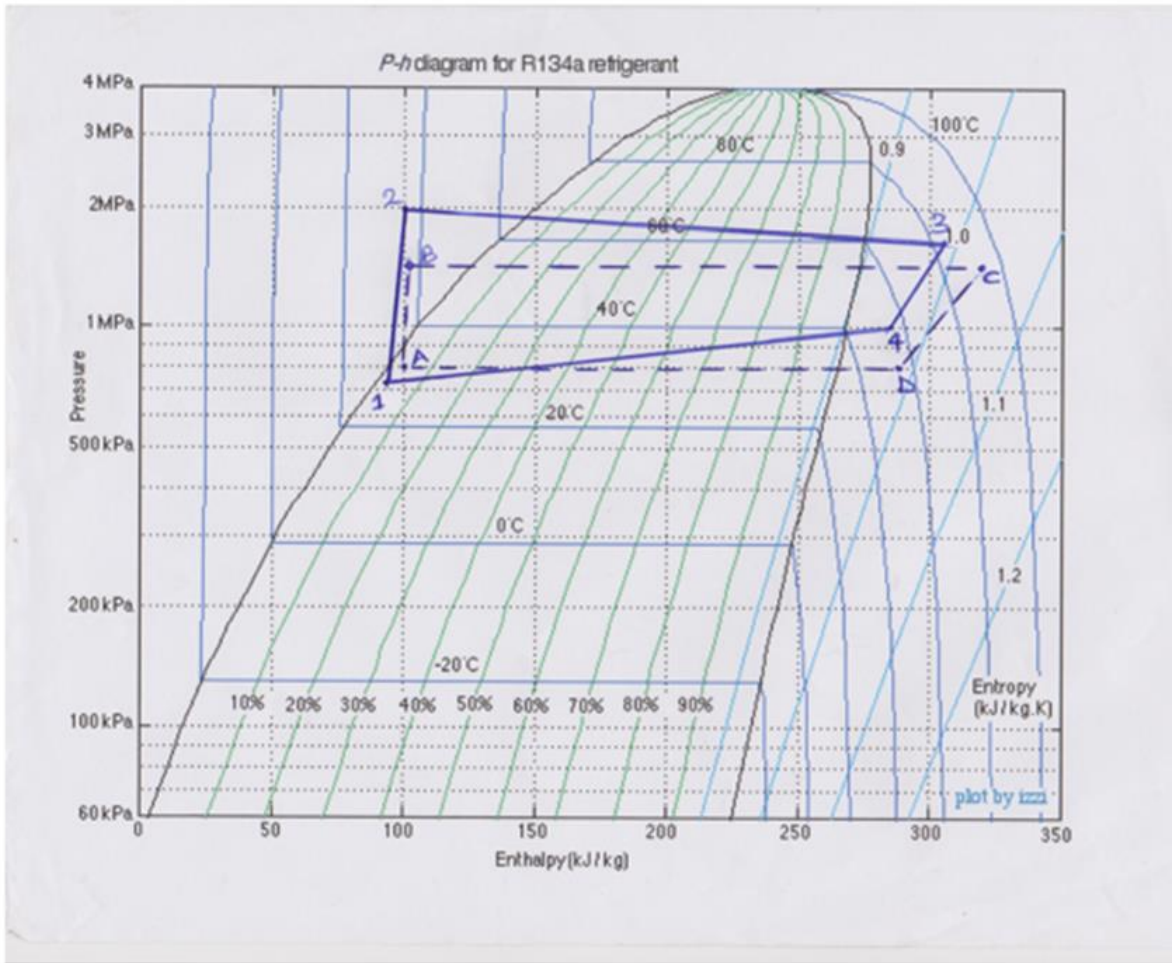


Figure 4.4 P-h diagram showing cycle 1 and 2

Figure 4.4 shows two notable results from the two set ups. Firstly, pressure losses were tremendously reduced in the system. Secondly, a small pressure differential yielded more power output at the scroll, the horizontal scale connecting C and D, compared to that connecting 3 and 4 on the enthalpy scale.

With regards to cavitation as discussed in section 3.5, both units behaved the same in response to flow rate of cooling fluid from the tap. Increased flow rate saw improved pump performance. Sight glasses reported similar expectations. It was thus concluded that the dryness factor of the fluid had a bearing on the pump performance, hence the working fluid had to be of zero (0) dryness factor. To be sure of this, a slight sub cooling had to be made in ranges not exceeding 5°C, by use of more efficient heat exchangers. Limiting factors were the cost of large heat exchangers and the lowest temperature achievable which was the ambient temperature.

4.6 SUMMARY OF PROTOTYPE 1 AND 2

From the experimental results, the first two prototypes were summarised as follows:

- Despite the high flow rates, the units could not produce more power output due to a limited pressure differential.
- Higher flow rates were achieved by running pump at high speeds, which resulted in high power input to the pump yet with low power output from the expander.
- Pump power demand was determined by the speed at which the pump was operated, more than any other factor.
- Poor evaporation resulted in reduced pressure differential and liquid flowing into the expander.
- Suction pressures had a tendency of increasing with running time thereby narrowing the pressure ratio and pushing the discharge pressure up.

The properties of refrigerants used can be found in *Appendices 1 to 5*.

4.7 FINAL PROTOTYPE

This section will discuss the experimental results of the final prototype shown in Figure 4.5, having been tested with both R-134a and R-245fa. The first part of this discussion will base on R-134a as a working fluid.

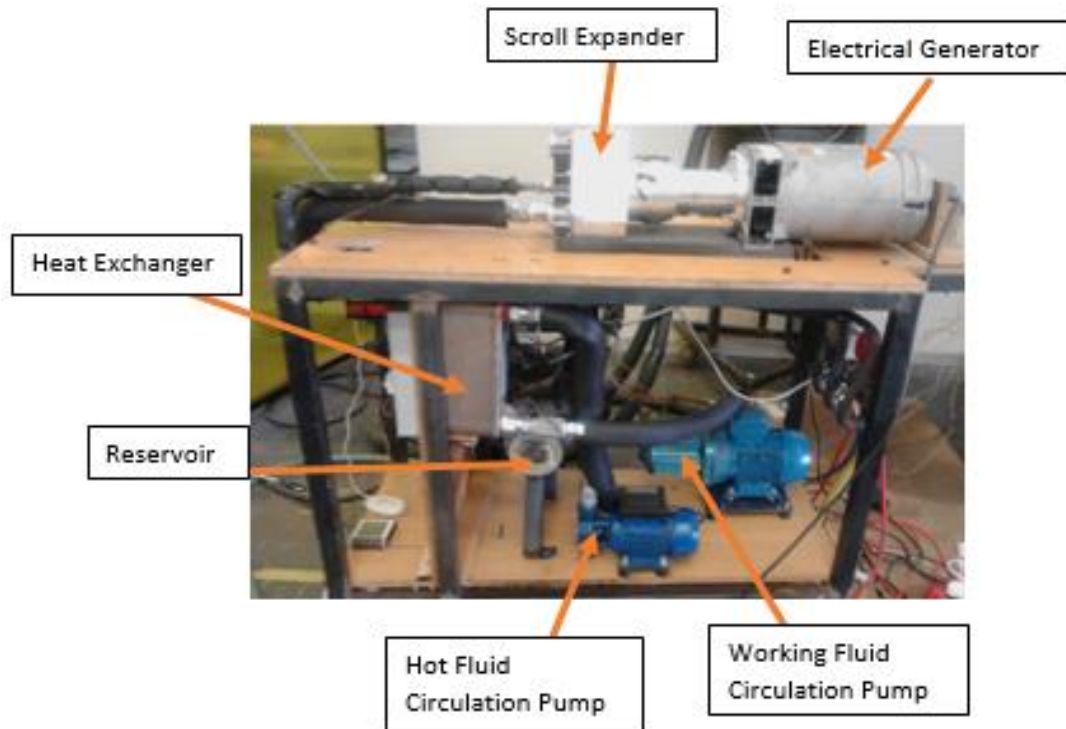


Figure 4.5 The final prototype

Comparisons of results with previous prototypes are also presented in areas of thermodynamic performances, mechanical power and electrical power. Scroll and pump speeds will also be discussed.

The speed of the feed pump was varied by a controller scaled 0 to 50 Hz., linearly representing 0 -1500 revs/min synchronous speed. This had a direct flow rate proportion ranging from 0 to about 4 litres per minute.

The specifications of the main components that form this prototype are presented in the Table 4.2. Note that a few other auxiliary components that make up this prototype have not been included in the table. These include the variable speed drive for the feed pump motor, the flow meters, pipes, unidirectional valves, flow control solenoid valves and pressure gauges.

Table 4.2 Specifications of main components

Component	Operating parameters	
Scroll expander	Pressure	13.8 bar
	Speed	3600 Revs/min
	Working fluid	R-134a and R-245fa
	Inlet temperature	175 °C
Plunger pump	Fluid condition	Liquid
	Flow	4 litres per minute
	Pressure	140 bar
	Max speed	3450 Revs/min
Heat exchangers	Heat load	15 kW
	Number of plates	28
	Heat transfer coefficient	511W/ m ² °C

4.7.1 Tests with R-134a

4.7.1.1 Thermal Efficiency

Thermodynamic performance of three cycles was compared in a P-h (Mourrier) chart for R-134a in Figure 4.6. The plot areas were obtained from the pressure reading and k- type thermocouple readings through a Data Acquisition module. Results were displayed as in Figure 4.7. All the three cycles operated under sub-critical conditions.

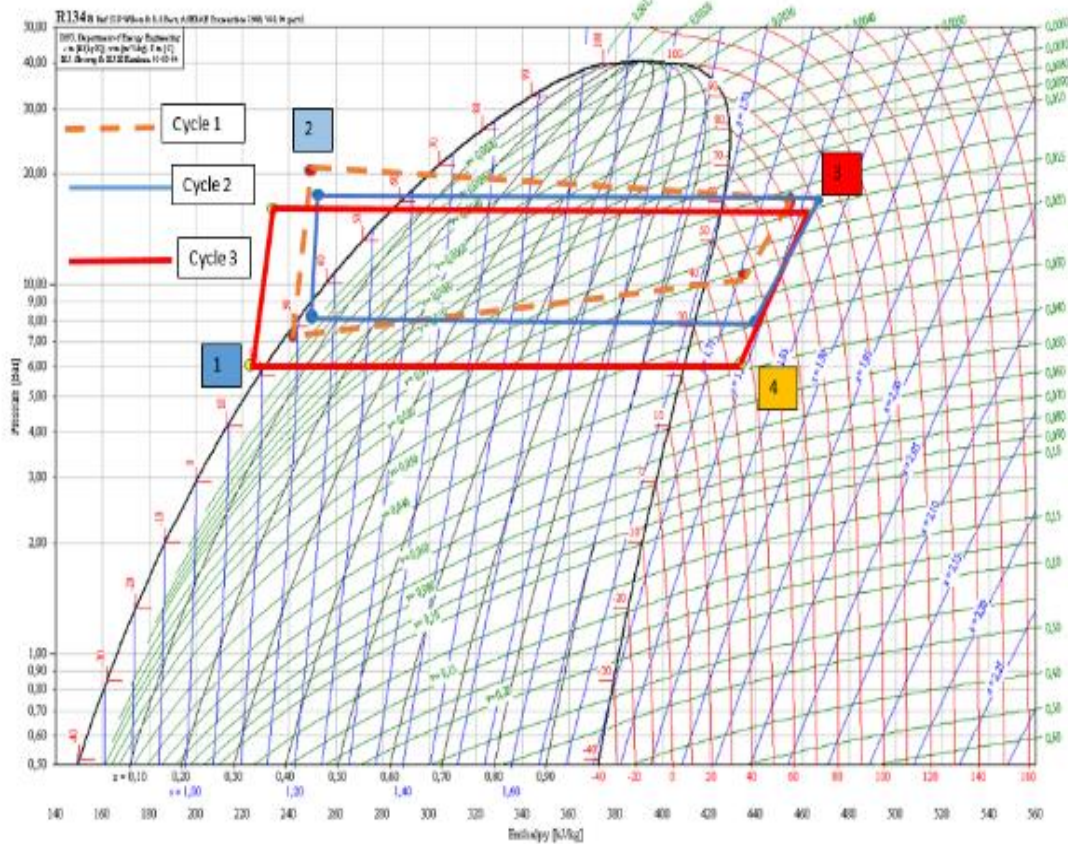


Figure 4.6 Thermodynamic performance of 3 prototypes tested with R-134a

TEMPpoint results were used to assist in plotting the cycles in Figure 4.6. The channels shown in Figure 4.7 with a temperature reading were a display of different positions in the cycle as read by thermocouples. For example, channel 10 which reads 47.53°C Figure 4.7) is the expander outlet temperature, while channel 21 shows an expander inlet temperature of 95.58°C. Observations on the P-h chart suggested that increasing the inlet temperature while maintaining the pressure could result in increased scroll thermodynamic power as Δh_{3-4} increased.

A summary of the results of thermodynamic performance from the plots in Figure 4.6 is presented in Table 4.3 The third cycle displayed a lower expander inlet pressure limit closing in to the recommended inlet pressure of 13 bar compared with the first two, which could

start at a pressure of 20 bar and gradually rise to as high as 23 bar. In the previous two setups it was also noted that the suction pressure was higher than expected under particular conditions and was increasing with running time. This caused a rise in condensation temperatures resulting in reducing performance. Later it was discovered that the expander exit port had a 12.5 mm union which was smaller than the required 25 mm outlet union. This meant that for every cycle there was residual pressure remaining which was gradually accumulating consequently reducing the pressure ratio. This might have contributed to low power output as it resulted in lowered expander speed.

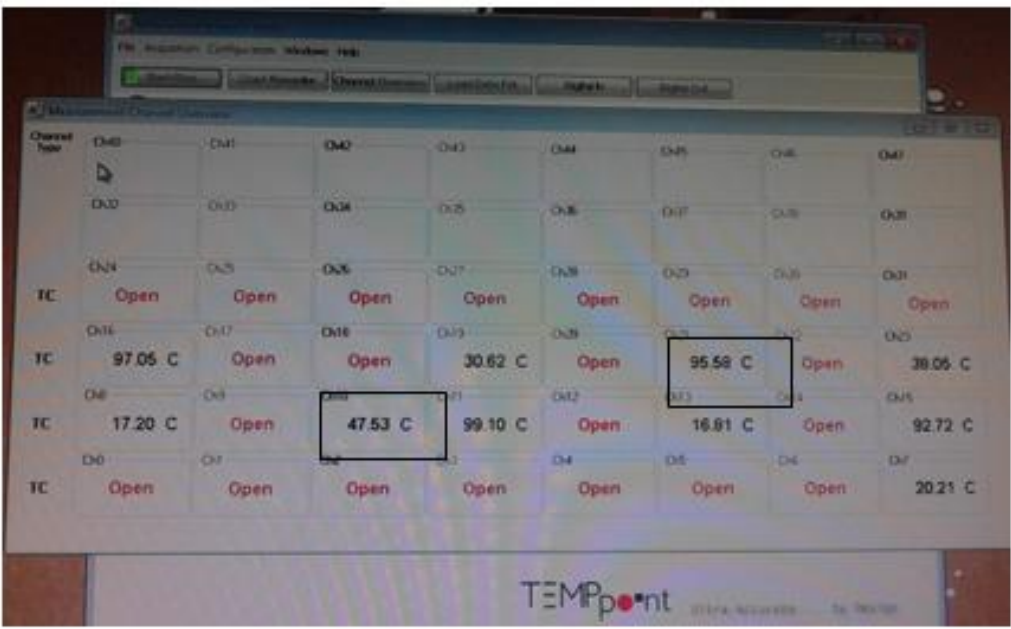


Figure 4.7 Temperature conditions at different positions in the cycle

A 25 mm fitting cleared the restriction and solved the problem resulting in low and maintained suction pressures as long as condensation was available. Also, to maintain required pressure ratio, a turbine inlet of 12 mm pipe diameter and an outlet of 35 mm were derived.

Table 4.3 Thermodynamic performance data for prototype 1,2 and3 (R-134a)

PARAMETERS	PROTOTYPE 1	PROTOTYPE 2	PROTOTYPE 3	UNITS
Volume flow (vf)	2	2	2	[l/min]
Mass flow	0.046	0.046	0.046	[kg/s]
Work in, pump	0.455	0.471	0.459	[kW]
Heat in, evaporator	9.555	10.238	10.465	[kW]
Work out, turbine	1.229	1.684	1.365	[kW]
Heat out, condenser	-8.782	-8.645	-9.555	[kW]
Thermal efficiency	0.081	0.156	0.087	
Carnot thermal efficiency	0.162	0.159	0.182	

As observed in the charts in Figure 4.6, the suction pressure of the third cycle was much lower, at 6 bar, giving sufficient pressure differential. The low pressure corresponded with the expected pressure at ambient temperature conditions of the fluid in use. The suction conditions remained unchanged as long as condensation was supplied, maintaining steady performance.

However, the results from Table 4.3 showed that prototype 2 had the highest turbine thermal work output followed by prototype 3 whilst prototype 1 had least power output with more frictional losses as evident by pressure drop. Some of the energy may have been used to overcome friction losses.

The 3rd prototype had more heat transfer to evaporator and from condenser suggesting that the heat exchangers were more efficient than those used in the first two prototypes. This was the only prototype with sub-cooling.

The second prototype had a higher thermal efficiency which was a result of operating at much higher pressure. This was in contrast with the electrical and mechanical power outputs of the prototypes. Carnot efficiency was observed to be greatest in prototype 3 possibly because the unit was able to operate at much lower temperatures on the suction side.

All units were compared at a flow rate of 2l/min but at different times of the year which had effect on the ambient conditions therefore the lowest possible operating temperature.

The method of analysing thermal power helped in deciding the component thermal capacities but could not be reliable in predicting the system mechanical and electrical power output in this research.

4.7.1.2 Mechanical, thermodynamic and electrical power

Shaft power was determined by making use of a setup as shown in Figure 4.8. In the arrangement, prototype 2 and 3 were compared while running on R-134a. The shaft power outputs in Figure 4.9 were compared with the thermodynamic power in Table 4.3. Prototype 2 gave 1.68 kW thermodynamic power while giving 182 W of shaft power, representing a difference of over 900%. Prototype 3 gave 1.365 kW of thermal power against 693 W of shaft power, representing a 196% difference. Refer to Table 4.4.

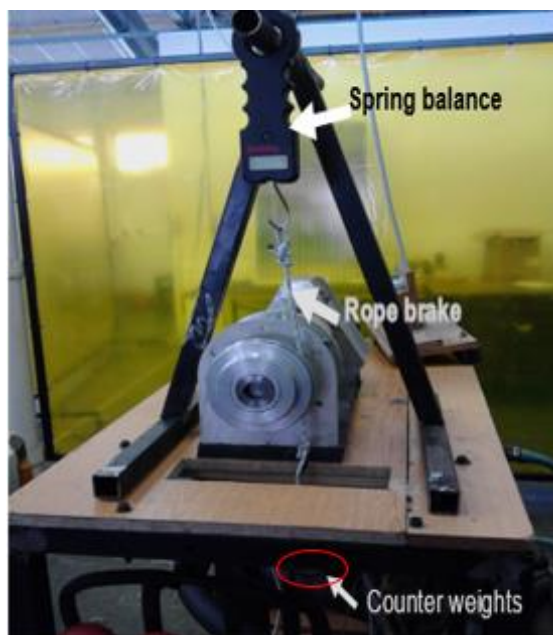


Figure 4.8 Apparatus for measuring shaft power

A further investigation was required to determine the correct interpretation, hence a comparison with electrical power.

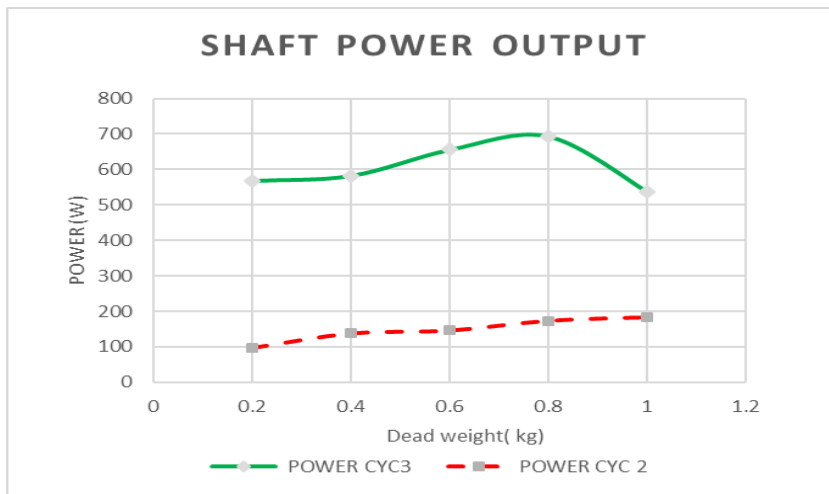


Figure 4.9 Comparison of shaft power - prototype 2 and 3 (R-134a)

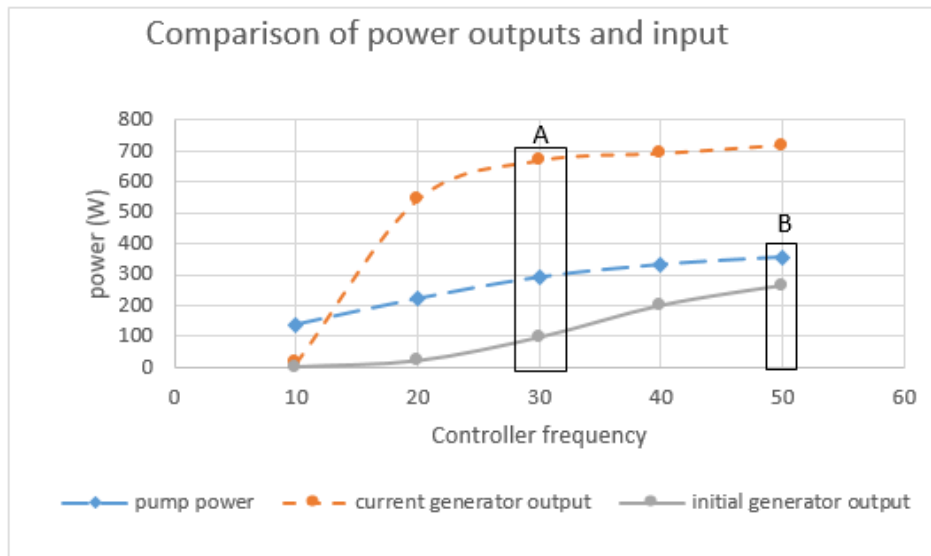


Figure 4.10 Electrical power input and output (R-134a).

Electrical power was compared for the two prototypes running on R-134a. Results are shown in Figure 4.10. Regions of optimal performance for both units are indicated A for prototype 3 and B for prototype 2 in the figure. Prototype 2 produced less than pump intake

while prototype 3 produced more. A comparison with shaft power showed a close relationship, unlike thermal performance, refer to Table 4.4. Therefore, it was suggested that thermodynamic efficiencies would not be a reliable way of suggesting unit performance in the case of this research. A comparison of all power outputs and inputs is presented in Table 4.4

Table 4.4 Expander power outputs and pump power inputs (R-134a)

SET UP	POWER (W)			
	THERMAL	SHAFT	ELECTRICAL	PUMP
1	1229	-	180	-350
2	1684	182	320	-350
3	1365	693	717	-280

4.7.1.3 Turbine speed

Figure 4.11 shows a comparison of generator power output and speed in relation to fluid flow rate. The engine displayed that flow rates about 2 litres per minute were optimum for system efficiency. At this flow rate, the working fluid effectively vaporised giving optimum power and highest rotational speeds. It was noticed that beyond this flow rate the sight glass at the inlet to turbine indicated passage of liquid/ vapour mixture instead of superheated vapour. This resulted in a drop in turbine inlet pressure, reducing the pressure differential which consequently resulted in a drop in speed and power.

The rated inlet-outlet pressure ratio for the expander was 3.5 to 1 in order to give an optimum power output. The best ratio that R-134a could provide was 3 to 1 since the recommended expander inlet pressure, by supplier Air Squared, was 14 bar and ambient pressures were about 5 bar. Operating at 16 bar gave the required pressure ratio. The first and second prototypes saw an increase in both suction and discharge pressure and could run at inlet

conditions higher than 22 bar when the exit pressures were 10 bar. The consequence was developing a lower pressure ratio, hence less rotational speed and less power.

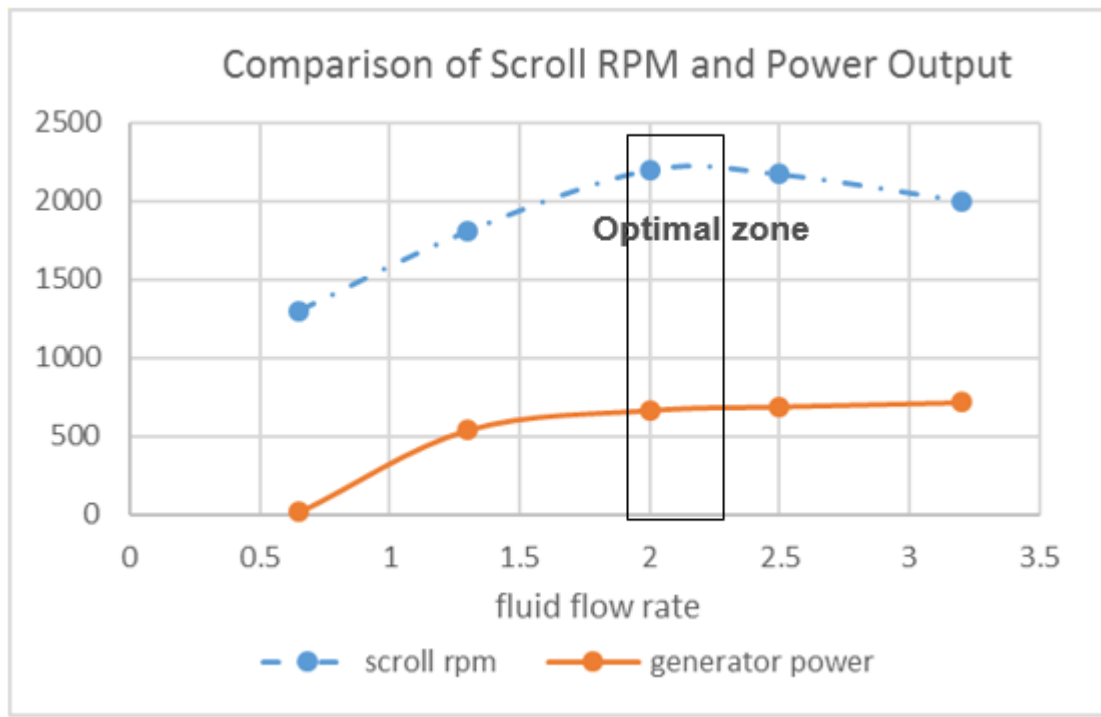


Figure 4.11 Power output and generator rotational speed (R-134a)

The new prototype had eliminated the rise of low pressure by increasing the expansion volume at the exit of the expander.

4.7.1.4 Relationship of pumping speed with scroll rotational speed

It was observed earlier in section 4.7.1.3 that the expander speed did not depend entirely on the flow rate. A comparison with the pump speed showed that increasing the pump speed did not necessarily increase the scroll speed even though it increased the flow rate as shown in Figure 4.12. More fluid flow reduced the performance of the expander.

This particular setup showed that a controller frequency of 30Hz which translated to 865 revs/ min for pump speed and 2200 revs/ min for expander, was optimal for the operation of the scroll expander as it gave the maximum speed and optimum power

(comparison with graph in Figure 4.11). Figure 4.12 shows that increasing pump speed increased the demand for power by the pump. This suggested that being able to run the pump at low speeds could increase system efficiency if optimum power was obtained.

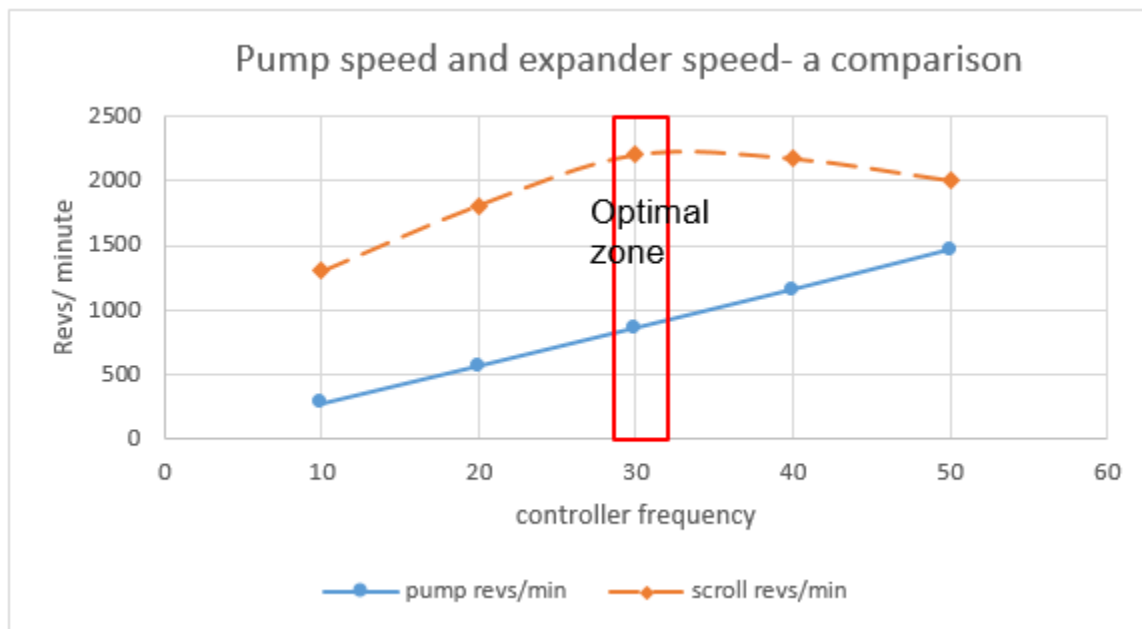


Figure 4.12 A comparison of pump and expander speeds (R-134a)

4.7.1.5 Effect of pressure differential

Section 4.7.1.3 suggested that a lapse in turbine performance with increased flow rate was linked to a reduction in pressure differential. Figure 4.13 shows the relationship between pump speed and pressure differential. The optimal zone was at 10.5 bar at which point the pumped fluid was able to evaporate and superheat sufficiently hence expanding adequately.

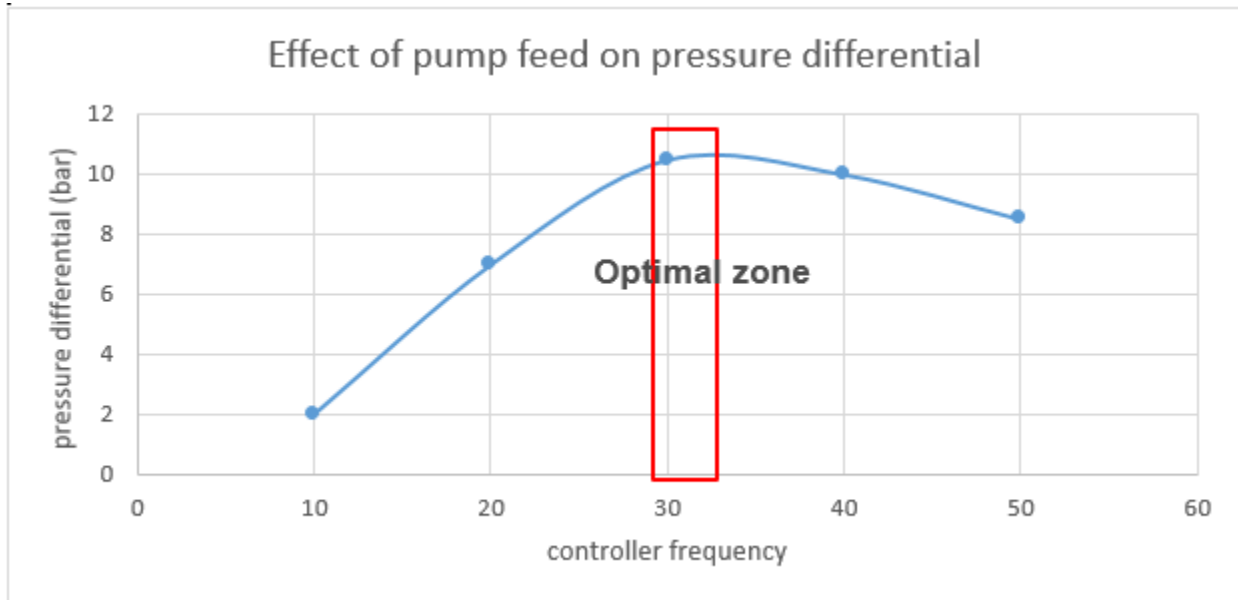


Figure 4.13 Effect of fluid feed on pressure differential (R-134a)

A gradual increase in pump speed revealed an increase in pressure and eventually a decrease, which narrowed the turbine pressure differential. The fluid flowed faster past the evaporator at high feeds, collecting less heat and leaving in a mixture phase. This resulted in the fluid not expanding sufficiently and less power output resulted.

4.7.2 Tests with R-245fa

As was suggested in the earlier section, R-245fa was charged into the system once it was assured that there were no leakages in the system and tests with R-134a had been concluded. The fluid was tested against two conditions. First it was tested under temperature ranges for R-134a test conditions of 100°C, then under raised conditions of 130°C which are a recommendation for R-245fa ⁽¹⁶⁾.

4.7.2.1 Pressure differential (R-245fa)

Figure 4.14 shows that increasing temperature also increased the pressure differential by increasing the upper limit pressure and maintaining the low pressure with a constant supply of condensing fluid. Performance was compared as labelled in working zones L for low

temperature and H for high temperature in the graph in Figure 4.14 and results are discussed in the following sections.

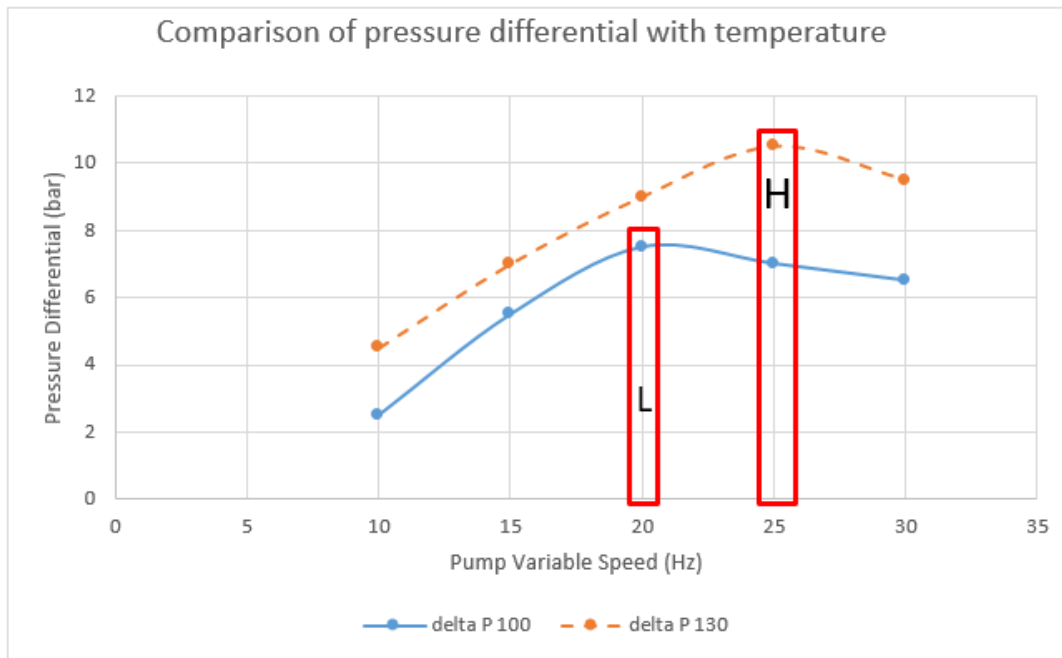


Figure 4.14 Pressure differential pattern with varying temperatures (R-245fa)

Increased evaporator temperature had a direct impact on the power output of the turbine as it was dependent on pressure differential. Zone H in the graph in Figure 4.14 shows that at high temperatures the pressure differential was greater and the pump could be run faster whilst maintaining sufficient evaporator performance. This suggested that the pump could be run at half speed and produce a differential about 11 bar. It was noted that at lower temperature increased flow rate resulted in reduced vaporisation and flooding of the turbine. It is evident in zone L in the graph that at 100°C the maximum pressure differential was 7.5 bar with 2/5 of the pump speed. Increasing pump speed beyond these limits had an effect of reducing power output as the evaporator was not able to evaporate most of the fluid.

4.7.2.2 Effect of temperature on scroll rotational speed

Under the same load, the scroll expander maintained an increase in speed which corresponded to an increase in power output under conditions of increased temperature, as presented in Figure 4.15. The scroll conditions were measured with a load attached to the expander, in this case a generator.

It was noted that at lower temperatures of 100°C the scroll expander rotational speed reduced increasingly compared to higher temperature conditions of 130°C.

Comparison of results in Figure 4.15 shows that optimal flow rate of 1.72l/min was required at low temperature to produce a maximum turbine speed of 2200 revs/ min while 2.3l/min produced 2570 rpm of turbine speed with load.

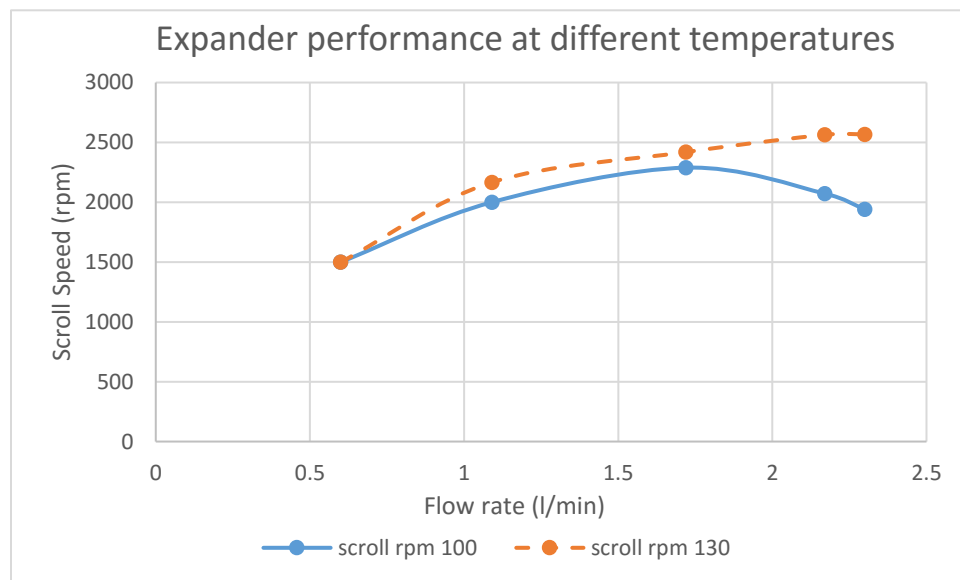


Figure 4.15 Variation in speed patterns with temperature (R-245fa)

4.7.2.3 Effect of temperature difference on power output

In Figure 4.16, a comparison of power output under different temperature conditions is shown. At lower temperatures the working fluid power output declined at lower pump speeds as compared to that at higher temperatures. For instance, the power curve started declining

at just about 20 Hz for lower temperature after reaching a maximum of 435 W, and at about 30 Hz and a power output of 650 W for the higher temperature conditions. This suggested that at lower temperature the evaporators could only transfer enough heat for lower flow rates resulting in less power. Sight glass observation showed that liquid refrigerant started entering the expander at the decline conditions, (Figure 4.10 - Figure 4.17) suggesting insufficient evaporation.

Comparison of R-245fa and R-134a revealed a slow reaction to input parameters for the former and a quick response for R-134a. As such it took a while to reach steady conditions with R-245fa. At higher temperatures, R-245fa reached higher limits of power output compared to R-134a. Also, at no load, R-245fa operated the expander to speeds as high as 8000 revs/min, compared to 4000 revs/min reached by R-134a. A considerable reduction in rotational speed occurred with R-245fa to ranges below 2600 revs/min while with R-134a the speed dropped to about 2600 revs/min. This observation suggested that R-134a had a steady power output in comparison with the other fluid.

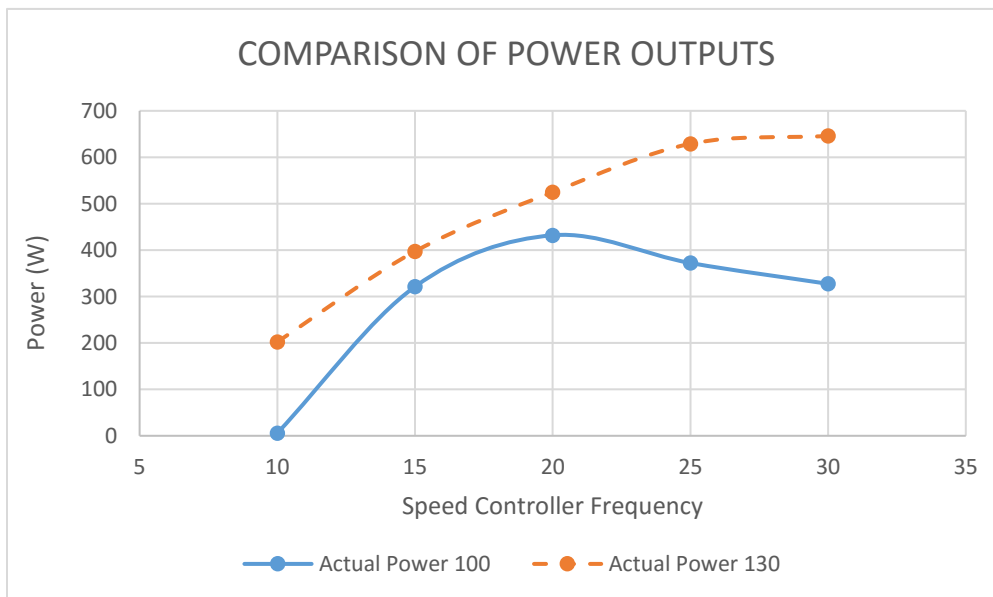


Figure 4.16 Power output curves at different temperatures. (R-245fa)

The reason R-245fa reached high speeds is the great pressure differential achieved during operation which exceeded ratios of 1:10. The most pressure differential reached by R-134a

was 1:3. Figure 4.17 shows a comparison of power output of the two working fluids, each one at its best temperature range. It was noted in the Figure that R-245fa gave the optimum power output of 740 W with the pump consumption of 250 W at 25 Hz which represented half the speed of the feed pump. Running pump at low speeds reduced the power consumption of the unit.

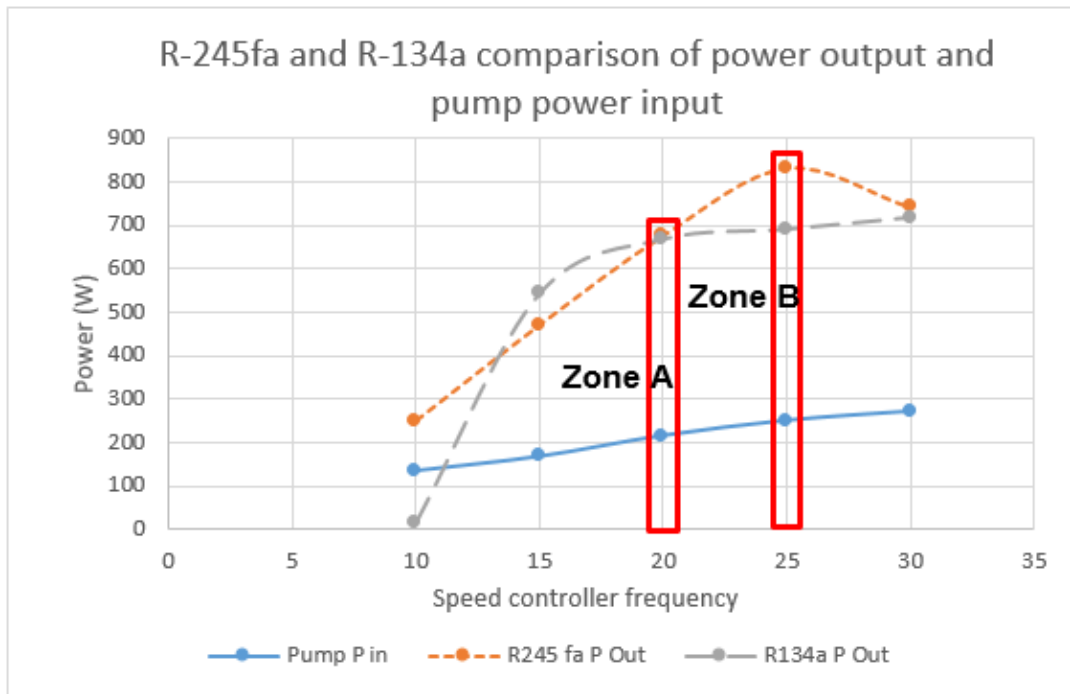


Figure 4.17 A comparison of power outputs (R-245fa)

R-134a was run optimally at 20 Hz and pump power of 215W which produced 667W.

Figure 4.18 shows a comparison of pressure differential with the flow rate for R-245fa. It was observed that the difference increased sharply to a maximum at pump speed of 25 Hz corresponding to pressure differential of 12.5 bar (Point A) and a flow rate of 2l/ min (Point B), beyond which the pressure differential declined.

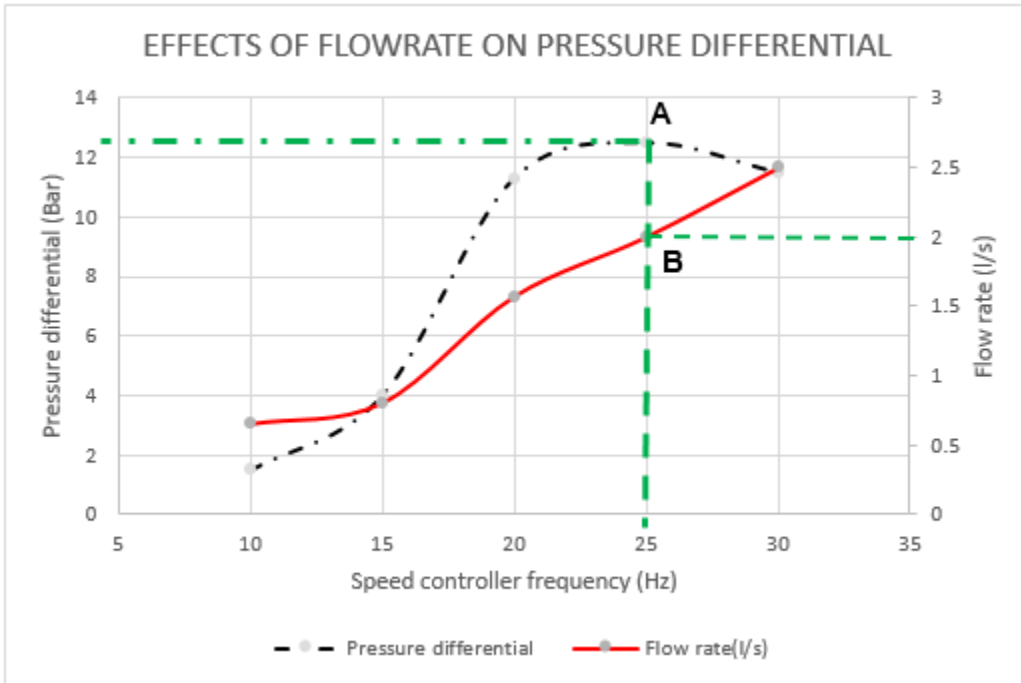


Figure 4.18 Effect of flow rate on pressure differential. (R-245fa)

Pressure differential, therefore, had a direct impact on performance, just as was observed with R-134a. It was noted that with sufficient condensation conditions, the minimum condenser pressure was 6 bar for R-134a and 1 bar for R-245fa while the recommended inlet pressure was 14 bar. The unit could be run to 16 bar.

4.7.2.4. Shaft power

A rope brake dynamometer was set up to measure shaft power as shown in Figure 4.19. Shaft power for R-245fa was compared at different flow rates. At much lower flow rates it was noted that the shaft simply stopped when dead weight was increased. When flow was increased, it still produced an increasing power output for increased dead loads. However, further increases in dead weight reduced the speed of the output shaft until it stopped and the magnetic coupling slipped. As shown in Figure 4.19, it was not possible to measure shaft power with more dead weights at 25 Hz as it had exceeded the capacity of the dynamometer which resulted in burning the rope or an instant slip at the magnetic coupling

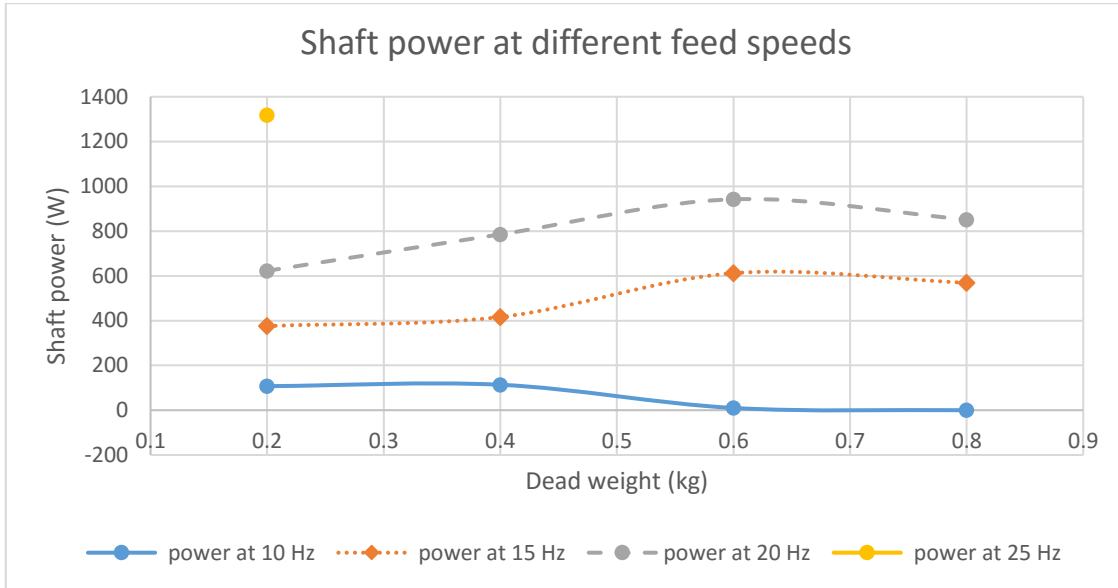


Figure 4.19 Shaft power output at different weights and flowrates (R-245fa)

It can be ascertained that the highest shaft power output was achieved by R-245fa which produced a value of 1.3 kW at 25 Hz and 942 W at 20Hz, both at 130°C.

4.7.2.5 Thermal efficiency

Lastly, a thermodynamic efficiency for R-245fa was investigated at temperatures of 100°C and 130°C. Thermal efficiencies were compared with those of R-134a. The P-h chart in Figure 4.20 was used to plot the cycles. The low temperature cycle showed less power output compared with the high temperature cycle. This was expected since increasing temperature increased thermal efficiency ⁽⁶⁶⁾ and performance of the cycle ⁽⁶⁷⁾. Table 4.5 shows a summary of results as obtained from the Mourrier Chart in Figure 4.20. The work output from a high temperature cycle was significantly high, deducing that the cycle was capable of producing more power than the low temperature one. As suggested earlier on, the low temperature cycle was observed to flood liquid into the expander. It is evident on the chart as the expander conditions are very close to the vapour saturation line and exit conditions are inside the vapour/ liquid mixture. This condition did not only reduce power output, but also would damage the expander internal components.

The high temperature cycle had a comparatively high power output - about 25% more than the low temperature one, and 6.4 % thermal efficiency. Refer to Table 4.5. Both situations gave thermal power output from turbine, which was much higher than that produced by R-134a, being 1.182 KW. This represented performance of 130% for similar temperature ranges and 188% for R-245fa at higher temperature. Refer to *Appendix 6* for Genetron simulation results.

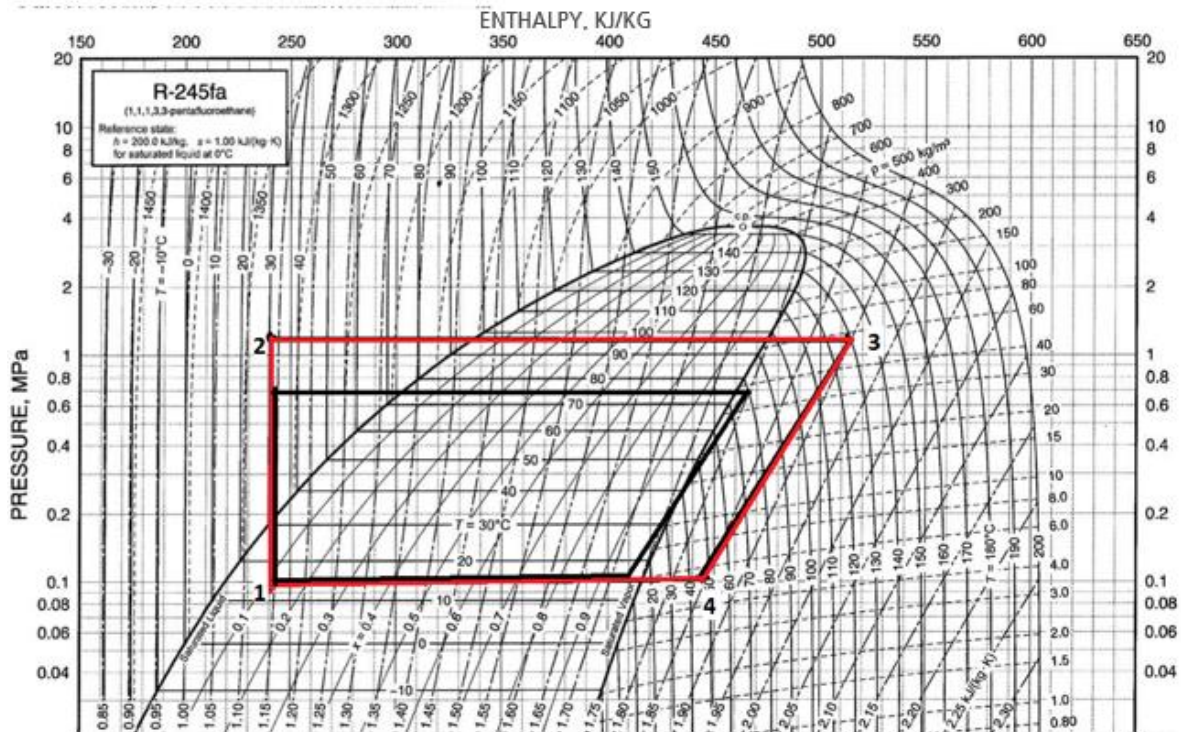


Figure 4.20 P-h diagram for R 245fa

Genetron simulation for the two working fluids predicted similar results in their proportions. However, other power output indicators did not agree with thermal power outputs as they were lower than the thermal power outputs.

Table 4.5 Thermal performance of low and high temperature cycles on R-245fa

PARAMETERS	TEMPERATURE		UNITS
	LOW	HIGH	
Volume flow (vf)	2	2	[l/min]
Mass flow	0.046	0.046	[kg/s]
Work in pump	0.228	0.228	[kW]
Heat in evaporator	10.238	12.285	[kW]
Work out turbine	2.503	3.185	[kW]
Heat out condenser	-7.963	-9.328	[kW]
Thermal efficiency	0.222	0.241	

A TEMPpoint display of results is shown in Figure 4.21 from which the cycle temperatures were obtained for use in the plotting of the Mourrier chart in Figure 4.20. The cycle thermodynamic plot was determined from the highlighted temperatures. The channels were presented as follows:

Inlet to expander channel 21 at 129.67°C (from evaporator)
Outlet from expander channel 10 at 55.44 °C (to condenser/recuperator)
Exit condenser channel 8 at 16.98°C (to pump)
Enter evaporator channel 19 at 42.45°C



Figure 4.21 TEMPpoint display for R 245fa at high temperature

In Figure 4.22 are the performance charts of the system tested on R-245fa at varying temperatures of the heat source. This was tested under two pump speeds of 20 Hz and 25Hz. It was noted that the power curve and expander rotational speed were stable for slower pump speed with changes in temperature. This could suggest that lesser amounts of working fluid were fully vaporised for a wide range of temperature though giving less power, while at 25Hz there was a drop in performance with a drop in temperature as increased fluid mass flow rates required more heat to convert to vapour. This suggested that maintaining the heat source conditions at high temperatures would guarantee performance of ORC heat engines.

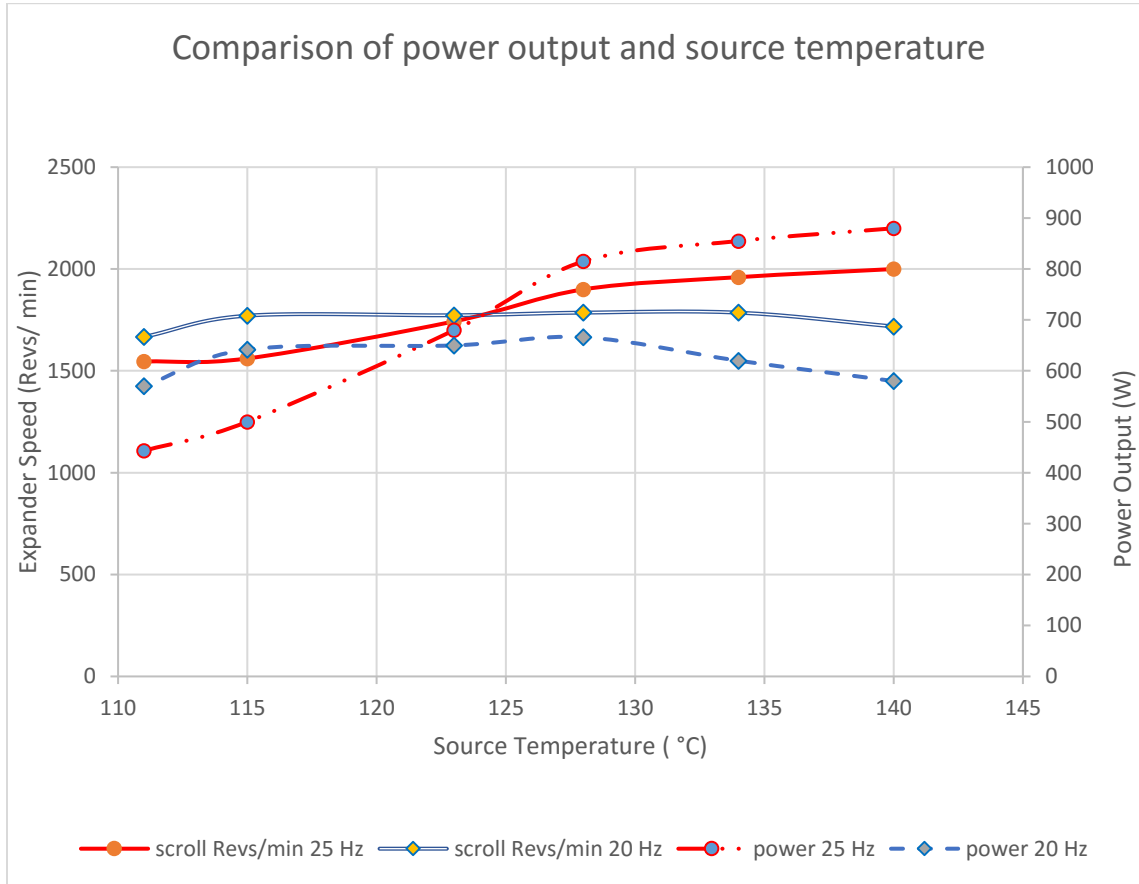


Figure 4.22 Power output and expander speeds for R-245fa

4.8 START UP

Investigations on start up without a motor were done with the recirculation pump coupled to a scroll expander through a chain /sprocket mechanism. The pump was cranked manually and when the expander reached a required power output, it started operating the pump. A load was attached to the turbine which measured the net shaft power output and electrical power by supplying different loads. The set-up is shown in Figure 4.23

An electrical generator was centrally fixed to the shaft from the turbine and one side of the bracket freely attached to a spring balance with a rigid connection. The three cables as shown in Figure 4.23 (blue) were attached to a variable load. As the scroll operated the pump, load in form of a variable resistor was altered which affected the rotational speed of

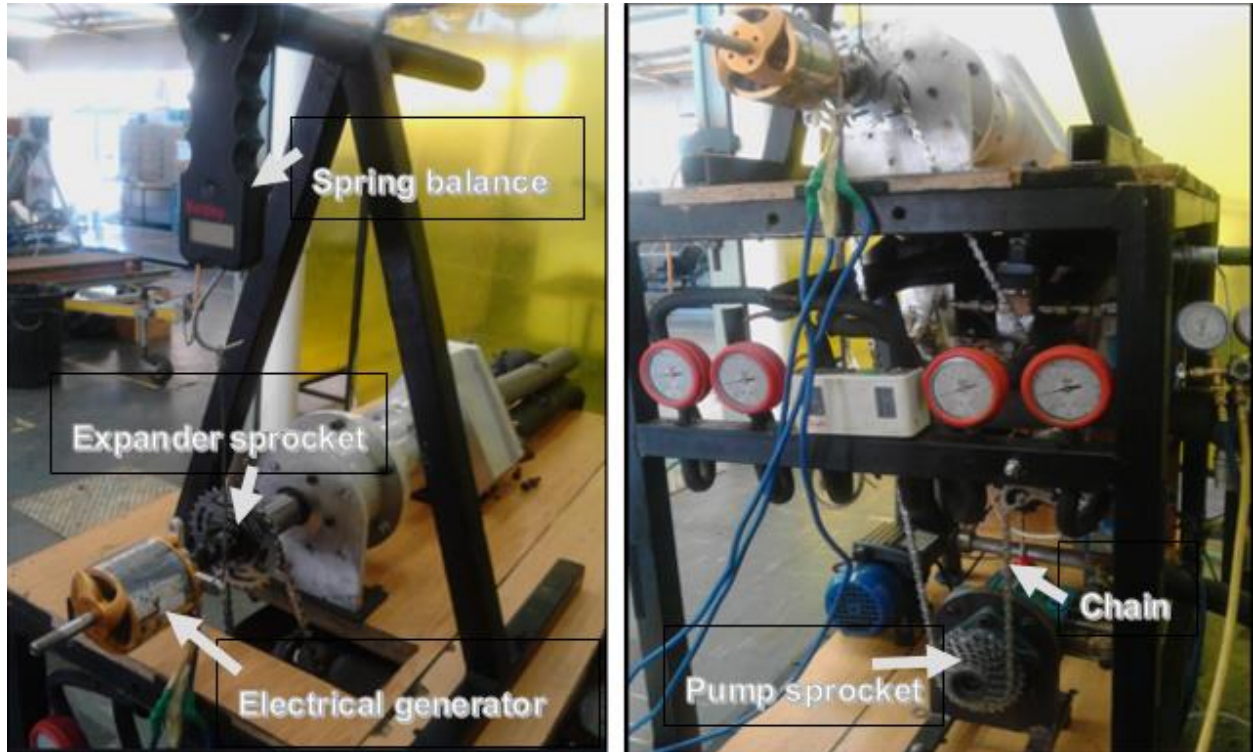


Figure 4.23 Manual start self-sustenance unit with power measuring devices

the output shaft and the reactional force was read from the spring balance in Figure 4.23. Shaft power was determined as shown in Figure 4.24. The highest registered power output with this set up was 512 W at 7kg and 1500 revs/min.

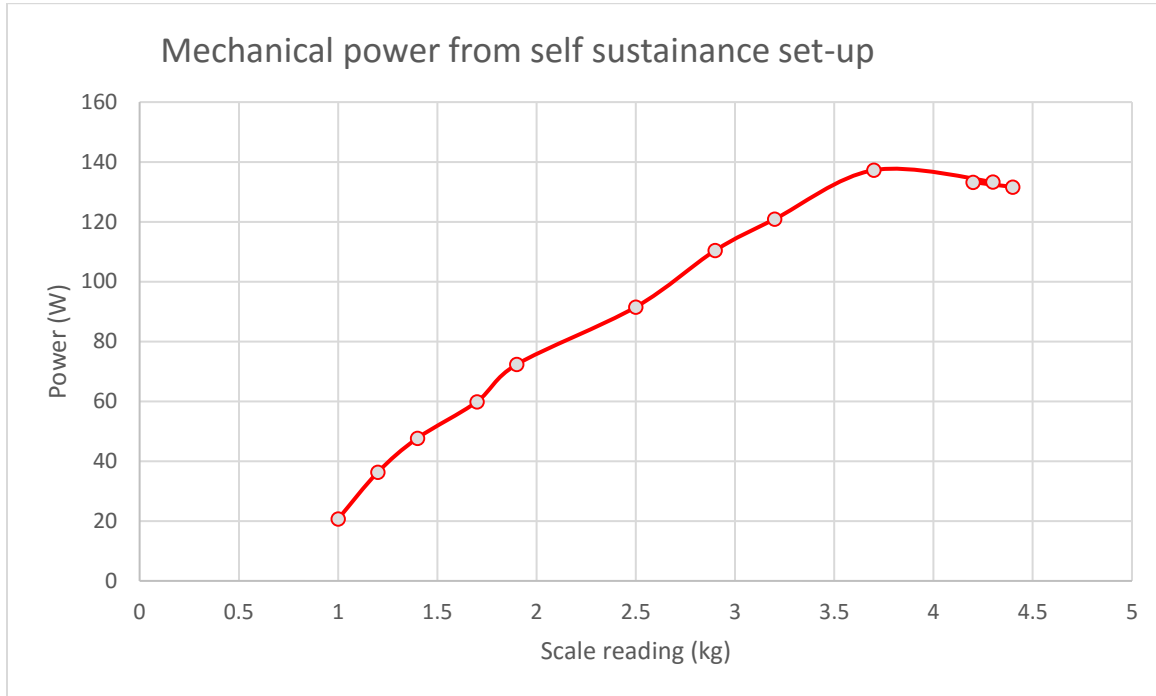


Figure 4.24 Results from a self-sustaining system

4.9 OVERALL EFFICIENCY

A heat source of 15 kW was supplied to heat the refrigerant and a pump power of 280 W was used to circulate the working fluid. A circulation pump for oil consumed 250 W. Other components were allocated 100 W. Total system consumption was 15630 W and an average of 850 W was realised from the system. Overall efficiency was therefore $\frac{850 \times 100}{15630}$, expressed as a percentage, which represented 5.44%

This efficiency looked lower compared to other power producing machines but bearing in mind that the heat source could be solar energy, industrial waste heat or geothermal energy, a 15 kW heat source may not be considered. This may bring the consumption to “630 W” raising the unit’s overall efficiency to as high as $\frac{850 \times 100}{630}$ which results to 135% “in economic sense” (if the heat source was not paid for by anyone), depending the technologies involved to harness the heat source.

4.10 SUMMARY OF RESULTS

- In most experiments, R-134a produced 750 W of power at a temperature of about 90 °C and pump speed of 30 Hz, representing input power of 292 W. (Figure 4.3 and Figure 4.10) R-245fa produced 850 W at a temperature of 130°C and pump speed of 25Hz, representing 250 W.
- R-134a started flooding the expander with liquid at speeds beyond 30 Hz while R-245fa did that beyond 25 Hz.
- R 245fa running at 25 Hz produced 880 W in one experiment at 140°C and reduced gradually to 500 W with a declined source temperature of 115°C, at which point liquid flooded into the expander. And the same was repeated at 20Hz where the power output was stable averaging 600 W, until at 115°C when liquid was observed entering the expander. This suggested that the fluid could only be effective at temperatures above 115°C (Figure 4.22) even though it had a steady power output at a lower flow rate of 20 Hz.

All the properties for refrigerants including Mourrier diagrams were taken from the ASHRAE booklet for refrigerant properties ⁽⁶⁸⁾.

A short clip can be watched on YouTube by following the link:

<https://youtu.be/PrPiu23EdSw>

CHAPTER 5

OBSERVATIONS

5.1 INTRODUCTION

In this chapter the major observations regarding the main issues encountered, observed and resolved during the research are highlighted.

5.2 FLOW RATE

A flow rate of 3.5 litres per minute was successfully achievable at the expense of more power input of about 330 W to the pump with power output in ranges of 300 W. The copper coil evaporators were able to vaporise fluid at such a flow rate despite the minimal power output in prototype 2. Condensation too was generally acceptable at cooling water flow rate of about 25 litres per minute. The third prototype, however, averaged 2 litres per minute of fluid flow rate for optimum evaporation. This was enough to produce power in ranges of 800 W or more with pump power of 280 W.

5.3 PRESSURE RISE

Initially a pressure build-up in the suction side was observed in both prototype 1 and 2, which was not an expected phenomenon. When the scroll outlet was upgraded to 25 mm, this situation was rectified. As long as adequate condensation was achieved, suction pressure remained constant and lower than static pressure. The volume ratio for the expander was therefore maintained by maintaining the pressure ratio. This condition allowed increase of high pressure without increasing low pressure resulting in a wider pressure differential which resulted in high power output.

5.4 SUCTION VOLUME

Increasing the suction volume increased the liquid stowage capacity, resulting in lower condensation pressures which corresponded to lower condensation temperatures. The best condensation temperatures achieved were same as atmospheric ambient temperatures of the time, which corresponded with pressure.

5.5 HEAT SOURCE

The heat source was observed to affect pressure differential making it a driving fuel of the Organic Rankine Cycle heat engine. Observation showed that a reduction in source temperature reduced the unit's power output. Also it encouraged incomplete evaporation, which resulted in less energised fluid entering the scroll expander. It was noted that at lower temperature, increased flow rate resulted in flooding the turbine.

5.6 TYPE OF WORKING FLUID

A comparison was done between R-134a and R-245fa, which revealed a 1:3 pressure ratio for the former and 1: 12 for the latter. However, mechanical and electrical power was in the same range. R-245fa, however, required more energy in the form of a high temperature heat sources. This gave R-134a an advantage that it could be utilised at much lower heat sources, in the range of 90-100 °C. Observation showed a very high speed for an unloaded generator of up to 4000 revs/min with R-134a, and 8000 revs/min for R-245fa. Both fluids operated at around 2600 revs/min or less when under load. This suggested that R-134a produced more power than R-245fa.

5.7 CAVITATION

It was observed that cavitation was a factor of condensation more than Net Positive Suction Head. Reducing cooling fluid resulted in cavitation for all the 3 prototypes, as tested with R-134a, and increasing the cooling water flow rate improved the performance of the unit. However, R-245fa had more tolerance to adverse conditions since completely closing off coolant showed no cavitation, despite the low power output from the turbine. Improvements in the final prototype included placing the reservoir above the pump which assured that the pump was always flooded with liquid, even under conditions of poor condensation, hence eliminating cavitation. It was found that the system required 6 kg for R 134a and 5 kg for R-245fa.

5.8 SELF-STARTING

A possibility for self-starting was investigated and was inconclusive. However, a manual start was achievable by cranking the pump to circulate the fluid manually to operate the expander which in turn took over running the pump. The expander kept accelerating until it slipped on the magnetic clutch. Control looked promising in the areas of regulating condensing water flow and working fluid flow.

CHAPTER 6

CONCLUSIONS AND SUMMARY

In conclusion, the results of the investigation can be summarised as follows:

6.1 THE PROBLEM

The research was to investigate factors that affected performance of the *Low Temperature ORC Heat Engine* and to optimise them. The following areas were investigated and optimised:

Working fluids R-134a and R-245fa were tested under various conditions and it was found that despite the good thermal efficiency of the latter, the mechanical and electrical power outputs were within the same range. R-134a was more prone to cavitation under poor condenser conditions than R-245fa, which was easier to condense as it boils at 15°C at atmospheric pressure compared with R-134a which boils at -26°C at same pressure. However, R-245fa was more expensive as it cost R11,000 per full unit charge, compared to R600 for R-134a.

Three types of heat exchangers were tested. The first was a 12.5 mm copper pipe which with inclusion of connecting pipes, resulted in significant friction. This was replaced by a set of parallel coils, increasing condensation as well as evaporation capacity and reducing friction losses. To further improve heat exchange capacity, a set of 20 KW soldered plate heat exchangers were employed.

Pressure build up in the system increased the suction pressures steadily reducing the pressure differential and consequently reduced power output of the heat engine. This was resolved by increasing the suction volume right from the exit of the expander. The result was that no partial pressure build ups occurred. The system maintained the suction pressure low and constant while increasing the discharge pressures to gain more power.

6.2 ISSUES RESOLVED

Several issues were resolved in this research. The first one was power output of the unit which increased from 200 W to an average of 800 W. This was due to improved pressure ratio which stood at 3:1 for R-134a and 12:1 for R-245fa. Initially it was hard to achieve a ratio of 2:1 for R-134a. Three methods were used to determine and confirm power output namely the rope brake dynamometer, Wattmeter, and a voltage and current reading. All indicated similar ranges of results.

Use of copper pipes reduced leakages and the cost of piping dropped significantly. Several fittings were removed from the previous unit reducing restrictions and cost.

Also a reduction and possible elimination of cavitation by allowing the pump to draw from the reservoir above it improved reliability. With adequate charge, the reservoir was guaranteed liquid refrigerant as long as adequate condensation was available.

A reduction in input power of about 50% was also achieved by running the feed pump at half the speed to achieve optimum flow rate, hence more power output.

6.3 FUTURE WORK

- There is need to investigate a way of reducing power input to the feed pump further as lowering power input increased the net power output. Thus far the smaller pump shows that it requires high rotational speed to achieve sufficient flow rates demanding more power, which defeats the purpose of saving on power input.
- An investigation on start-up without external source was inconclusive. A few options such as cranking the pump and use of a separate photovoltaic panel battery inverter set for start-up may be investigated. Cranking as suggested earlier on is possible with a challenge in controlling the unit, which requires further investigation.
- The ORC heat engine can be compressed further and redesigned to improve aesthetics since NSPH has been found not to affect performance.
- The issue of noise reduction may be considered.

- Automation can also be considered to monitor and control power and other associated parameters such as temperature, pressure and fluid flow. Fault identification and coding may also be considered in this arrangement.

REFERENCES

1. Gian Paolo Beretta. International Journal of Environmental Technology and Management on "Sustainable development: a joined goal of energy efficiency and environmental impact". World Energy Consum Electr. 2014;
2. Teleman Y. Rankine Cycles , Modeling and Control. 2016;2016. Available from: <http://lup.lub.lu.se/luur/download?func=downloadFile&recordId=8522986&fileId=8522991>
3. Zhou S, Turnbull A. NPL Report MATC (A) 95 Steam Turbine Operating Conditions, Chemistry of Condensates, and Environment Assisted Cracking – A Critical Review Steam Turbine Operating Conditions, Chemistry of Condensates, and Environment Assisted Cracking – A Critical Review. 2002;(May).
4. Humm JC. An Organic Rankine Cycle (ORC) heat engine using a rock thermal battery as the heat source. Nelson Mandela Metropolitan University; 2015.
5. Taylor L, Water M, Krumdieck S. Development of a Low Temperature Geothermal Organic Rankine Cycle Standard. 35th Newzeal Geotherm Work. 2013;(November).
6. Di Nicola G, Brandoni C, Di Nicola C, Giuliani G. Triple point measurements for alternative refrigerants. J Therm Anal Calorim. 2012;108(2):627–31.
7. Zilke TA. 2009 ASE Refrigerant recovery and recycling training booklet. 2009.
8. Mcdonald A, Hill H. A study of current working practices for refrigeration field service engineers RR839. 2011;
9. Takaishi TEA. Approach to High Efficiency Diesel and Gas Engines. Mitsubishi Heavy Ind Ltd Tech Rev. 2008;45(1).
10. Lahimer AA, Alghoul MA, Yousif F, Razykov TM, Amin N, Sopian K. Research and development aspects on decentralized electrification options for rural household. Renew Sustain Energy Rev [Internet]. Elsevier; 2013;24:314–24. Available from: <http://dx.doi.org/10.1016/j.rser.2013.03.057>

11. Camacho EF, Samad T, Garcia-sanz M, Hiskens I. Control for Renewable Energy and Smart Grids. 2011;
12. Tchanche BF, Papadakis G, Lambrinos G, Frangoudakis A. Fluid selection for a low-temperature solar organic Rankine cycle. *Appl Therm Eng* [Internet]. Elsevier Ltd; 2009;29(11–12):2468–76. Available from: <http://dx.doi.org/10.1016/j.applthermaleng.2008.12.025>
13. Bell LE. REVIEW Cooling, Heating, Generating Power, and Recovering Waste Heat with Thermoelectric Systems. 2008;321(September):1457–61.
14. Dumont O, Quoilin S, Lemort V. Experimental investigation of a reversible heat pump / organic Rankine cycle unit designed to be coupled with a passive house to get a Net Zero Energy Building. *Int J Refrig* [Internet]. Elsevier Ltd and IIR; 2015;54:190–203. Available from: <http://dx.doi.org/10.1016/j.ijrefrig.2015.03.008>
15. Orosz MS, Mueller A, Quolin S, Hemond H. Small scale solar orc system for distributed power. 1(3).
16. Muhammad U, Imran M, Lee DH, Park BS. Design and experimental investigation of a 1kW organic Rankine cycle system using R245fa as working fluid for low-grade waste heat recovery from steam. *Energy Convers Manag* [Internet]. Elsevier Ltd; 2015;103:1089–100. Available from: <http://www.sciencedirect.com/science/article/pii/S0196890415006962>
<http://linkinghub.elsevier.com/retrieve/pii/S0196890415006962>
17. Yamamoto T, Furuhata T, Arai N, Mori K. Design and testing of the organic Rankine cycle. *Energy*. 2001;26(239–251):239–51.
18. Tchanche BF, Papadakis G, Lambrinos G, Frangoudakis A. Fluid selection for a low-temperature solar organic Rankine cycle. *Appl Therm Eng* [Internet]. Elsevier Ltd; 2009;29(11–12):2468–76. Available from: <http://dx.doi.org/10.1016/j.applthermaleng.2008.12.025>
19. Lakew AA, Bolland O. Working fluids for low-temperature heat source. *Appl Therm*

- Eng. 2010;30(10):1262–8.
20. Bertrand TF, Papadakis G, Lambrinos G, Author C. Criteria for working fluids selection in low-temperature solar organic Rankine cycles. 1st Int Congr Heating, Cool Build. 2008;(October 2008):1–8.
 21. Drescher U, Bru D. Fluid selection for the Organic Rankine Cycle (ORC) in biomass power and heat plants. 2007;27:223–8.
 22. Sustainable Energy Ireland. Refrigerants Choice , Regulatory Requirements and Energy Efficiency. Refrig Spec Work Gr Refrig [Internet]. 2011;(2037). Available from: www.sei.ie
 23. Ingersoll Rand. Climate Change Regulation and the Next Generation of Refrigerants. 2014; Available from: <http://www.trane.com/commercial/uploads/pdf/cso/138/Refrigerants.pdf>
 24. Black AJ, Head G. EU f-gas regulations : impact on R404A and the opportunity for R442A(RS-50). 2014;(May):50–3.
 25. Yamada N, Mohamad MNA, Kien TT. Study on thermal efficiency of low- to medium-temperature organic Rankine cycles using HFO-1234yf. Renew Energy [Internet]. Elsevier Ltd; 2012;41:368–75. Available from: <http://dx.doi.org/10.1016/j.renene.2011.11.028>
 26. Kang SH. Design and experimental study of ORC (organic Rankine cycle) and radial turbine using R245fa working fluid. Energy. 2012;41(1):514–24.
 27. Heberle F, Preißinger M, Brüggemann D. Zeotropic mixtures as working fluids in Organic Rankine Cycles for low-enthalpy geothermal resources. Renew Energy [Internet]. Elsevier Ltd; 2012;37(1):364–70. Available from: <http://dx.doi.org/10.1016/j.renene.2011.06.044>
 28. Nouman J. Comparative studies and analyses of working fluids for Organic Rankine Cycles - ORC. 2012;

29. Brasz LJ, Bilbow WM. Ranking of Working Fluids for Organic Rankine Cycle Applications. *Int Refrig Air Cond Conf.* 2004;1–8.
30. Liu BT, Chien KH, Wang CC. Effect of working fluids on organic Rankine cycle for waste heat recovery. *Energy.* 2004;29(8):1207–17.
31. Dong B, Xu G, Cai Y, Li H. Analysis of zeotropic mixtures used in high-temperature Organic Rankine cycle. *Energy Convers Manag* [Internet]. Elsevier Ltd; 2014;84:253–60. Available from: <http://dx.doi.org/10.1016/j.enconman.2014.04.026>
32. Jung HC, Krumdieck S. Analysis of Zeotropic Mixture in a Geothermal Organic Rankine Cycle Power Plant With an Air-Cooled Condenser. 2013;(November).
33. Liu Q, Duan Y, Yang Z. Effect of condensation temperature glide on the performance of organic Rankine cycles with zeotropic mixture working fluids. *Appl Energy* [Internet]. Elsevier Ltd; 2014;115:394–404. Available from: <http://dx.doi.org/10.1016/j.apenergy.2013.11.036>
34. Rowshanzadeh R. “ Performance and cost evaluation of Organic Rankine Cycle at different technologies ” (Master thesis). *Sustain Energy Eng* (Master thesis). 2014;1(1).
35. Clemente S, Micheli D, Reini M, Tacconi R. Bottoming organic Rankine cycle for a small scale gas turbine: A comparison of different solutions. *Appl Energy* [Internet]. 2013;106:355–64. Available from: <http://dx.doi.org/10.1016/j.apenergy.2013.02.004>
36. Costall a. W, Gonzalez Hernandez a., Newton PJ, Martinez-Botas RF. Design methodology for radial turbo expanders in mobile organic Rankine cycle applications. *Appl Energy* [Internet]. Elsevier Ltd; 2015;1–15. Available from: <http://linkinghub.elsevier.com/retrieve/pii/S0306261915002573>
37. Fiaschi D, Manfrida G, Maraschiello F. Thermo-fluid dynamics preliminary design of turbo-expanders for ORC cycles. *Appl Energy.* 2012;97:601–8.
38. Gao P, Jiang L, Wang LW, Wang RZ, Song FP. Simulation and experiments on an ORC system with different scroll expanders based on energy and exergy analysis.

- Appl Therm Eng [Internet]. Elsevier Ltd; 2015;75:880–8. Available from: <http://linkinghub.elsevier.com/retrieve/pii/S1359431114009156>
39. Chang J-C, Chang C-W, Hung T-C, Lin J-R, Huang K-C. Experimental study and CFD approach for scroll type expander used in low-temperature organic Rankine cycle. Appl Therm Eng [Internet]. Elsevier Ltd; 2014;73(2):1444–52. Available from: <http://linkinghub.elsevier.com/retrieve/pii/S1359431114007467>
 40. Durmaz A, Pugh R. Novel Application of Organic Rankine Cycle (ORC) Technology for Waste Heat Recovery From Reheat Furnace Evaporative Cooling System. AISTech - Iron Steel Technol Conf Proc. 2012;(September 2011):1625–33.
 41. Gharbi N El, Kheiri A, Ganaoui M El, Blanchard R. Numerical optimization of heat exchangers with circular and non-circular shapes. Case Stud Therm Eng [Internet]. Elsevier; 2015;6:194–203. Available from: <http://dx.doi.org/10.1016/j.csite.2015.09.006>
 42. Admiraal DM, Bullard CW, Conditioning A. Heat Transfer in Refrigerator Condensers and Evaporators Acustar Division of Chrysler Ford Motor Company Frigidaire Company General Electric Company. Development. 1993;61801(217).
 43. Evans T. The different types of air conditioning equipment for IT environments. APC White Pap [Internet]. 2004;24. Available from: <http://www.dcsarabia.com/whitepapers/48.pdf>
 44. Park CY, Hrnjak P. Experimental and numerical study on microchannel and round-tube condensers in a R410A residential air-conditioning system. Int J Refrig. 2008;31(5):822–31.
 45. Gillain. Brazed heat exchangers. 2014; Available from: www.gillain.com
 46. Transfer DH. solutions concept, product and application of BPHE concept. brazed plate heat Exch [Internet]. 2014; Available from: Website: www.dhtnet.com
 47. Richardson ES. Thermodynamic performance of new thermofluidic feed pumps for Organic Rankine Cycle applications. Appl Energy [Internet]. Elsevier Ltd;

- 2016;161:75–84. Available from: <http://dx.doi.org/10.1016/j.apenergy.2015.10.004>
48. Baral S, Kim D, Yun E, Kim K. Energy, Exergy and Performance Analysis of Small-Scale Organic Rankine Cycle Systems for Electrical Power Generation Applicable in Rural Areas of Developing Countries. *Energies* [Internet]. 2015;8(2):684–713. Available from: <http://www.mdpi.com/1996-1073/8/2/684/>
 49. Christopher, Brennen E. Cavitation and bubble dynamics [Internet]. *Annual Review of Fluid Mechanics*. 1977. 145-185 p. Available from: <http://arjournals.annualreviews.org/doi/abs/10.1146/annurev.fl.09.010177.001045>
 50. Wilson S. Net Positive Suction Head (NPSH) -White Paper. GRUNDFOS WHITE Pap. 2009;WP 17.
 51. Pei G, Li J, Li Y, Wang D, Ji J. Construction and dynamic test of a small-scale organic rankine cycle. *Energy* [Internet]. Elsevier Ltd; 2011;36(5):3215–23. Available from: <http://dx.doi.org/10.1016/j.energy.2011.03.010>
 52. Lee Y-R, Kuo C-R, Liu C-H, Fu B-R, Wang C-C. Response of a 50kW Organic Rankine Cycle System Subject to Influence of Evaporators. *Energy Procedia* [Internet]. Elsevier B.V.; 2014;61:635–8. Available from: <http://linkinghub.elsevier.com/retrieve/pii/S1876610214030161>
 53. DANFOSS. Brazed Plate Heat Exchanger. CATALOGUE [Internet]. DKQB.PK.00. Available from: danfoss@danfoss.com. www.danfoss.com
 54. Li T, Zhu J, Hu K, Kang Z, Zhang W. Implementation of PDORC (parallel double-evaporator organic Rankine cycle) to enhance power output in oilfield. *Energy* [Internet]. Elsevier Ltd; 2014;68:680–7. Available from: <http://dx.doi.org/10.1016/j.energy.2014.03.007>
 55. Power from the sun. Power cycles for electrical generation [Internet]. Available from:
 56. Delgado-Torres AM, García-Rodríguez L. Analysis and optimization of the low-temperature solar organic Rankine cycle (ORC). *Energy Convers Manag*. 2010;51(12):2846–56.

57. Li M, Wang J, He W, Wang B, Ma S, Dai Y. Experimental Evaluation of the Regenerative and Basic Organic Rankine Cycles for Low-Grade Heat Source Utilization. 2013;(September):190–8.
58. Vanslambrouck B, Vankeirsbilck I, Gusev S, Paepe M De. Efficiency comparison between the steam cycle and the organic Rankine cycle for small scale power generation. Renew Energy World Conf Expo North Am [Internet]. 2012;32(0):13. Available from: <http://hdl.handle.net/1854/LU-3078894>
59. Cengel, Y. a. M. AB. Thermodynamics, an Engineering approach. 5 th Editi. text. New York: Mc Graw Hill; 2008. 551-589 p.
60. Cengel Y a., Klein S, Beckman W. Heat Transfer, a Practical Approach. 3rd Editio. McGraw Hill, editor. 2002. 896 p.
61. Ziviani D, Woodland BJ, Georges E, Groll EA, Braun JE, Horton WT, et al. Organic Rankine Cycle (ORC) Simulation Tool †. :1–36.
62. Woodland BJ, Braun, James E EAG, Horton WT. Experimental Testing of an Organic Rankine Cycle with Scroll-type Expander. 2012;2505.
63. Richardson ES. Thermodynamic performance of new thermofluidic feed pumps for Organic Rankine Cycle applications Thermofluidic pump. Appl Energy [Internet]. Elsevier Ltd; 2016;161:75–84. Available from: <http://dx.doi.org/10.1016/j.apenergy.2015.10.004>
64. Du Pont technical Information. Properties, Uses, Storage, and Handling. 2014;
65. Gopinath R. Design of a Rope Brake Dynamometer. 2014;20(5):650–5.
66. Wu W, Zhao L, Ho T. Experimental investigation on pinch points and maximum temperature differences in a horizontal tube-in-tube evaporator using zeotropic refrigerants. 2012;56:22–31.
67. Koç A, Adnan G, Tandiro A. Parametric optimization and exergetic analysis comparison of subcritical and supercritical organic Rankine cycle (ORC) for biogas

fuelled combined heat and power (CHP) engine exhaust gas waste heat.
2016;111:923–32.

68. ASHRAE. Thermophysical Properties of Refrigerants. ASHRAE Handbook-Fundamentals. 2002;718:2002.

8. APPENDICES

Appendix 1: Properties of saturated refrigerant R-134a

R134a - TetraFlouroEthane Saturation Properties - Pressure Table											
Pressure	Temp	volume (m ³ /kg)		energy (kJ/kg)		enthalpy (kJ/kg)			entropy (kJ/kg.K)		
kPa	deg C	vf	vg	uf	ug	hf	hfg	hg	sf	sfg	sg
60	-36.935	0.00071	0.31123	3.8148	209.13	3.8574	223.943	227.8	0.01641	0.94805	0.96446
80	-31.115	0.00072	0.23755	11.17	212.47	11.228	220.242	231.47	0.04717	0.90998	0.95715
100	-26.361	0.00073	0.19256	17.225	215.2	17.298	217.162	234.46	0.07195	0.87993	0.95188
120	-22.31	0.00073	0.16214	22.419	217.52	22.507	214.473	236.98	0.09283	0.85501	0.94784
140	-18.76	0.00074	0.14015	26.996	219.56	27.1	212.08	239.18	0.11095	0.83367	0.94462
160	-15.588	0.00074	0.12349	31.107	221.37	31.226	209.894	241.12	0.12701	0.81495	0.94196
180	-12.712	0.00075	0.11042	34.852	223	34.987	207.893	242.88	0.14148	0.79824	0.93972
200	-10.076	0.00075	0.09988	38.301	224.5	38.452	206.018	244.47	0.15466	0.78313	0.93779
220	-7.6377	0.00076	0.09119	41.506	225.88	41.672	204.268	245.94	0.16678	0.76934	0.93612
240	-5.3653	0.00076	0.08391	44.503	227.16	44.686	202.614	247.3	0.17803	0.75662	0.93465
260	-3.235	0.00077	0.0777	47.325	228.36	47.524	201.036	248.56	0.18853	0.74481	0.93334
280	-1.2277	0.00077	0.07236	49.993	229.48	50.209	199.531	249.74	0.19838	0.73379	0.93217
300	0.67206	0.00077	0.0677	52.527	230.54	52.759	198.091	250.85	0.20767	0.72343	0.9311
320	2.4768	0.00078	0.06361	54.943	231.54	55.192	196.708	251.9	0.21647	0.71367	0.93014
340	4.1969	0.00078	0.05998	57.253	232.49	57.519	195.371	252.89	0.22483	0.70442	0.92925
360	5.8412	0.00078	0.05674	59.469	233.4	59.751	194.079	253.83	0.2328	0.69564	0.92844
400	8.9306	0.00079	0.05121	63.651	235.09	63.967	191.613	255.58	0.24771	0.67927	0.92698
500	15.735	0.00081	0.04112	72.955	238.77	73.358	185.972	259.33	0.28033	0.64375	0.92408
600	21.572	0.00082	0.0343	81.046	241.85	81.538	180.892	262.43	0.30809	0.61376	0.92185
700	26.713	0.00083	0.02937	88.266	244.5	88.849	176.201	265.05	0.3324	0.58761	0.92001
800	31.327	0.00085	0.02563	94.825	246.82	95.501	171.819	267.32	0.35414	0.56429	0.91843
900	35.526	0.00086	0.02269	100.86	248.87	101.64	167.65	269.29	0.37387	0.54313	0.917
1000	39.388	0.00087	0.02032	106.48	250.7	107.35	163.67	271.02	0.39199	0.52367	0.91566
1200	46.315	0.00089	0.01672	116.73	253.84	117.8	156.1	273.9	0.42451	0.48861	0.91312
1400	52.422	0.00092	0.01411	125.97	256.4	127.26	148.89	276.15	0.45326	0.45733	0.91059
1600	57.906	0.00094	0.01213	134.47	258.5	135.97	141.93	277.9	0.47923	0.42872	0.90795
1800	62.895	0.00096	0.01056	142.38	260.2	144.11	135.1	279.21	0.50307	0.40203	0.9051
2000	67.481	0.00099	0.00929	149.83	261.55	151.81	128.33	280.14	0.52524	0.37674	0.90198
2500	77.577	0.00106	0.00694	167.06	263.51	169.7	111.16	280.86	0.57551	0.31695	0.89246
3000	86.203	0.00114	0.00528	183.14	263.35	186.56	92.63	279.19	0.62145	0.25778	0.87923

Appendix 2: Properties of superheated refrigerant R134a

R-134a - TetraFlouroEthane Superheated Properties												
P=0.06 MPa (-36.3 C)					P=0.10 MPa (-26.4 C)				P=0.14 MPa (-18.8 C)			
Temp	volume	energy	enthalpy	entropy	volume	energy	enthalpy	entropy	volume	energy	enthalpy	entropy
Deg C	v (m ³ /kg)	u (kJ/kg)	h (kJ/kg)	s (kJ/kg.K)	v (m ³ /kg)	u (kJ/kg)	h (kJ/kg)	s (kJ/kg.K)	v (m ³ /kg)	u (kJ/kg)	h (kJ/kg)	s (kJ/kg.K)
Sat.	0.31123	203.13	227.8	0.96446	0.19256	215.2	234.46	0.95188				
-20	0.33608	220.6	240.77	1.0175	0.19841	219.66	239.5	0.97208	0.14015	219.56	239.18	0.94462
-10	0.35049	227.55	248.58	1.0477	0.20743	226.75	247.49	1.003	0.14606	225.91	246.36	0.97237
0	0.36476	234.66	256.54	1.0774	0.2163	233.96	255.59	1.0332	0.15263	233.23	254.6	1.0031
10	0.37893	241.93	264.66	1.1066	0.22506	241.3	263.81	1.0628	0.15908	240.66	262.93	1.0331
20	0.39303	249.36	272.94	1.1353	0.23373	248.8	272.17	1.0918	0.16544	248.23	271.39	1.0624
30	0.40705	256.95	281.38	1.1636	0.24233	256.45	280.68	1.1203	0.17172	255.93	279.97	1.0912
40	0.42102	264.71	289.98	1.1916	0.25088	264.25	289.34	1.1485	0.17795	263.79	288.7	1.1195
50	0.43495	272.64	298.74	1.2191	0.25938	272.22	298.16	1.1762	0.18412	271.8	297.57	1.1474
60	0.44884	280.74	307.67	1.2463	0.26784	280.35	307.13	1.2035	0.19025	279.96	306.6	1.1749
70	0.46269	288.99	316.76	1.2732	0.27626	288.64	316.26	1.2305	0.19635	288.28	315.77	1.202
80	0.47652	297.42	326.01	1.2998	0.28466	297.09	325.55	1.2572	0.20243	296.75	325.09	1.2288
90	0.49032	306	335.42	1.326	0.29303	305.69	335	1.2836	0.20847	305.99	334.57	1.2553
100	0.5041	314.75	344.99	1.352	0.30138	314.46	344.6	1.3097	0.2145	314.17	344.2	1.2815
P=0.18 MPa (-12.7 C)					P=0.20 MPa (-10.1 C)				P=0.24 MPa (-5.4 C)			
Temp	volume	energy	enthalpy	entropy	volume	energy	enthalpy	entropy	volume	energy	enthalpy	entropy
Deg C	v (m ³ /kg)	u (kJ/kg)	h (kJ/kg)	s (kJ/kg.K)	v (m ³ /kg)	u (kJ/kg)	h (kJ/kg)	s (kJ/kg.K)	v (m ³ /kg)	u (kJ/kg)	h (kJ/kg)	s (kJ/kg.K)
Sat.	0.11042	223	242.88	0.93972	0.09988	224.5	244.47	0.93779	0.08391	227.16	247.3	0.93465
-10	0.1119	225.02	245.16	0.94844								
0	0.11722	232.48	253.58	0.97983	0.10481	232.09	253.05	0.96979	0.08617	231.29	251.97	0.95192
10	0.1224	240.01	262.04	1.0102	0.10955	239.67	261.58	1.0005	0.09026	238.99	260.65	0.98313
20	0.12748	247.64	270.59	1.0399	0.11419	247.35	270.19	1.0303	0.09423	246.75	269.36	1.0134
30	0.13248	255.41	279.26	1.069	0.11874	255.15	278.89	1.0595	0.09812	254.61	278.16	1.0429
40	0.13742	263.32	288.05	1.0975	0.12323	263.08	287.72	1.0882	0.10193	262.59	287.06	1.0718
50	0.1423	271.37	296.98	1.1256	0.12766	271.15	296.68	1.1163	0.1057	270.71	296.08	1.1001
60	0.14715	279.57	306.05	1.1533	0.13206	279.37	305.78	1.1441	0.10942	278.97	305.23	1.128
70	0.15196	287.92	315.27	1.1805	0.13642	287.73	315.02	1.1714	0.1131	287.37	314.51	1.1555
80	0.15674	296.42	324.63	1.2074	0.14074	296.25	324.4	1.1983	0.11675	295.91	323.93	1.1825
90	0.16149	305.08	334.14	1.234	0.14505	304.92	333.93	1.2249	0.12038	304.61	333.5	1.2092
100	0.16622	313.88	343.8	1.2602	0.14933	313.74	343.6	1.2512	0.12398	313.45	343.2	1.2356
P=0.28 MPa (-1.2 C)					P=0.32 MPa (2.5 C)				P=0.40 MPa (8.9 C)			
Temp	volume	energy	enthalpy	entropy	volume	energy	enthalpy	entropy	volume	energy	enthalpy	entropy
Deg C	v (m ³ /kg)	u (kJ/kg)	h (kJ/kg)	s (kJ/kg.K)	v (m ³ /kg)	u (kJ/kg)	h (kJ/kg)	s (kJ/kg.K)	v (m ³ /kg)	u (kJ/kg)	h (kJ/kg)	s (kJ/kg.K)
Sat.	0.07236	229.48	249.74	0.93217	0.06361	231.54	251.9	0.93014	0.05121	235.09	255.58	0.92698
10	0.07646	238.28	259.69	0.968	0.06609	237.54	258.69	0.95445	0.05151	235.98	256.58	0.93053
20	0.07997	246.13	268.52	0.99867	0.06925	245.5	267.66	0.98558	0.05421	244.18	265.86	0.96276

Appendix 2: Properties of superheated refrigerant R134a (cont...)

	100	0.04220	305.11	400.0	1.203															
		P=1.2 MPa (46.3 C)					P=1.4 MPa (52.4 C)					P=1.6 MPa (57.9 C)								
Temp		volume	energy	enthalpy	entropy		volume	energy	enthalpy	entropy		volume	energy	enthalpy	entropy					
Deg C		v (m ³ /kg)	u (kJ/kg)	h (kJ/kg)	s (kJ/kg.K)		v (m ³ /kg)	u (kJ/kg)	h (kJ/kg)	s (kJ/kg.K)		v (m ³ /kg)	u (kJ/kg)	h (kJ/kg)	s (kJ/kg.K)					
Sat.		0.01672	253.84	273.9	0.91312		0.01411	256.4	276.15	0.91059		0.01213	258.5	277.9	0.90795					
50		0.0172	257.63	278.27	0.92673															
60		0.0184	267.56	289.64	0.9614		0.01501	264.47	285.47	0.9389		0.01237	260.9	280.69	0.91636					
70		0.0195	277.21	300.61	0.99385		0.01606	274.62	297.11	0.97331		0.01343	271.76	293.25	0.95351					
80		0.02053	286.75	311.39	1.0248		0.01702	284.51	308.34	1.0056		0.01436	282.09	305.07	0.98747					
90		0.02151	296.27	322.07	1.0546		0.01792	294.28	319.37	1.0364		0.01522	292.17	316.52	1.0194					
100		0.02244	305.8	332.73	1.0836		0.01878	304.01	330.3	1.0661		0.01602	302.14	327.77	1.05					
110		0.02335	315.38	343.4	1.1118		0.0196	313.76	341.2	1.0949		0.01677	312.08	338.91	1.0795					
120		0.02423	325.04	354.11	1.1394		0.02039	323.55	352.1	1.123		0.0175	322.02	350.02	1.1081					
130		0.02509	334.78	364.88	1.1664		0.02116	333.41	363.03	1.1504		0.0182	332	361.13	1.136					
140		0.02593	344.62	375.73	1.193		0.0219	343.35	374.01	1.1773		0.01888	342.05	372.26	1.1633					
150		0.02675	354.56	386.66	1.2192		0.02264	353.38	385.07	1.2038		0.01955	352.17	383.45	1.19					
160		0.02757	364.62	397.69	1.2449		0.02336	363.51	396.21	1.2298		0.02019	362.39	394.7	1.2163					
170		0.02837	374.79	408.83	1.2704		0.02406	373.75	407.44	1.2554		0.02083	372.7	406.03	1.2421					
180		0.02916	385.08	420.07	1.2954		0.02476	384.1	418.77	1.2807		0.02146	383.11	417.44	1.2676					
		(Source of data:	NIST Chemistry WebBook					Accessed: May 2007												
		P=1.8 MPa (62.9 C)					P=2.0 MPa (67.5 C)													
Temp		volume	energy	enthalpy	entropy		volume	energy	enthalpy	entropy										
Deg C		v (m ³ /kg)	u (kJ/kg)	h (kJ/kg)	s (kJ/kg.K)		v (m ³ /kg)	u (kJ/kg)	h (kJ/kg)	s (kJ/kg.K)										
Sat.		0.01056	408.35	427.36	1.7007		0.00929	409.7	428.28	1.6976										
70		0.01133	416.68	437.07	1.7293		0.00957	412.91	432.06	1.7086										
80		0.01226	427.61	449.67	1.7655		0.01054	424.7	445.77	1.7481										
90		0.01309	438.07	461.63	1.7989		0.01136	435.66	458.38	1.7833										
100		0.01385	448.32	473.25	1.8305		0.01211	446.24	470.45	1.816										
110		0.01457	458.46	484.68	1.8607		0.01279	456.63	482.21	1.8471										
120		0.01525	468.58	496.02	1.8899		0.01344	466.93	493.8	1.877										
130		0.0159	478.7	507.32	1.9183		0.01405	477.21	505.31	1.9059										
140		0.01653	488.86	518.61	1.946		0.01464	487.49	516.78	1.934										
150		0.01714	499.08	529.93	1.9731		0.01521	497.82	528.24	1.9614										
160		0.01773	509.38	541.3	1.9996		0.01576	508.21	539.74	1.9883										
170		0.01832	519.77	552.74	2.0257		0.0163	518.68	551.28	2.0146										
180		0.01889	530.25	564.25	2.0514		0.01683	529.23	562.89	2.0405										
A		(Source of data:	NIST Chemistry WebBook					Accessed: Oct 2010												

Appendix 3: Mourrier (P-h) chart for R-134a

Licensed for single user. © 2009 ASHRAE, Inc.

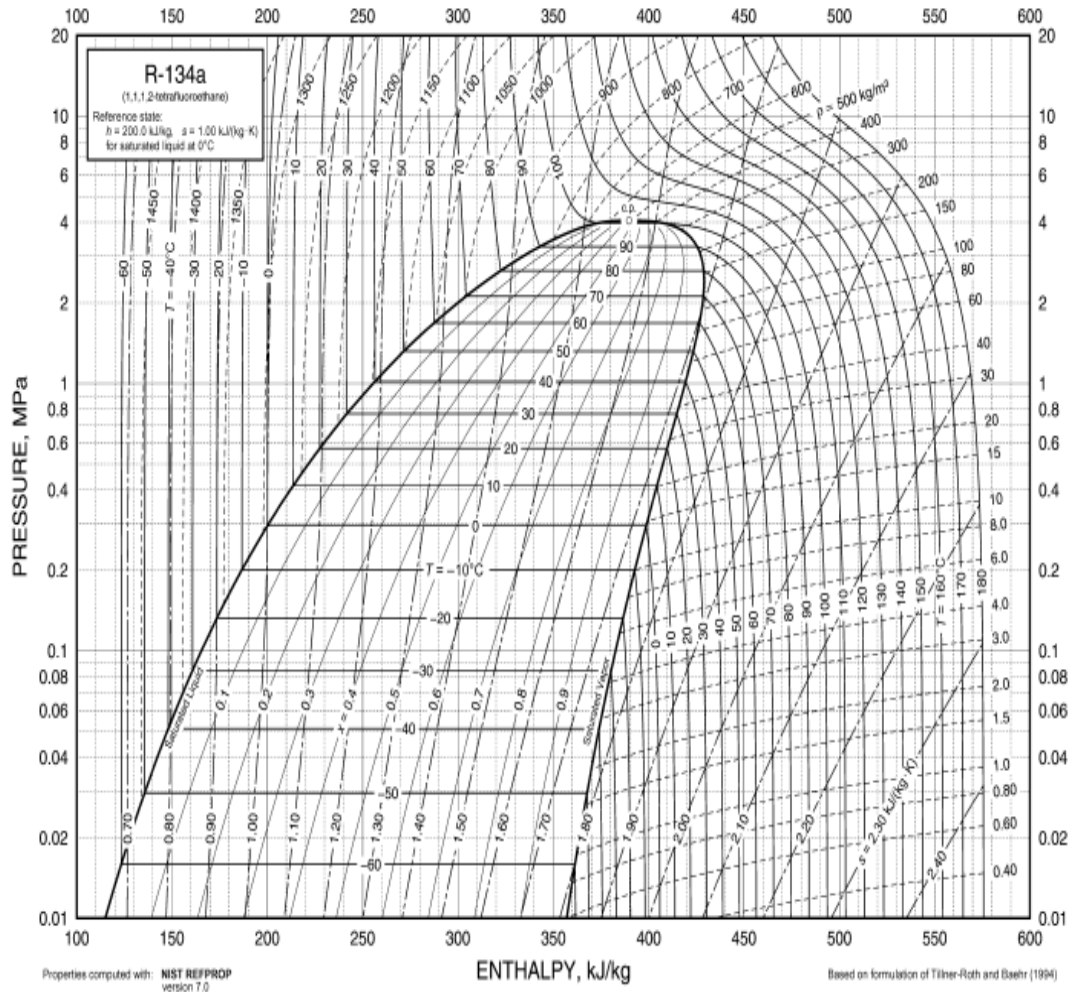


Fig. 8 Pressure-Enthalpy Diagram for Refrigerant 134a

30.16

2009 ASHRAE Handbook—Fundamentals (SI)

Appendix 4: Properties of saturated refrigerant R-245fa

Thermophysical Properties of Refrigerants

30.25

Refrigerant 245fa (1,1,1,3,3-Pentafluoropropane) Properties of Saturated Liquid and Saturated Vapor

Temp., °C	Pres-sure, MPa	Density, kg/m ³	Volume, m ³ /kg	Enthalpy, kJ/kg		Entropy, kJ/(kg-K)		Specific Heat c _p , kJ/(kg-K)		c _p /c _v	Velocity of Sound, m/s		Viscosity, μPa·s		Thermal Cond., mW/(m ² ·K)		Surface Tension, mN/m	Temp., °C
				Liquid	Vapor	Liquid	Vapor	Liquid	Vapor		Liquid	Vapor	Liquid	Vapor	Liquid	Vapor		
-60	0.00127	1548.7	0.380	126.06	361.82	0.6949	1.8009	1.200	0.701	1.101	1041	1203	2026.	7.36	115.5	9.08	24.67	-60
-50	0.00281	1525.2	4.9084	138.12	368.68	0.7501	1.7834	1.208	0.725	1.099	994	1227.	1501.	7.71	111.9	9.27	23.47	-50
-40	0.00572	1501.6	2.5079	150.34	375.67	0.8033	1.7702	1.218	0.751	1.098	948	1250.	1174.	8.06	108.5	9.54	22.26	-40
-30	0.01085	1477.7	1.3726	162.48	382.76	0.8547	1.7606	1.229	0.778	1.098	902	1271.	951.2	8.40	106.2	9.89	21.03	-30
-20	0.01937	1453.6	0.79638	174.84	389.94	0.9044	1.7541	1.242	0.806	1.099	859	1290.	790.1	8.75	102.1	10.30	19.78	-20
-10	0.03277	1429.0	0.48886	187.34	397.18	0.9528	1.7502	1.257	0.837	1.100	815	1307.	668.3	9.09	99.0	10.77	18.52	-10
0	0.05292	1404.0	0.30955	200.00	404.47	1.0000	1.7486	1.274	0.868	1.103	773	1321.	573.2	9.42	95.9	11.31	17.25	0
2	0.05795	1398.9	0.28419	202.55	405.95	1.0093	1.7484	1.277	0.875	1.104	765	1323.	556.7	9.49	95.3	11.48	16.99	2
4	0.06336	1393.8	0.26129	205.11	407.39	1.0186	1.7484	1.281	0.881	1.104	756	1325.	540.8	9.56	94.7	11.55	16.74	4
6	0.06916	1388.7	0.24057	207.68	408.86	1.0278	1.7484	1.284	0.888	1.105	748	1328.	525.6	9.62	94.0	11.67	16.48	6
8	0.07538	1383.5	0.22180	210.25	410.32	1.0369	1.7485	1.288	0.895	1.106	740	1330.	511.0	9.69	93.4	11.79	16.22	8
10	0.08204	1378.3	0.20477	212.84	411.79	1.0461	1.7487	1.292	0.901	1.107	731	1332.	497.0	9.76	92.8	11.91	15.97	10
12	0.08917	1373.1	0.18929	215.45	413.25	1.0552	1.7489	1.296	0.908	1.108	723	1334.	483.5	9.82	92.2	12.04	15.71	12
14	0.09677	1367.9	0.17520	218.02	414.72	1.0642	1.7492	1.299	0.915	1.109	715	1335.	470.6	9.89	91.5	12.17	15.46	14
15.14 ^b	0.10133	1364.9	0.16774	219.51	415.55	1.0694	1.7494	1.302	0.919	1.109	710	1336.	463.4	9.93	91.2	12.24	15.31	15.14
16	0.10488	1362.6	0.16236	220.63	416.18	1.0733	1.7496	1.303	0.922	1.110	707	1337.	458.1	9.96	90.9	12.30	15.20	16
18	0.11352	1357.3	0.15063	223.24	417.65	1.0822	1.7500	1.307	0.929	1.111	698	1338.	446.1	10.02	90.3	12.43	14.94	18
20	0.12270	1352.0	0.13992	225.86	419.12	1.0912	1.7504	1.312	0.936	1.112	690	1339.	434.5	10.09	89.7	12.56	14.69	20
22	0.13247	1346.6	0.13012	228.49	420.58	1.1001	1.7509	1.316	0.943	1.113	682	1341.	423.3	10.16	89.0	12.70	14.43	22
24	0.14283	1341.3	0.12113	231.13	422.04	1.1090	1.7515	1.320	0.950	1.114	674	1341.	412.5	10.22	88.4	12.84	14.17	24
26	0.15383	1335.8	0.11288	233.78	423.51	1.1178	1.7521	1.324	0.958	1.115	666	1342.	402.1	10.29	87.8	12.98	13.92	26
28	0.16547	1330.4	0.10530	236.44	424.97	1.1267	1.7527	1.329	0.966	1.117	657	1343.	392.0	10.36	87.2	13.12	13.66	28
30	0.17779	1324.9	0.09833	239.10	426.46	1.1355	1.7534	1.333	0.973	1.118	649	1343.	382.3	10.42	86.5	13.27	13.40	30
32	0.19061	1319.3	0.09191	241.76	427.89	1.1442	1.7541	1.338	0.980	1.120	641	1344.	372.8	10.49	85.9	13.42	13.15	32
34	0.20466	1313.7	0.08599	244.46	429.35	1.1529	1.7549	1.342	0.988	1.121	633	1344.	363.7	10.56	85.3	13.57	12.89	34
36	0.21907	1308.1	0.08053	247.15	430.81	1.1617	1.7557	1.347	0.996	1.123	625	1344.	354.8	10.62	84.6	13.72	12.63	36
38	0.23436	1302.4	0.07548	249.86	432.26	1.1703	1.7566	1.352	1.003	1.125	617	1344.	346.2	10.69	84.0	13.87	12.38	38
40	0.25046	1296.7	0.07080	252.57	433.71	1.1790	1.7574	1.357	1.011	1.126	609	1343.	337.9	10.76	83.4	14.02	12.12	40
42	0.26741	1291.0	0.06647	255.29	435.16	1.1876	1.7583	1.362	1.019	1.128	600	1343.	329.8	10.83	82.7	14.18	11.87	42
44	0.28522	1285.2	0.06246	258.03	436.61	1.1962	1.7593	1.367	1.028	1.130	592	1342.	321.9	10.89	82.1	14.34	11.61	44
46	0.30394	1279.3	0.05873	260.77	438.05	1.2048	1.7603	1.373	1.036	1.132	584	1341.	314.3	10.96	81.4	14.50	11.36	46
48	0.32358	1273.4	0.05527	263.52	439.49	1.2133	1.7613	1.378	1.044	1.135	576	1340.	306.9	11.03	80.8	14.66	11.10	48
50	0.34417	1267.4	0.05205	266.29	440.93	1.2219	1.7623	1.383	1.053	1.137	568	1338.	299.7	11.10	80.2	14.83	10.85	50
52	0.36576	1261.4	0.04905	269.07	442.36	1.2304	1.7633	1.389	1.061	1.139	560	1337.	292.6	11.17	79.5	15.00	10.60	52
54	0.38836	1255.3	0.04625	271.85	443.78	1.2389	1.7644	1.395	1.070	1.142	552	1335.	285.8	11.24	78.9	15.17	10.34	54
56	0.41201	1249.2	0.04365	274.65	445.21	1.2474	1.7655	1.401	1.079	1.145	544	1333.	279.1	11.32	78.2	15.34	10.09	56
58	0.43674	1243.0	0.04122	277.46	446.62	1.2558	1.7666	1.407	1.088	1.147	536	1331.	272.6	11.39	77.6	15.51	9.84	58
60	0.46259	1236.8	0.03894	280.29	448.04	1.2642	1.7678	1.413	1.098	1.150	527	1328.	266.2	11.46	76.9	15.69	9.59	60
62	0.48957	1230.4	0.03682	283.12	449.44	1.2727	1.7689	1.419	1.107	1.153	519	1326.	260.1	11.54	76.3	15.86	9.34	62
64	0.51773	1224.1	0.03482	285.97	450.84	1.2811	1.7701	1.426	1.117	1.157	511	1323.	254.0	11.61	75.6	16.04	9.09	64
66	0.54710	1217.6	0.03296	288.83	452.23	1.2894	1.7713	1.433	1.127	1.160	503	1320.	248.1	11.69	75.0	16.23	8.84	66
68	0.57771	1211.1	0.03121	291.70	453.62	1.2978	1.7724	1.439	1.137	1.164	495	1316.	242.3	11.77	74.4	16.41	8.59	68
70	0.60960	1204.4	0.02957	294.59	455.00	1.3062	1.7736	1.447	1.147	1.168	487	1313.	236.7	11.85	73.7	16.60	8.35	70
72	0.64279	1197.8	0.02803	297.49	456.36	1.3145	1.7748	1.454	1.158	1.172	479	1309.	231.2	11.93	73.1	16.79	8.10	72
74	0.67732	1191.0	0.02658	300.40	457.72	1.3229	1.7760	1.461	1.169	1.176	470	1305.	225.8	12.01	72.4	16.98	7.85	74
76	0.71323	1184.1	0.02521	303.33	459.08	1.3312	1.7773	1.469	1.180	1.181	462	1300.	220.5	12.10	71.8	17.18	7.61	76
78	0.75056	1177.2	0.02393	306.28	460.42	1.3395	1.7785	1.477	1.192	1.186	454	1295.	215.3	12.18	71.2	17.38	7.37	78
80	0.78931	1170.1	0.02272	309.24	461.75	1.3478	1.7797	1.486	1.204	1.191	446	1290.	210.2	12.27	70.5	17.58	7.13	80
82	0.82956	1163.0	0.02158	312.21	463.06	1.3561	1.7809	1.494	1.217	1.196	437	1285.	205.3	12.37	69.9	17.79	6.88	82
84	0.87132	1155.7	0.02050	315.20	464.37	1.3644	1.7821	1.503	1.230	1.202	429	1279.	200.4	12.46	69.3	18.00	6.65	84
86	0.91464	1148.4	0.01949	318.21	465.66	1.3727	1.7833	1.512	1.243	1.209	421	1274.	195.6	12.56	68.6	18.22	6.41	86
88	0.95955	1140.9	0.01853	321.24	466.94	1.3810	1.7845	1.522	1.257	1.215	412	1267.	190.9	12.66	68.0	18.44	6.17	88
90	1.0061	1133.3	0.01762	324.28	468.20	1.3893	1.7856	1.532	1.272	1.223	404	1261.	186.3	12.76	67.4	18.66	5.93	90
92	1.0543	1125.6	0.01676	327.34	469.45	1.3976	1.7868	1.543	1.287	1.230	396	1254.	181.8	12.87	66.7	18.89	5.70	92
94	1.1042	1117.7	0.01594	330.42	470.68	1.4059	1.7879	1.554	1.303	1.239	387	1247.	177.3	12.98	66.1	19.13	5.47	94
96	1.1559	1109.7	0.01517	333.52	471.89	1.4142	1.7890	1.565	1.320	1.247	379	1239.	172.9	13.10	65.5	19.38	5.24	96
98	1.2093	1101.6	0.01444	336.64	473.09	1.4225	1.7901	1.577	1.337	1.257	370	1231.	168.6	13.22	64.9	19.63	5.01	98
100	1.2646	1093.3	0.01374	339.78	474.26	1.4308	1.7912	1.590	1.356	1.267	362	1223.	164.3	13.35	64.3	19.89	4.78	100
105	1.4130	1071.8	0.01215	347.74	477.09	1.4516	1.7936	1.625	1.408	1.297	340	1200.	154.0	13.70	62.8	20.39	4.22	105
110	1.5698	1049.1	0.01074	355.85	479.74	1.4725	1.7959	1.667	1.469	1.335	319	1174.	143.9	14.09	61.3	21.36	3.68	110
115	1.7417	1025.0	0.00949	364.13	482.30	1.4936	1.7977	1.716	1.544	1.383	296	1146.	134.2	14.54	59.9	22.34	3.15	115
120</																		

Appendix 5: Mourrier (P-h) chart for R-245fa

Licensed for single user. © 2009 ASHRAE, Inc.

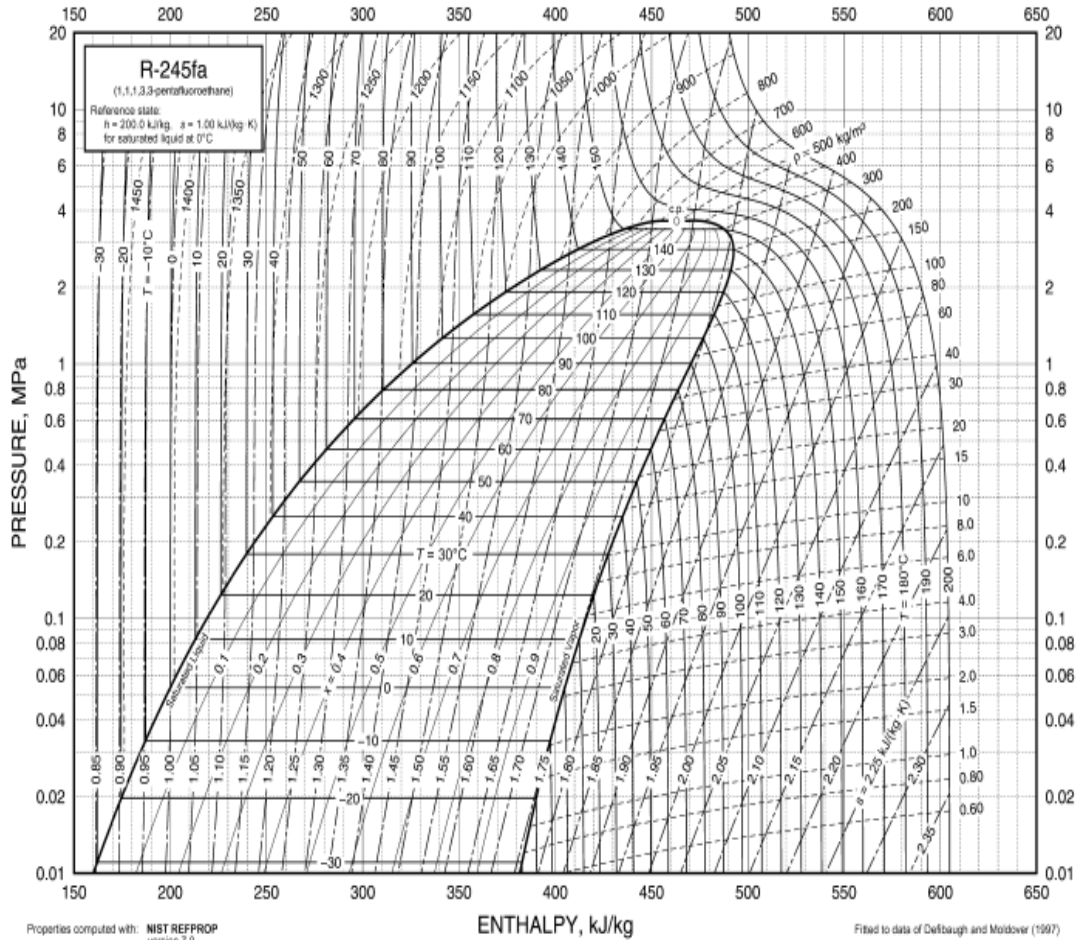
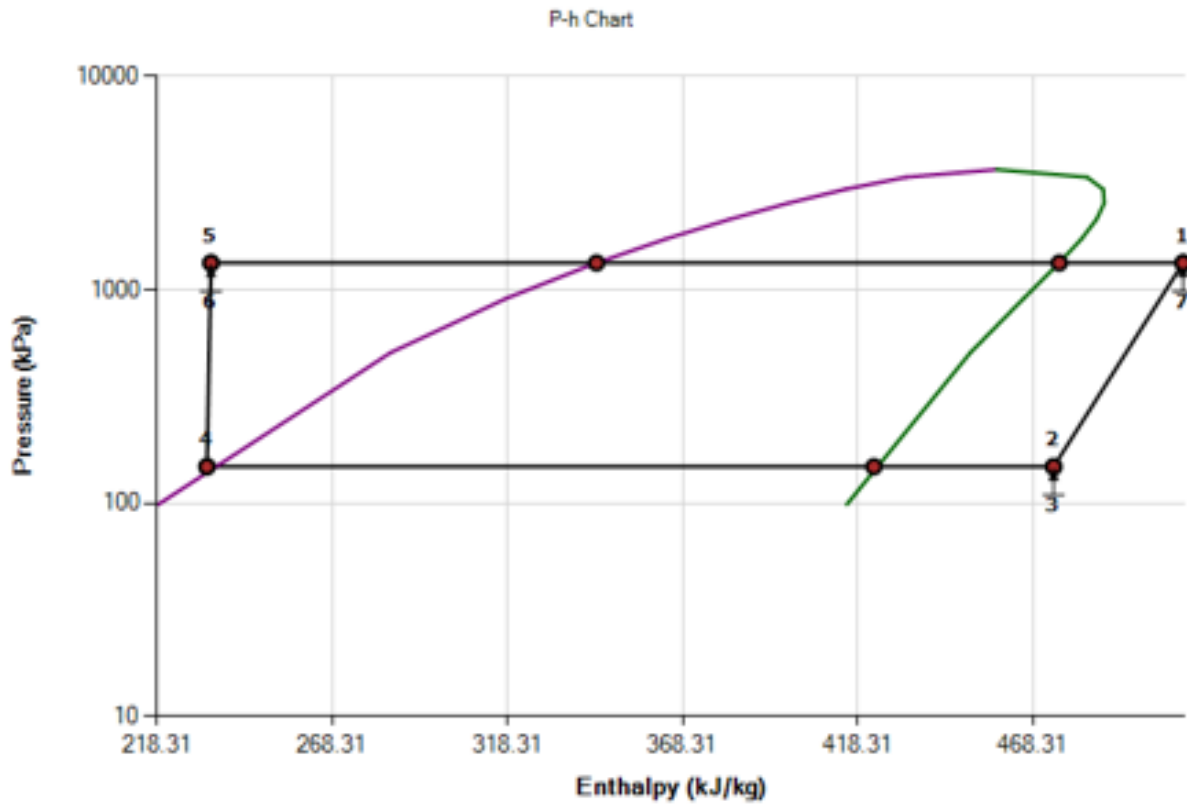


Fig. 11 Pressure-Enthalpy Diagram for Refrigerant 245fa

30.24

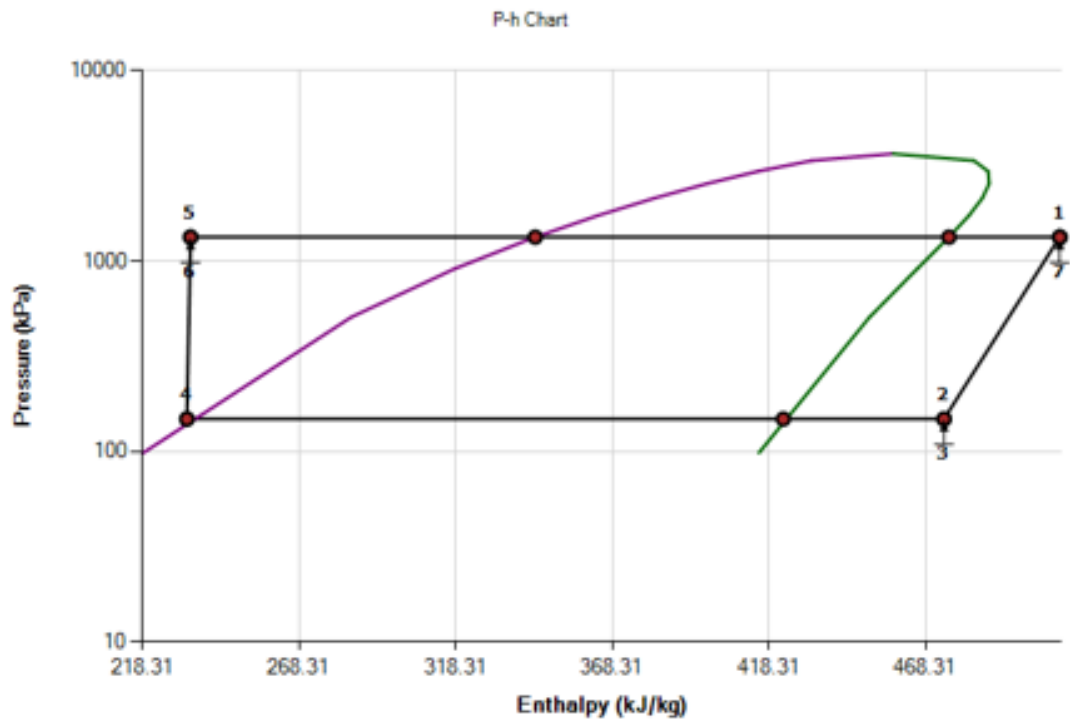
2009 ASHRAE Handbook—Fundamentals (SI)

Appendix 6a: Simulation of thermal performance of R-245fa at low temperature



Performance Parameters				
Refrigerant	R245FA		Thermal Eff.	- 0.1326
GWP	858		Turb. Exit Quality	- 1
Mass Flow	kg/s	0.02707	Turb. Exit Superheat	°C 53.33
Boiler Heat Input	W	7508.15	Boiler Temp.	°C 102.43
Turbine Output	W	1000	Condensation Temp.	°C 25
Heat Rejection Cond.	kW	6.54	Pump Power	kW 0.032

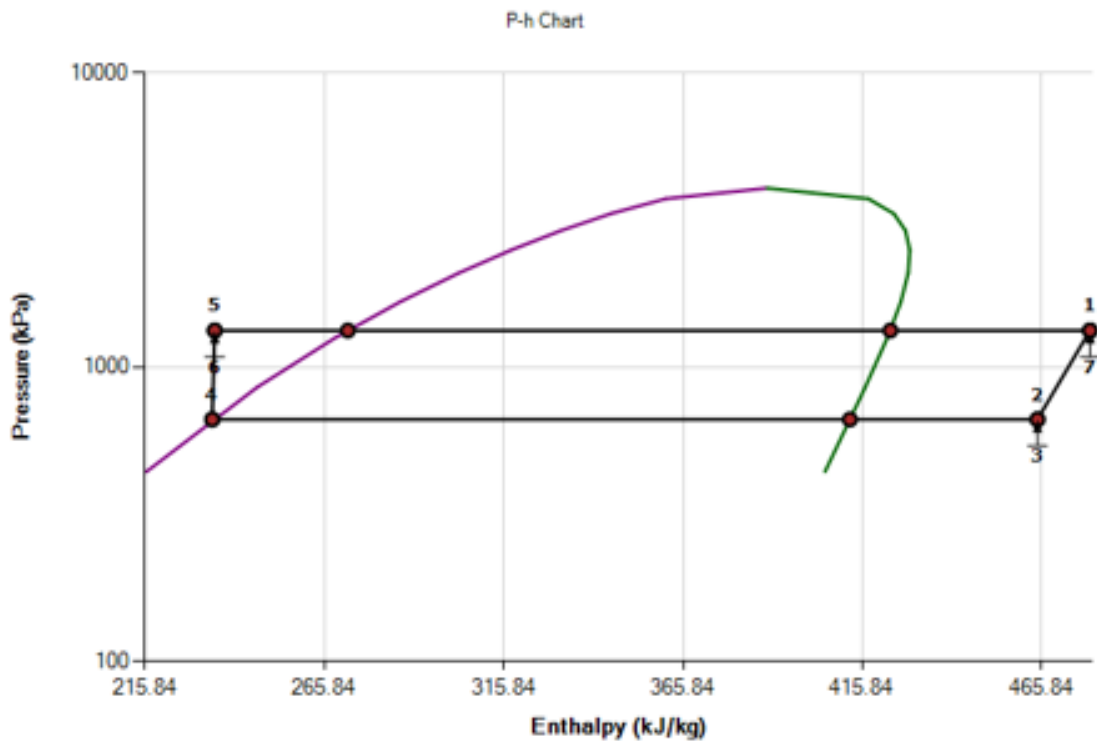
Appendix 6b: Simulation of thermal performance of R-245fa at high temperature



Performance Parameters

Refrigerant	R245FA	Thermal Eff.	-	0.1326	
GWP	858	Turb. Exit Quality	-	1	
Mass Flow	kg/s	0.03605	Turb. Exit Superheat	°C	53.34
Boiler Heat Input	W	10000	Boiler Temp.	°C	102.43
Turbine Output	W	1331.88	Condensation Temp.	°C	25
Heat Rejection Cond.	kW	8.711	Pump Power	kW	0.043

Appendix 6c: Simulation of thermal performance of R-134a



Performance Parameters

Refrigerant	R134A	Thermal Eff.	-	0.0598	
GWP	1300	Turb. Exit Quality	-	1	
Mass Flow	kg/s	0.06763	Turb. Exit Superheat	°C	52.73
Boiler Heat Input	W	16500	Boiler Temp.	°C	50.49
Turbine Output	W	990.11	Condensation Temp.	°C	25
Heat Rejection Cond.	kW	15.56	Pump Power	kW	0.05

Appendix 7: Pressure conversion tables

PRESSURE CONVERSION TABLE

by :H.Tring/T.Stec

MILLIBAR	TORR (mm of Hg)	MICRON (millitorr)	INCHES HG	PSI Pounds Per Square Inch	PASCAL (Pa)
1013 (1 atmosphere)	760 (1 atmosphere)	760000 (1 atmosphere)	0 (1 atmosphere)	14.69 (1 atmosphere)	101,325 (1 atmosphere)
1000	750	750,000	0.42	14.5	100,000
800	600	600000	6.32	11.6	80,000
533	400	400,000	14.22	7.73	52,300
267	200	200,000	22.07	3.87	25,700
133	100	100,000	25.98	1.93	13,300
60	45	45,000	28.15	0.87 (8.7×10^{-1})	6,000
27	20	20,000	29.14	0.39 (3.9×10^{-1})	2,700
1.33	1.0	1,000	29.88	0.02 (2.0×10^{-2})	133
0.93 (9.3×10^{-1})	0.7 (7.0×10^{-1})	700	29.89	0.013 (1.3×10^{-2})	93
0.78 (7.8×10^{-1})	0.6 (6.0×10^{-1})	600	29.9	0.011 (1.1×10^{-2})	78
0.66 (6.6×10^{-1})	0.5 (5.0×10^{-1})	500	29.9	0.009 (9.0×10^{-3})	66
0.53 (5.3×10^{-1})	0.4 (4.0×10^{-1})	400	29.9	0.008 (8.0×10^{-3})	53
0.40 (4.0×10^{-1})	0.3 (3.0×10^{-1})	300	29.91	0.006 (6.0×10^{-3})	40
0.26 (2.6×10^{-1})	0.2 (2.0×10^{-1})	200	29.91	0.004 (4.0×10^{-3})	26
0.13 (1.3×10^{-1})	0.10 (1.0×10^{-1})	100	29.92	0.002 (2.0×10^{-3})	13
0.09 (9.0×10^{-2})	0.07 (7.0×10^{-2})	70		0.0013 (1.3×10^{-3})	9
0.08 (8.0×10^{-2})	0.06 (6.0×10^{-2})	60		0.0011 (1.1×10^{-3})	8
0.07 (7.0×10^{-2})	0.05 (5.0×10^{-2})	50		0.0009 (9.0×10^{-4})	7
0.05	0.04	40		0.0008	5

Appendix 8: Properties of ORC heat engine working fluids

	Name or Number	NBP [K]	Critical temp. [K]	Critical pr. [kPa]	Safety group	Atm. life time	ODP	GWP (100 yr)	Expansion
1	R245ca	298,13	447,42	3925	-	6,5	0	726	dry
2	R11	296,708	470,96	4407,6	A1	45	1	4750	isentropic
3	R245fa	288,14	427	3651	B1	7,7	0	1050	dry
4	R601b Neopentane	282,5	433,6	3196			0	20	dry
5	R21	281,86	451,33	5181	B1	1,7	0,04	151	wet
6	R236ea	279,2	412,29	3502		11	0	1410	dry
7	Cis-butene	276,72	435,6	4225,5					isentropic
8	R114	276,6	427,7	3257	A1	190	0,58	9180	dry
9	Trans-butene	273,88	428,46	4027	A3	0,018	0	20	dry
10	R600 BUTANE	272,5	425	3800	A3	0,018	0	20	dry
11	R236fa	271,6	397,9	3200	A1	242	0	9820	dry
12	Perfluorobutane	270,99	386,18	2323					dry
13	RC318	267	388,2	2780	A1	3200	0	10300	dry
14	Butene	266,69	419,14	4005					dry
15	Isobutene	266	506,96	4010					dry
16	R142b	263,9	410,1	4060	A2	17,2	0,06	2220	isentropic
17	Sulfur dioxide	263	430,5	7090	B1		0		wet
18	Isobutane	261,3	407,7	3630	A3	0,016	0	20	dry
19	R124	261	395,3	3062	A1	5,9	0,02	619	dry
20	R152a	258,98	386,26	4517	A2	1,5	0	140	wet
21	R227ea	256,7	374,8	2930	A1	38,9	0	3580	dry
22	R1234ze [E]	254	382,4	3640		0,045	0	6	dry
23	CF3i	251,15	396,29	3953					wet
24	DME	248,2	400,23	5340	A3	0,015	0		wet
25	R134a	247	374	4059	A1	14,6	0	1300	wet
26	R1234yf	243,5	367,7	3380	A2L	0,029	0	4,4	dry
27	R12	243,2	385	414	A1	100	0,82	10900	wet
28	C270 Cyclopropane	241,8	398,2	5580		0,44	0	20	wet
29	Ammonia	239,7	405,25	11333	B2L	0,02	0	1	wet
30	R161	235,4	375,2	5090		0,18	0	12	wet
31	R22	232,2	369,1	4990	A1	11,9	0,04	1790	wet
32	R290 Propane	231	369,7	4247	A3				wet
33	R1270 Propylene	225,4	364,1	4560	A3	0,001	0	20	wet
34	Carbonyl sulfide	222,84	378,62	6370					wet
35	Hydrogen sulfide	212,7	372,95	9000					wet